LOCALIZATION OF BROADBAND OCEAN ACOUSTIC SOURCES

Matthew Andrew Dzieciuch

COMMUNICATIONS & SIGNAL PROCESSING LABORATORY
Department of Electrical Engineering and Computer Science
The University of Michigan
Ann Arbor, Michigan 48109

August 1990

Technical Report No. 277

#277

LOCALIZATION OF BROADBAND OCEAN ACOUSTIC SOURCES

by

Matthew Andrew Dzieciuch

A dissertation submitted in partial fulfillment
of the requirements for the degree of
Doctor of Philosophy
(Electrical Engineering)
in The University of Michigan
1990

Doctoral Committee:

Professor Theodore G. Birdsall, Chairman
Assistant Professor Alfred O. Hero
Professor Donald J. Patterson
Professor Emeritus William L. Root
Associate Professor Demosthenis Teneketzis
Associate Research Scientist Kurt Metzger

To my Mom and Dad,
Jennifer and James.

ACKNOWLEDGEMENTS

No dissertation can be finished without the assistance and support of others. This dissertation is no different. A number of people have helped me, both directly and indirectly, to complete this thesis and I shall forever be grateful.

First and foremost, I would like to thank Ted Birdsall for being my advisor and a great teacher. His door was always open and he was always quick with encouragement and generous with his time. His example provided me with an exceptional role model of how to be a scientific investigator. My many adventures with Kurt Metzger, taught me how to make things work even when disaster seemed just around the corner. He also served on my committee and his insights and comments were invaluable.

Also, I would like to thank the members of my doctoral committee, Professors Root, Teneketzis, Hero, and Patterson, for their time and guidance in seeing this work to its conclusion.

Carol Van Aken and Dawn Wacker of the Communications and Signal Processing Laboratory took care of administrative details and made a big university seem small.

Many friends are made during graduate school and the struggles we went through together will always be some of my favorite memories. Particularly, Paul and Suzette Puzinauskas who became part of my family and kept me from going insane. Lunch will never be the same. Also my housemate Nick Petrick, whose disposition brightened the cloudiest skies.

Also, I was blessed by friendship with Dennis Buckley, Dave Childs, Kevin Sietz, whom I have known since grade school and have been like brothers to me.

I believe that one learns as much from other students as from ones teachers. Paul Min, Mark Andersland, Manju Hegde and Fuad Khan were uncommon classmates and will be lifelong friends.

Finally, I want to thank my family, in particular my Mom and my Dad, for encouraging me to stay in school. Their love and understanding has made my life a rich one indeed.

This dissertation was made possible by funding from the Office of Naval Research and the Office of Naval Technology.

TABLE OF CONTENTS

LIST OF FIGURES

LIST OF APPENDICES

Appendix

ABSTRACT

LOCALIZATION OF BROADBAND OCEAN ACOUSTIC SOURCES

by
Matthew Andrew Dzieciuch

Chairman: Theodore G. Birdsall

Underwater acoustic propagation is characterized by multipath or multimode propagation. Signal processors can be designed to take advantage of the channel complexity if the environment is known. The proposed technique, channel matched filtering (CMF), synthetically backpropagates the wave front to a hypothesized source location. Passive estimates of source location can be made without knowledge of signal characteristics. CMF is demonstrated to be a good performer in the wideband case, as well as the narrowband case where matched field processing, a localization technique appropriate for narrowband sources, has previously been employed. Several ad hoc variants on CMF are also developed. Extensions of matched field processing for broadband signals are made as well. CMF and its variants are developed in the time domain which leads to computational efficiencies over the broadband matched field processor. Comparisons of the various techniques are made with various signal bandwidths and with channels perturbed by internal waves. Accurate and efficiently calculated impulse responses of the ocean acoustic channel are necessary for the successful application of the CMF technique. Gaussian beam theory

(GBT) is developed for the propagation model since it provides impulse responses which are shown to approach the accuracy of mode based models, while the computational complexity of GBT is of the same order as ray based models. A procedure is developed here for the specification of the initial conditions of the GB model corresponding to an ideal point source which compares favorably with the accuracy of mode based models. Impulse responses are shown to be easily obtainable from GBT providing an efficient characterization of the channel in the time domain. Time front visualization of a propagating spatial impulse together with amplitude and phase information given by GBT provide great insight into the nature of ocean acoustic propagation.

CHAPTER I

INTRODUCTION

Rapid progress has been made recently in the mapping of the ocean's temperature and current fields. It is now possible to measure the fluctuations in the sound speed field, with tomographic techniques, over ocean basin regions, [13]. Since sonar signal processors have long suffered from the lack of environmental information, it is reasonable to ask how this data can be used effectively in source detection and localization problems.

In the late seventies, oceanographers faced a crisis. General circulation models of the ocean's current fields were impossible to validate, [36]. Traditional measurements made by current meters, expendable bathythermographs and similar instruments are point measurements. That is to say, the instruments provide data about one point in the ocean volume at one particular moment. While the instruments themselves were not particularly expensive, it was clear that to gather the amount of data necessary for meaningful analysis would be prohibitively expensive. Researchers realized that a new synoptic method of oceanic observation was needed in order to adequately sample the current field.

After some very innovating analysis and experimentation a new oceanographic technique was invented, [37]. This technique, ocean acoustic tomography, provided the means necessary to monitor the current and temperature fields in a large area

from a relatively few sites. Instead of direct measurement of ocean properties, the ocean acoustic characteristics were observed via long range propagation experiments involving deep moored sources and receivers. Since the acoustic impulse response is dependent on the ocean current and temperature fields, measurement of the ocean acoustic channel provides information about these variables.

The science of acoustics has found wide use in the ocean because sound waves have the remarkable property of being able to propagate over very long ranges. Electromagnetic energy, on the other hand, is not able to penetrate the sea to any great depth. Therefore, sound is much more suitable for the remote sensing of the ocean interior than electromagnetic waves, which are quickly attenuated by conductive turbid saltwater.

It is well known that low frequency sound (less than 1kHz) can travel several megameters underwater without prohibitive attenuation, [42]. The transmission of energy over such great distances is facilitated by two facts. The first is that sound has low attenuation at low frequencies. This implies that the medium does not absorb the sound energy. The second is that the sound speed profile has a minimum at a depth of approximately one kilometer. This implies that the energy is ducted as in a waveguide and that boundary losses are not incurred for purely refracted rays. Another well documented characteristic of the ocean acoustic channel is multipath propagation. The typical point to point impulse response of the channel is the sum of several time delayed, amplitude weighted, phase shifted arrivals.

Ocean acoustic tomography takes advantage of the long range multipath propagation of underwater sound. The technique is fairly simple to describe but difficult to implement, [23]. First, accurate measurements of the multipath time delays between a number of moored transceivers are made. Then, using historical data to model a reference ocean, perturbations between the reference ocean and the actual observations are calculated. The necessary changes in the current and temperature

fields are then determined by using standard linear inverse theory. Since this is a vastly underdetermined problem, the fields are restricted to a few oceanographically efficient modes. Finally, the fields can be tracked in time by using a Kalman filter that smooths the data.

There are several advantages of acoustic tomography over traditional point measurements. First, tomography naturally smooths small scale local variability because the observed travel time is integrated over the entire propagation path. Secondly, the number of data points increases quadratically with the number of moorings as compared to linearly with point measurements. And thirdly, the technique takes advantage of the fact that multiple arrivals can be separated and used individually. This also increases the number of data points.

The efforts of physical oceanographers to include ocean acoustics into their models resulted in a major step forward. Sonar signal processors can also benefit by including ocean acoustic modeling in their efforts. Sonar signal processing has always been hampered by a complicated multipath environment, [45]. It can be demonstrated however, that the complex arrival structure can be used to the signal processor's advantage. The essential element is, of course, good modeling of ocean acoustic properties. The study of techniques which utilize precise knowledge of the acoustic propagation is the proposed thesis problem.

Assume that ocean acoustic tomography can give the signal processor accurate environmental information, that is to say the temperature, density and current fields are known well enough in the region of interest to allow one to infer the sound speed field and thus to make a good estimate of the channel impulse response. Based on this assumption, it is interesting to construct a solution to a standard sonar problem and to compare the result to a solution which does not contain environmental information.

In this thesis we try to solve the passive source location problem, using environmental information provided by a technique such as ocean acoustic tomography.

Passive source location without environmental information is a standard problem in ocean acoustics with many applications, [22]. A standard solution is to deploy two vertical hydrophone arrays. The two arrays operate in a passive or *listen only* mode. Also, the source waveform is unknown. Initially, the arrays are beamformed to reduce directional noise. Then the beamformer outputs are used as inputs to a generalized cross–correlator [8]. The output is a time delay estimate which localizes the source along a hyperbola with the two arrays at the foci.

In order to deal with the multipath propagation problem a new signal processor is proposed in this thesis, which synthetically back-propagates the wavefront to a hypothesized source location. This method, called channel matched filtering here, was inspired by phase conjugation techniques used in optical processors to reduce the effect of atmospheric distortion, [53]. The motivation for the back–propagation approach is to refocus the signal energy, which is dispersed both in time and space, to a particular source location. By concentrating the energy, signal detectability should increase. By searching over a set of hypothesized source locations, a source position estimate can be made. In fact it will be shown that a single vertical array can localize a source along a circle with the array at the center. Furthermore if the ocean has some range variability in its sound speed, the ambiguity can be reduced even more.

The channel matched filtering (CMF) algorithm is similar to the matched field processing first described by Bucker [7]. The approach taken here removes the narrowband restriction. By combining the broadband information in the manner described by Baggeroer, Kuperman, and Schmidt, [1], a better position estimate can be made. Since the CMF algorithm is implemented in the time domain, however, calculation of the estimator is more efficient, as well as providing an alternate and perhaps more transparent viewpoint of the problem. Recently, Clay [11] described a similar technique in terms of **impulse** responses, but does not combine the theory

with an ocean acoustic model. Wax and Kailath, [47], have also considered the optimal source localization problem, as a maximum likelihood estimate of position but not specifically for the multipath ocean acoustic environment.

As mentioned above, the key element of the signal processing is an accurate acoustic propagation model. Also, the acoustic model needs to be numerically efficient, since the channel matched filtering algorithm searches over range and depth, and therefore the model is run repeatedly. A further requirement is that it be a broadband model since no assumption about the source signal is made. These are severe requirements. Propagation models generally available do not perform as well as an advanced signal processor may desire. Therefore a recently developed modeling technique has been explored for use in underwater acoustics.

The new ocean acoustic propagation model, called the Gaussian beam method, was first described in the optics literature, [27], and has been more recently applied to seismic signal processing by Červený, [9], [10]. It was first applied to the underwater sound environment by Porter [38]. The idea is to approximate the wave equation along the path that the sound energy travels. A number of unique results are obtained in this thesis. Acoustic fields, magnitude and phase, and channel impulse responses can be accurately and efficiently calculated. By plotting amplitude and phase modulated time fronts, valuable insight into the nature of the propagation problem can be gained. Finally a procedure is defined which specifies initial conditions for accurate modeling.

There are two parts to this thesis. The first part is about ocean acoustic propagation modeling which is covered in chapters two and three. The second part is about signal processing techniques which are covered in chapter four.

Chapter Two contains a basic review of underwater sound. A simple environmental model adequate for computer simulations is described first. Then the wave equation is derived from fundamental physical principles. Finally, both mode and

ray theories of sound propagation are considered as solutions to the wave equation.

Chapter Three gives an approximate solution to the wave equation known as the Gaussian beam method. First the method is derived from the wave equation and the basic approximations are explained as was originally presented by Červený, [9], [10]. Next, the subject of choosing initial conditions to accurately model an ideal point source is discussed. A number of approaches, including minimum beamwidth and beam reciprocity, are explored. A procedure is developed here that minimizes the error due to approximation of the wave equation by a Taylor series. Then the numerical procedure used to calculate acoustic fields and channel impulse responses is described. It is found, in this thesis, that impulse responses can be accurately and efficiently calculated using this method. Finally, comparisons are made to the more exact mode solution in a specific situation where a mode solution exists.

Chapter Four describes a recent development in sonar signal processing called matched field processing. This algorithm uses a spatial matched filter to search for the source location. An extension to multiple frequency processors is made in two ways: coherent and incoherent integration of the signal spectrum. Next, a new signal processing algorithm for source localization is presented. The algorithm is called channel matched filtering. Variations of this theme are also be presented that rely only upon the channel phase and time delay characteristics. Finally, environmental mismatch issues are simulated by ocean internal wave modeling.

There are two appendices. The first appendix provides a list of the computer code that was used as an acoustic model. Also there is a brief discussion of how the program works. The second appendix presents a brief discussion of linear ocean internal waves. These are the main source of ocean variability considered in this work.

CHAPTER II

OCEAN ACOUSTIC MODELING

Good modeling of ocean acoustic propagation is essential for good sonar signal processing. In the problem under consideration here, the model should be able to accurately predict all important phenomena. Also, the model should be computationally efficient so that the signal processing algorithms which depend on it can be reasonably implemented. Thus when comparing models, the criteria of model efficiency or ease of calculation are just as important as model accuracy and consistency.

There are two main schools of thought in acoustic modeling, [44]. They are the ray–based and mode–based approaches. Each has its advantages in certain situations. There are limits, however, to the usefulness of both models. Roughly, mode theory is a high accuracy, low efficiency model; while ray theory is a lower accuracy, high efficiency model.

The mode model gives the best results in a range independent environment (the sound speed is a function of depth only), where the wave equation is separable. For a weakly range dependent environment, an adiabatic mode model can be used if the sound speed fluctuation with range is small enough so that there is no mode coupling. Both of these models give good amplitude and phase results for their respective situations. The computational complexity of these models also make them difficult and expensive to implement. Mode models are generally used when one is

in a shallow water environment and bottom interaction is important. Also they are important when one wishes to investigate frequency dispersion effects. The parabolic approximation method could also be used. It sacrifices some accuracy for ease of calculation. Even so, all these models give results only at a single frequency and therefore must be run many times for a broadband signal.

As far as ease of use is concerned, simple ray tracing codes cannot be beaten. They are easy to implement, cheap to run, and can handle range dependent environments easily. For the most part they give correct time of arrival information, which is frequency independent. Amplitude and phase results are suspect, if not completely erroneous, especially around caustics and shadow zones. Ray models tend to be used in a deep water situation when there are too many modes present for efficient calculation and bottom interaction is not important.

A simple, but very useful introduction to underwater sound is given in the book by Urick, [45]. This book is highly recommended as an introduction to sonar systems. A more thorough discussion of ocean acoustic propagation was published by Tolstoy and Clay, [44]. For a more recent reference which includes material on the scattering of sound by a fluctuating ocean, the investigator should consult the monograph edited by Flatté, [18].

In this chapter, a description of the ocean acoustic environment is given first. Then, the wave equation is derived from basic physical principles. Finally, a review of the basic mode-based and ray-based wave propagation models is presented as well as some examples. In the next chapter a newer model is developed, Gaussian beam theory, which compromises between the accuracy of modal solutions and the efficiency of ray solutions.

In order to simplify this discussion, only two–dimensional models are considered here. Full three–dimensional models are significantly more difficult to design and to execute. Almost all important propagation phenomena are present in a two–

dimensional vertical slice of the ocean.

The Ocean Acoustic Environment

The ocean is a turbulent, rotating fluid, whose properties are ever changing. The property of most concern to the acoustic modeler is the sound speed field. It is a function of the ocean's temperature, salinity, and pressure. Also, the field varies with time. It is affected by currents which move water masses of varying temperature and salinity through the ocean. Also, the sound speed is affected by internal waves, which are slowly moving density waves that move throughout the ocean's volume.

Perhaps the most remarkable property of the abyssal ocean is that it acts as a waveguide for acoustic energy. This is because there exists a sound channel where the speed of sound has a minimum at a middle depth of the water column. This means that all sound is refracted back toward the center of the "waveguide".

A popular model for the sound speed as it varies with depth is the Munk profile. It is a simple, analytical formula derived from physical principles, [35]. To derive it one starts with the empirical thermodynamic equation of state for seawater relating temperature, pressure and salinity, and combines it with the Brunt–Väisälä frequency, a measure of the stability of the water column. The result is an expression for the sound speed which decreases exponentially with depth until it reaches a minimum, then it increases linearly. The sound speed, c, can then be written

$$c(z) = c_0[1 + \epsilon(e^{-\eta} + \eta - 1)] \tag{2.1}$$

where z is depth,

$$\eta = 2(z - z_1)/\mathrm{B} \tag{2.2}$$

and typical parameter values are

$$c_0 = 1492.0\,\mathrm{meters/second} \tag{2.3}$$

$$\epsilon = 7.4 \times 10^{-3} \tag{2.4}$$

$$z_1 = 1300\,\text{meters} \tag{2.5}$$

$$\mathrm{B} = 1300\,\text{meters}. \tag{2.6}$$

Although the Munk profile is reasonable for mid–latitudes, Figure 2.1 shows a comparison between it and a profile measured in the Greenland Sea, [32]. The Greenland Sea is an Arctic environment where the water temperature is nearly constant everywhere except near the surface. The two profiles are very similar at greater depths but at shallower depths the agreement is terrible. Still, if only a general representation at middle latitudes is desired, the Munk profile is a convenient and accurate prototype and therefore will be employed throughout this thesis.

Another consideration is the volume attenuation of seawater, in which sound energy is lost to heat and molecular dissociation. At low frequencies, attenuation is exponentially proportional to the square of frequency, about 25 decibels per megameter per (kilohertz)^2. This imposes a practical limit, signals must have temporal frequencies of less than 400 Hertz to be heard at long ranges (greater than 100 kilometers). Figure 2.2 shows attenuation vs. frequency, see [45]. There are several loss mechanisms. The dominant ones are due to the viscosity of water and the ionic relaxation of magnesium sulfate ($MgSO_4$) molecules in seawater.

Although attenuation due to a lossy medium is important, its effects will be omitted here. This is because there is a more dominant effect that must be included: the loss due to cylindrical spreading. As a comparison, the absorption loss of a source at 100 Hertz at a range of 1 megameter is about 0.1 decibels, while the spreading loss is about 60 decibels.

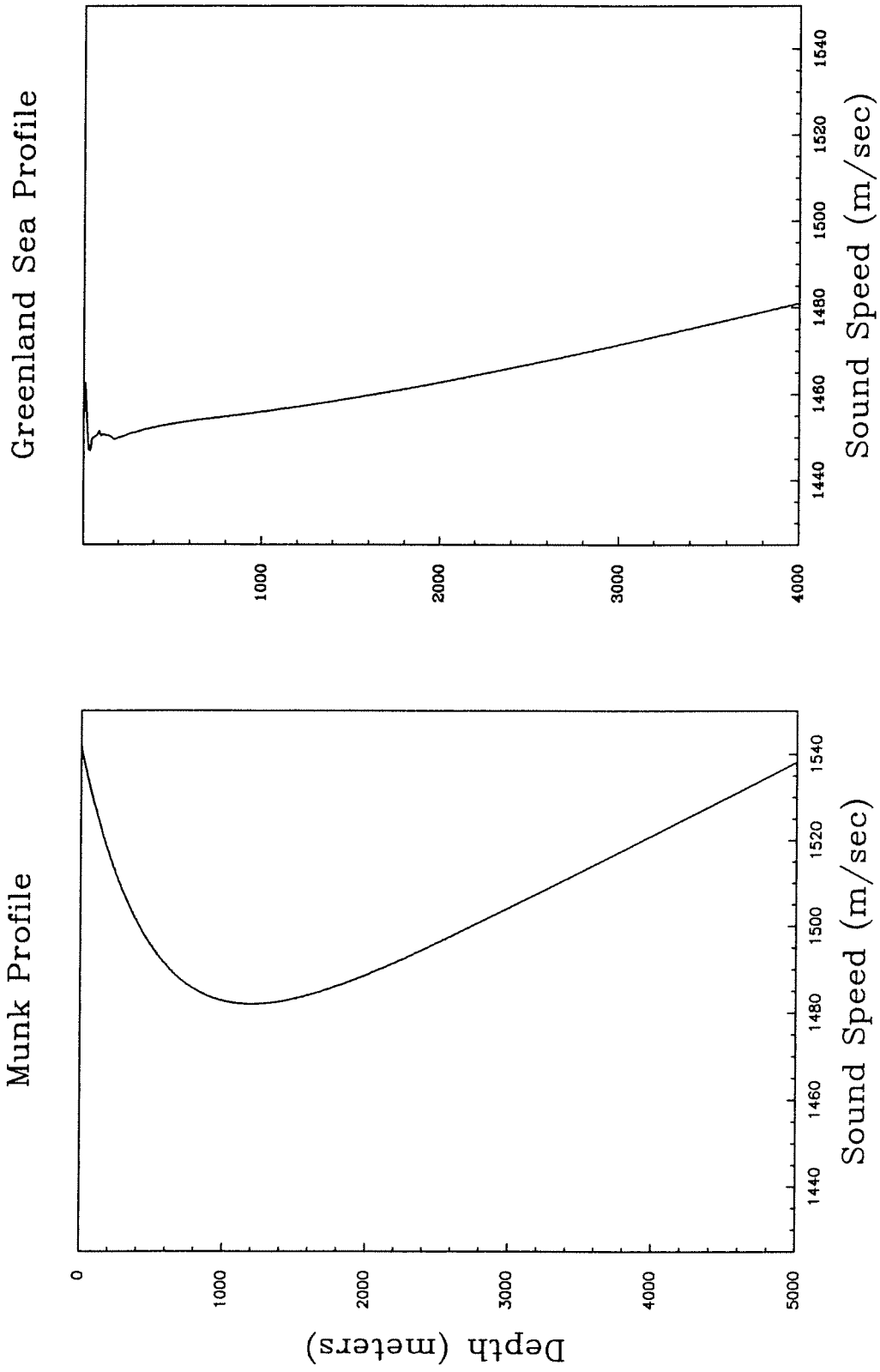

Figure 2.1: Sound Speed Profiles.

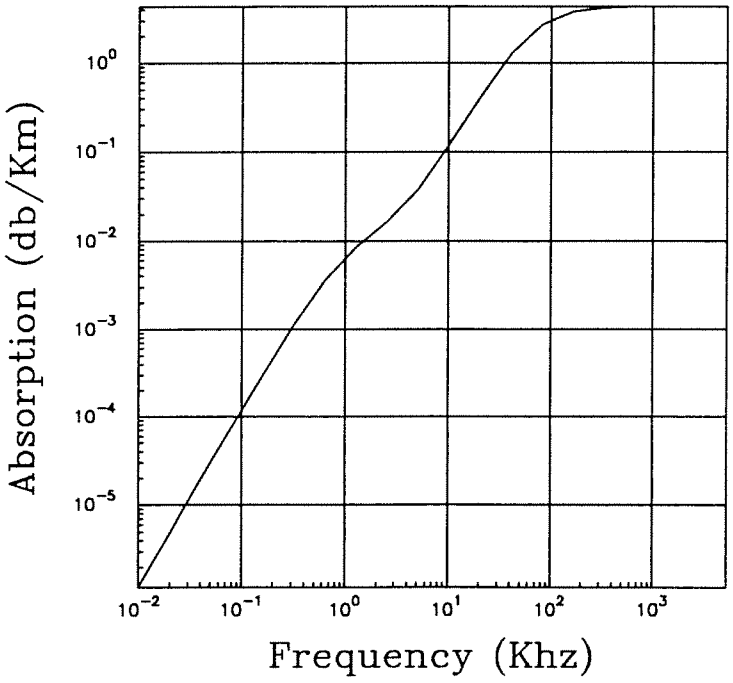

Figure 2.2: Attenuation Coefficient vs. Frequency.

The Wave Equation

All ocean acoustic modeling is based on the wave equation. The development shown here follows Bold, [5]. The acoustic wave equation is derived from three well known physical principles, Newton's second law, the conservation of mass, and Hooke's law. To understand how sound propagates in a fluid consider the mechanical forces which act on a differential element of fixed volume in space.

The equation of motion in three dimensions for the differential volume of fluid is described by Newton's second law

$$\nabla p + \rho \frac{\partial \mathbf{u}}{\partial t} = 0 \tag{2.7}$$

where $\mathbf{u}$ is the vector of fluid velocity through the differential volume element, ρ is the density, and p is the signal pressure.

According to the principle of conservation of mass, any change in the density of the fixed volume must be because some amount of mass either flowed into or out of the volume. Accordingly, the continuity equation can be written

$$\frac{\partial \rho}{\partial t} + \nabla \cdot (\rho \mathbf{u}) = 0. \tag{2.8}$$

This relates the density change per unit time to the divergence of fluid flow through the fixed volume.

Hooke's law is a stress–strain relation. It states that the density change of the fluid is linearly proportional to the pressure acting on that volume of fluid. This is a very good approximation for small signals. Hooke's law is expressed as

$$\rho = \rho_0 \left(1 + \frac{p}{\kappa}\right) \tag{2.9}$$

where κ is the bulk modulus. The bulk modulus is defined as the excess pressure divided by the fractional density change.

Now there are two scalar equations and one vector equation with five unknowns; pressure, density and the three components of velocity. To derive the wave equation, solve for the pressure. Start by taking the time derivative of the continuity equation

$$\frac{\partial^2 \rho}{\partial t^2} + \nabla \cdot \rho \frac{\partial \mathbf{u}}{\partial t} + \nabla \cdot \mathbf{u} \frac{\partial \rho}{\partial t} = 0. \tag{2.10}$$

Then by taking the second time derivative of Hooke's law

$$\frac{\partial^2 \rho}{\partial t^2} = \frac{\rho_0}{\kappa} \frac{\partial^2 p}{\partial t^2} \tag{2.11}$$

and applying the $\nabla \cdot$ operator to Newton's law

$$\nabla^2 p = -\nabla \cdot \rho \frac{\partial \mathbf{u}}{\partial t} \tag{2.12}$$

and substituting into (2.10) results in

$$\nabla^2 p - \frac{1}{c^2} \cdot \frac{\partial^2 p}{\partial t^2} = \nabla \cdot \left(\frac{\partial \rho}{\partial t} \mathbf{u}\right). \tag{2.13}$$

When the signal pressure is much less than the ambient pressure, the right side of the equation becomes essentially zero and the scalar wave equation for pressure can be written

$$\nabla^2 p - \frac{1}{c^2} \cdot \frac{\partial^2 p}{\partial t^2} = 0 \tag{2.14}$$

where

$$c = \sqrt{\frac{\kappa}{\rho_0}} \tag{2.15}$$

is the sound speed. This is an excellent description of small signal sound propagation. For a discussion of the fundamental approximations see [18]. Similar equations can be written in terms of particle density or velocity. Pressure is used in the following discussion because that is what most contemporary hydrophones measure.

The Modal Solution

There is no general analytical solution to the wave equation, (2.14). It is possible to solve it in certain cases. The instance in which we are interested occurs when the sound speed does not vary with range. In this case, there is a straightforward solution to the wave equation based on the separation of variables. The solution is a vertical eigensolution multiplied by a range varying Hankel function. The amplitude and phase response of the channel can then be accurately calculated anywhere in the channel.

Let's take a closer look at the derivation of the modal solution. First, write the wave equation in a cylindrical coordinate system,

$$\frac{\partial^2 p}{\partial r^2} + \frac{1}{r}\frac{\partial p}{\partial r} + \frac{\partial^2 p}{\partial z^2} + \frac{1}{c^2}\frac{\partial^2 p}{\partial t^2} = 0 \tag{2.16}$$

where z is the depth of the ocean measured from the ocean surface and r is the range. Using cylindrical symmetry changes a three dimensional problem into one with only

two dimensions. Now assume a time harmonic solution of the form

$$p(r,z) = p_h(r)p_v(z)e^{j\omega t}. \tag{2.17}$$

The wave equation then separates into two equations. A horizontal part

$$\frac{\partial^2 p_h}{\partial r^2} + \frac{1}{r}\frac{\partial p_h}{\partial r} + k^2 p_h = 0 \tag{2.18}$$

and a vertical part

$$\frac{\partial^2 p_v}{\partial z^2} + \left(\frac{\omega^2}{c^2} - k^2\right) p_v = 0 \tag{2.19}$$

where k is the constant of separation.

The horizontal solution is

$$p_h(r) = H_0^{(2)}(kr) \approx \sqrt{\frac{2}{\pi kr}} e^{-j(kr-\frac{\pi}{4})} \text{ as } r \to \infty \tag{2.20}$$

where $H_0^{(2)}(\cdot)$ is the zero-order Hankel function of the second kind, [44]. Often the Hankel function is often approximated by an exponential. This is reasonable since in most situations the receiver is in the far field of the source.

The vertical equation has no analytical solution for arbitrary sound speed profiles. It must be solved numerically. Assume that the surface and the bottom are parallel boundaries. The fact that the surface acts as a pressure release interface results in the boundary condition

$$p_v(0) = 0. \tag{2.21}$$

The condition at the bottom is more complicated. Physically all that is required is that the pressure is constant across the interface. This means that some energy is transferred to the bottom. In reality, this does occur. At long ranges, though, the more strict boundary condition

$$p_v(z_{bottom}) = 0 \tag{2.22}$$

applies because any solution which does not meet (2.22), will quickly decay. Therefore, it can be assumed that any energy in the continuous k spectrum will be absorbed

by the bottom, so only the discrete modes propagate to long ranges. This implies a discrete spectrum of k values. Some examples of modal functions are shown in figure 2.3. For a typical deep water case with a Munk profile there are as many as five hundred significant modes. The modal functions can be shown to be orthogonal,

$$\int_0^\infty p_v^{(m)}(z)\, p_v^{(n)}(z)\, dz = \delta_{mn}. \tag{2.23}$$

The procedure for calculating modal functions is to use the shooting method, [41]. First make a guess of the eigenvalue (or wavenumber) k, and then calculate the eigenfunction (or modal function) by matching the boundary condition at one end and extrapolating the solution to the other end. Using the error at the far boundary, Newton–Raphson iteration can be done to converge to the correct value of k.

In order to make a good initial guess for k, it is wise to first solve equation (2.19) approximately using the WKB method. To do this, rewrite the separated vertical mode equation as

$$\frac{\partial^2 p_v}{\partial z^2} + \alpha^2 p_v = 0 \tag{2.24}$$

with the dummy variable

$$\alpha^2 = \frac{\omega^2}{c^2} - k^2. \tag{2.25}$$

Now assume a solution of the form

$$p_v(z) = P(z) e^{j\phi(z)} \tag{2.26}$$

which when substituted into (2.24) gives a real and an imaginary equation. The imaginary equation

$$P\frac{d^2\phi}{dz^2} + 2\frac{dP}{dz}\frac{d\phi}{dz} = 0 \tag{2.27}$$

has the solution

$$P(z) = P_0 \left(\frac{d\phi}{dz}\right)^{-1/2}. \tag{2.28}$$

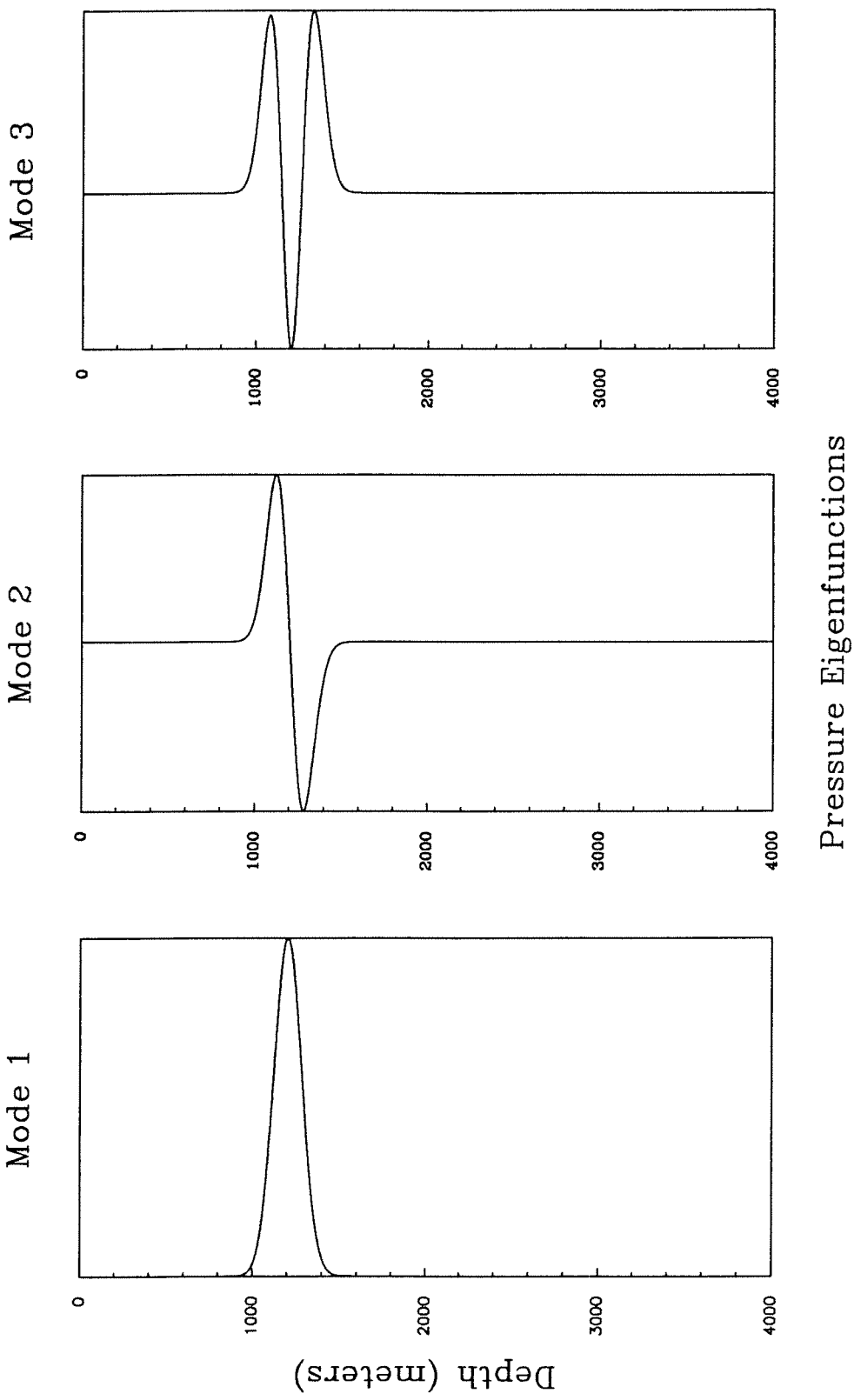

Figure 2.3: Typical Acoustic Vertical Modes.

In order to solve the real equation

$$\frac{d^2P}{dz^2} - \left[\left(\frac{d\phi}{dz}\right)^2 - \alpha^2\right] P = 0 \tag{2.29}$$

we must make the assumption that P is slowly varying, that is to say the amplitude of the solution varies much slower than the phase, as expressed by

$$\frac{d^2P}{dz^2} \approx 0. \tag{2.30}$$

Now we have the solution for ϕ,

$$\phi = \int_0^{z_{bottom}} \alpha \, dz. \tag{2.31}$$

Since the solution must be continuous, ϕ must satisfy the Bohr–Sommerfield condition

$$\phi = \int_{z_1}^{z_2} \alpha \, dz = (n - 1/2)\pi \tag{2.32}$$

where z_1 and z_2 are the roots of

$$\alpha^2 = \frac{\omega^2}{c^2} - k^2 = 0. \tag{2.33}$$

This condition implies that the mode must have an integer number of cycles during the interval that α is imaginary.

It is well known that, in the absence of currents, the acoustic channel is reciprocal. This means that the transfer function of the channel between two points is the same regardless of which point is the source and which point is the receiver. In order to calculate the acoustic field it is necessary to sum the contributions from all the modes. Using the reciprocity condition and summing over the modes we get

$$p(r, z_r, t) = \sum_{m=1}^{M} p_v^{(m)}(z_s)\, p_v^{(m)}(z_r)\, e^{-j(kr - \frac{\pi}{4})}\, e^{-j\omega t} \tag{2.34}$$

where z_s is the source depth and z_r is the receiver depth.

An example of a sound field is plotted in figures 2.4 and 2.5. Shown are the magnitude and phase of the acoustic field of a 1200 meter deep source operating

at 250 Hertz as a function of range and depth. The magnitude plot clearly shows shadow zones where little acoustic power is present and convergence zones where power is focused. The phase plot reveals little physical insight but does show the complicated structure of the field. One thing that can be noticed is that there is a jump in the phase along a caustic, (a place where rays cross that will be described in more detail in the next section). Indeed more careful inspection reveals that the phase changes by 90 degrees across the caustic boundary.

The modal solution depends upon the crucial assumption that the sound speed is range independent. It is not able to cast any light in the case of a range dependent sound speed. Although this does not pose a large problem for theoretical work it is not acceptable in practical situations. Also note that the modal solution gave results only at a single frequency. This is a large problem for theoreticians as well as practitioners of ocean acoustics since the model must be run many times to approximate a broadband signal.

The Ray Solution

Another solution to the wave equation is given by the ray method. This method makes the assumption that the sound energy has a much smaller wavelength (or higher frequency) than the typical dimensions of the medium it is propagating in. This is equivalent to saying that we expect the solution to be locally a plane wave. In the normal deep water ocean situation, ray acoustics gives a useful description of sound energy propagation. This situation is characterized by water that is nearly five kilometers deep and frequencies that are greater than ten cycles per second. In other words the depth of the water should be much greater than the wavelength of the acoustic energy. The usual case is

$$\frac{h}{\lambda} > 10^2 \tag{2.35}$$

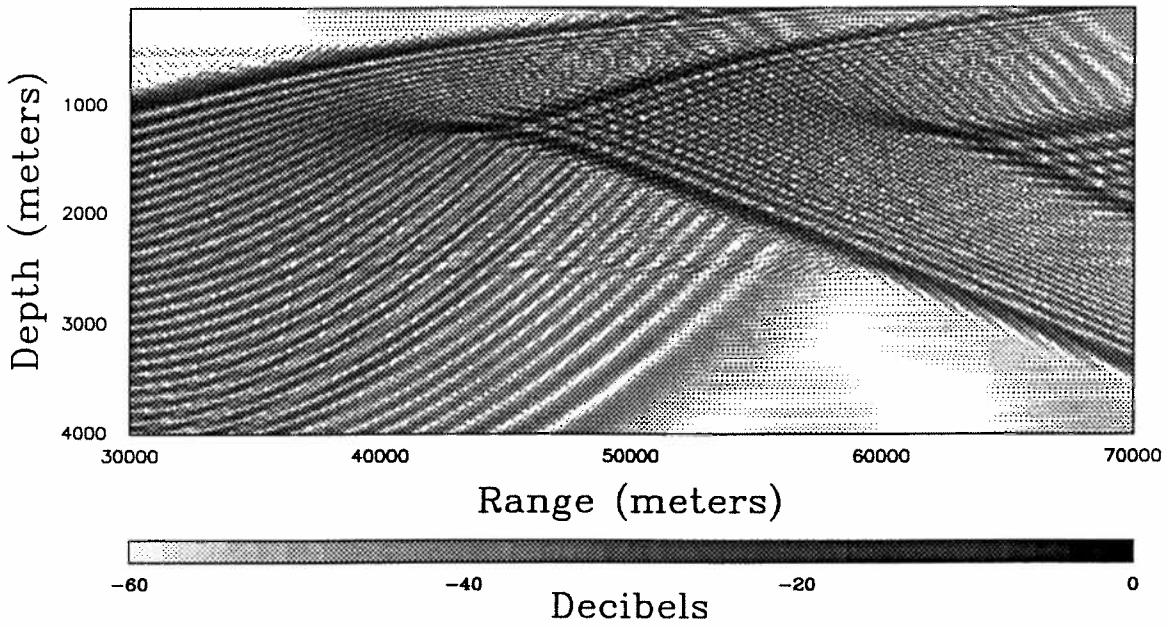

Figure 2.4: Modal Acoustic Field Magnitude.

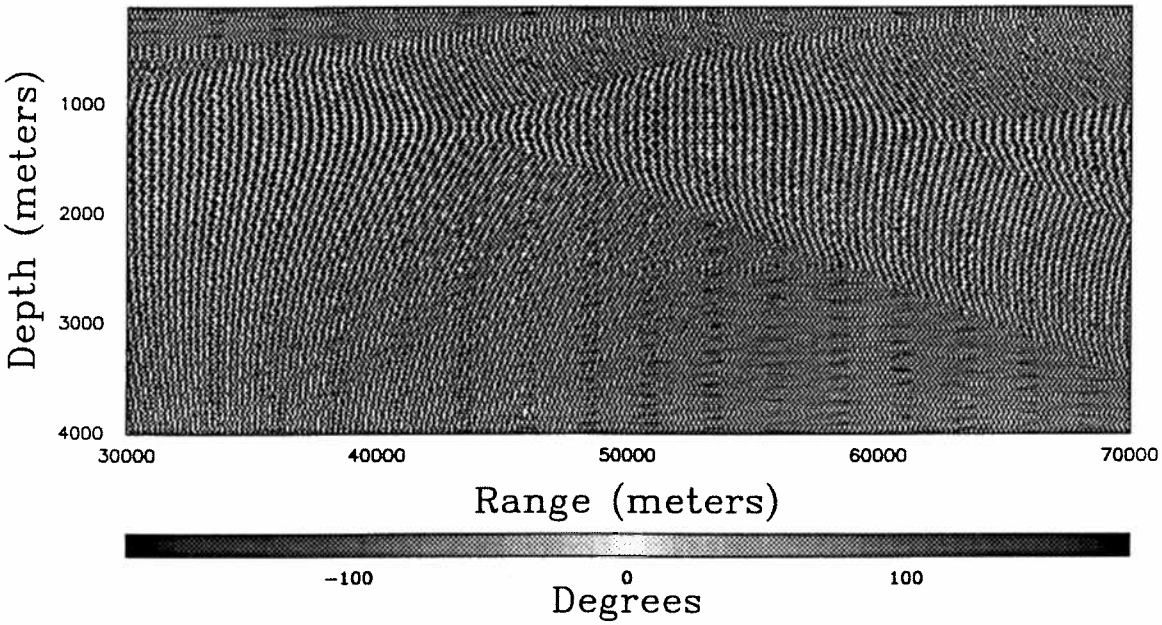

Figure 2.5: Modal Acoustic Field Phase.

where h is the depth of the water and λ is the wavelength.

The basic assumption of ray theory is that all arrivals are plane waves. A plane wave can be represented by

$$p(x,y,z,t) = A(x,y,z)e^{j\omega(t-T(x,y,z))}. \tag{2.36}$$

If the function $T(x,y,z)$ is set equal to a constant then it represents an isotemporal surface or a timefront. In order to find $T(x,y,z)$, insert the plane wave solution into the wave equation

$$\left(\nabla^2 A - \omega^2 A \nabla T \cdot \nabla T - j\omega[A\nabla^2 T + 2\nabla A \cdot \nabla T]\right) e^{j\omega(t-T)} = -\frac{\omega^2}{c^2} A e^{j\omega(t-T)}. \tag{2.37}$$

Now make the high frequency approximation by taking the limit of this equation as ω gets arbitrarily large. This results in

$$|\nabla T|^2 = \frac{1}{c^2} \tag{2.38}$$

which is known as the eikonal equation.

The direction in which T increases the fastest at (x,y,z) is by definition the direction of the raypath. In fact the gradient of T defines the raypath by,

$$\nabla T = \frac{1}{c}\frac{d\mathbf{r}}{ds} \tag{2.39}$$

where $\mathbf{r}$ is the coordinate vector defining the raypath and ds is an element of incremental length along the path. To solve for the ray path $\mathbf{r}$, take the gradient of the eikonal equation to get

$$2(\nabla T \cdot \nabla)\nabla T = \frac{-2}{c^3}\nabla c. \tag{2.40}$$

Now substitute the definition of the gradient of T into equation (2.40) and use the fact

$$\frac{d}{ds} = \sum_i \frac{\partial x_i}{ds}\frac{\partial}{\partial x_i} = \frac{d\mathbf{r}}{ds} \cdot \nabla \tag{2.41}$$

from vector calculus. Finally the result is

$$\frac{d}{ds}\left(\frac{1}{c}\frac{d\mathbf{r}}{ds}\right) = -\frac{1}{c^2}\nabla c \tag{2.42}$$

which is the ray equation, a numerically solvable system.

The computational procedure to solve for the ray path is easy. First write three scalar ray equations. For example, in the x direction,

$$\frac{d}{ds}\left(\frac{1}{c}\frac{dx}{ds}\right) = -\frac{1}{c^2}\frac{\partial c}{\partial x}. \tag{2.43}$$

This can be rewritten as a system of two first order differential equations

$$a = \frac{1}{c}\frac{dx}{ds} \tag{2.44}$$

$$\frac{da}{ds} = -\frac{1}{c^2}\frac{\partial c}{\partial x}. \tag{2.45}$$

where a is a new dummy variable. These can be integrated numerically using a straight forward technique such as the Runge–Kutta method, [41]. The initial conditions are the starting point and initial direction (or gradient) of the ray.

An example of a ray trace is shown in figure 2.6. A number of rays are traced leaving a point source which is at a depth of 1200 meters. A number of features can be seen in this diagram.

The amplitude of the field can be estimated by using the distances between adjacent rays. The width of the ray tube is inversely proportional to the arrival amplitude. This method works well except in two well known cases, where rays converge and where no rays are present.

Caustics are defined as points where two adjacent rays (narrowly separated in initial angle) converge. In this situation ray theory predicts an infinite amplitude arrival. While this is obviously not physically possible, it is remarkable that accurate amplitude estimates can still be made on the far side of the caustic, that is using rays that have already passed through a singularity.

Shadow zones are the second situation which is poorly modeled by ray theory. These are regions where rays indicate that no acoustic energy is propagated. The boundaries are sharply defined by caustics. In the real world, energy is present in the

shadow zones, especially near the boundaries of the shadow. A more correct model would include this effect.

In figure 2.6, the region at a range of 45 kilometers and depth of 1200 meters is known as a convergence zone. There is a focusing of the sound energy here that reoccurs periodically.

Using the ray model with an impulsive source predicts a number of time delayed impulses at the receiver. An example of an eigenray trace is shown in figure 2.7, with both the source and the receiver at a depth of 1200 meters, 100 kilometers apart. An eigenray is a ray that leaves the source at specific angle (eigenangle) and passes exactly through the receiver's location. The separate ray paths for each arrival are clearly shown.

Finally, figure 2.8 shows a time front generated by connecting the end points of ray paths whose time delay along the path is the same and is about 70 seconds. The four sheets of the time front clearly show four arrivals, that one would receive depending on the receiver depth. The cusps trace the caustic boundaries as the front evolves in time. Also shown in the upper figure is the same time front where the depth and range are on the same scale.

Ray tracing codes are straightforward to implement, can incorporate range dependent environments easily, and are frequency independent. The difficulty with this type of model is that the amplitude prediction is not accurate in certain well known regions.

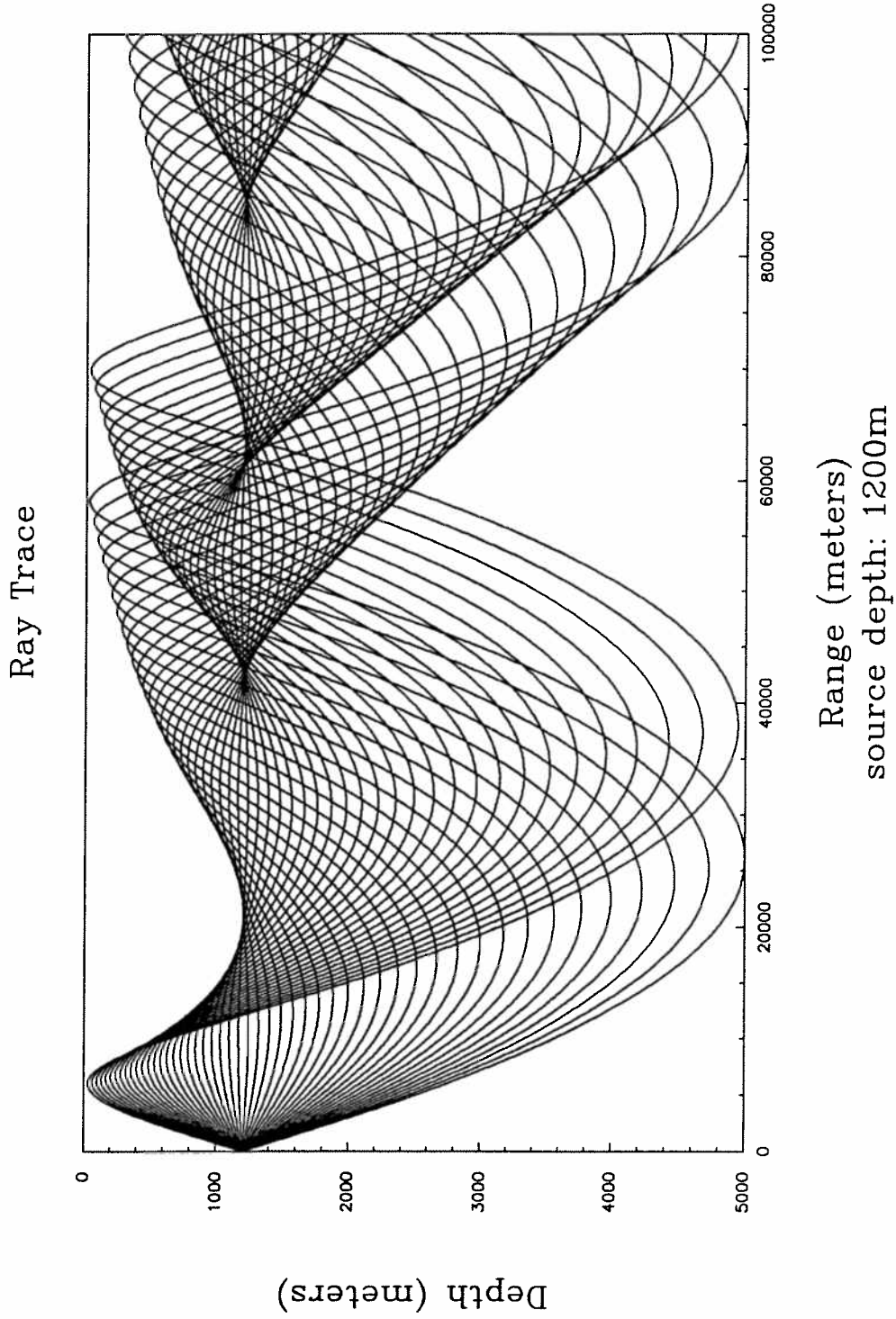

Figure 2.6: Ray Trace.

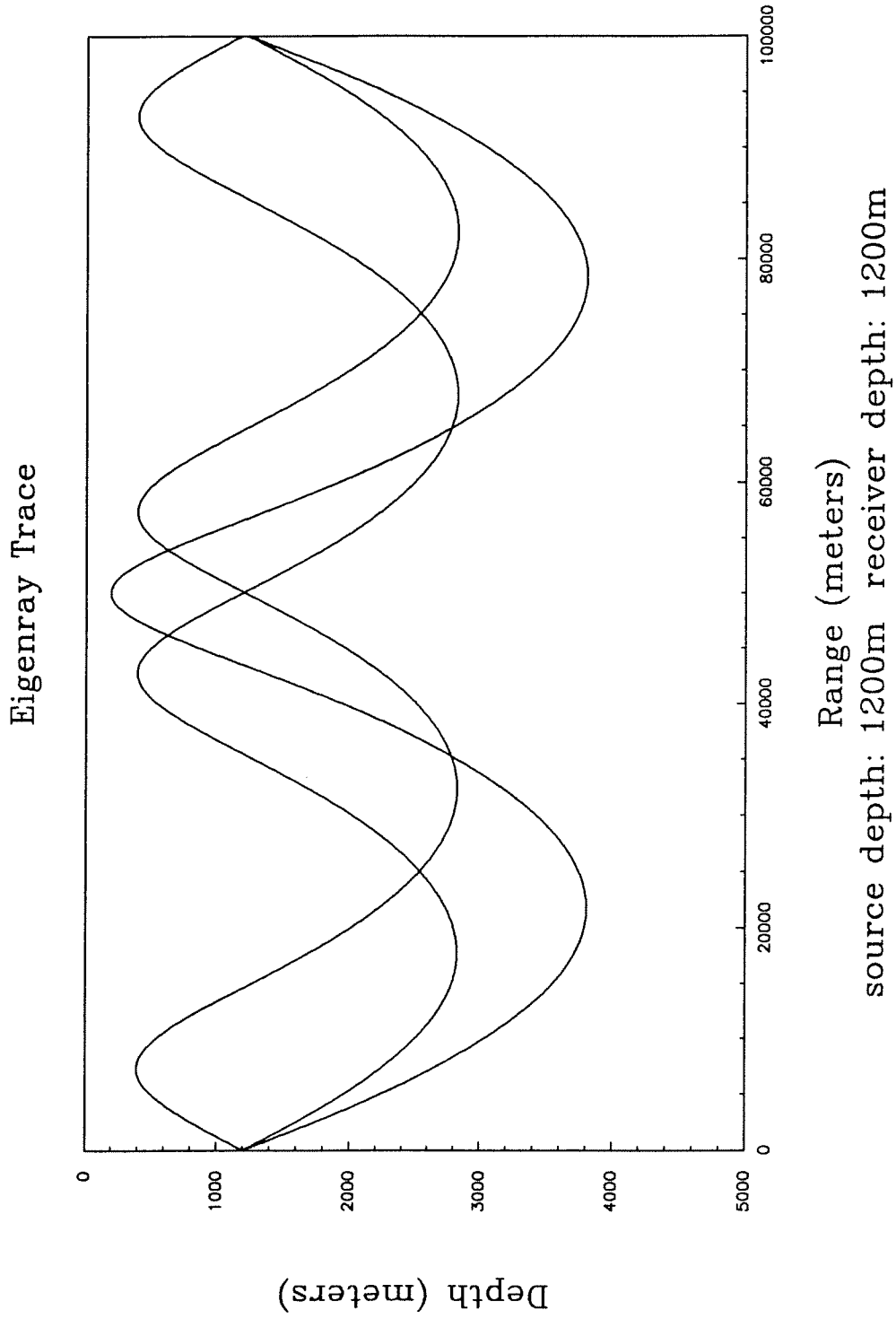

Figure 2.7: Eigenrays.

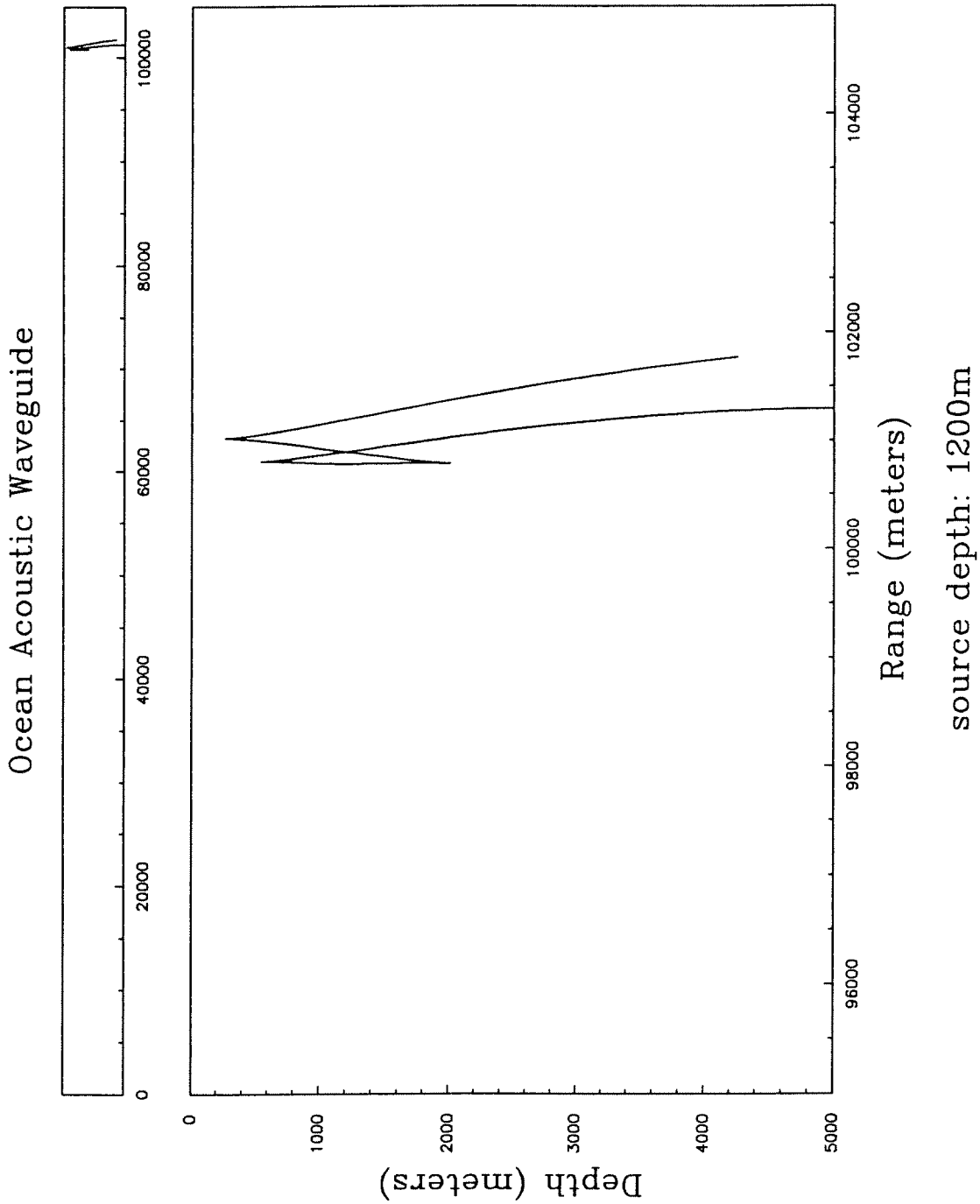

Figure 2.8: Time Front.

CHAPTER III

THE GAUSSIAN BEAM SOLUTION

As indicated in the previous chapter, modeling the impulse response of the ocean acoustic channel is difficult. None of the standard models really does the job that is required for the signal processing algorithms to be considered in this thesis. The main problem is that neither of the two well established modeling techniques can achieve both high accuracy and high efficiency simultaneously.

The mode model, while being very accurate, is difficult to use. The cost is complexity of calculation and a very small collection of boundary geometries that admit solutions. A necessary assumption is that the sound speed be range independent. The solution entails the calculation of eigenfunctions which are frequency dependent. So for a broadband signal the eigenfunctions must be calculated across the spectrum, and then the calculated transfer function (Fourier coefficients) can be used to synthesize an impulse response.

Tracing rays on a digital computer is a fairly easy thing to do. This accounts for the popularity of ray theory. The arrival time estimates are very accurate and it is easy to include a range dependent sound speed profile. The main disadvantage with ray theory is that the amplitude estimate is not always accurate. The theory predicts infinite amplitude at caustics, which are where neighboring ray paths cross. It also predicts zero amplitude in shadow zones. This does not match physical reality.

Another problem is that in order to get accurate time of arrival estimates one must trace eigenrays, rays that connect the source and receiver. Practically speaking this means that many rays with different initial conditions must be traced until a ray that goes through (or comes close to) the receiver location is found.

A recently proposed model is developed here, which gives reasonable results for time of arrival, amplitude, and phase of a propagating signal without being difficult or expensive to use. Another advantage is that it can use a range dependent sound speed profile and it does not require eigenray tracing for accurate time of arrival estimates. The theory is based on the idea of Gaussian beams which have been used to model propagation phenomena in geophysics [9] and in laser cavities [31]. It was first applied to an ocean acoustic environment by Porter and Bucker [38], in order to calculated propagation losses at a particular frequency. In this thesis, the model is extended to calculated impulse responses of the ocean acoustic channel and to provide amplitude estimates for timefront analysis.

In this chapter, the method of Gaussian beam propagation will be derived following the development of Červený, [9], [10]. Then the important consideration of matching the field to an ideal point source field by tuning the initial conditions will be covered. A discussion of various possible initial conditions can be found in Müller, [33]. An argument is made in this thesis that the most accurate result can be obtained by minimizing the beamwidth of the beam closest to the receiver. The numerical procedure for calculating impulse responses and fields will be described and examples will be compared to the more exact modal solution. It will be shown that the impulse response solution can be calculated for little more effort than a single frequency calculation. Also it is revealed that the phase behavior of the Gaussian beam solution closely models that of the real ocean.

Derivation

It is well known that the high frequency wave field propagates mostly along rays. Gaussian beam theory seeks solutions to the wave equation which are concentrated close to each selected ray Ω. Define an orthogonal coordinate system (s, n) along the ray. The coordinate s measures the arc length along the ray from an arbitrary reference point, n represents a length coordinate in the direction perpendicular to Ω at s. Rewrite the wave equation in the new coordinate system. The parabolic approximation to the wave equation is used to obtain solutions close to the ray. A complete derivation is given by Červený [9].

The starting point in Gaussian beam theory is the wave equation in two dimensional Cartesian coordinate system

$$\frac{\partial^2 p}{\partial x^2} + \frac{\partial^2 p}{\partial z^2} = \frac{1}{c^2}\frac{\partial^2 p}{\partial t^2}. \tag{3.1}$$

where x is the range coordinate and z is the depth coordinate. As mentioned above, high frequency acoustic energy is known to travel along rays, therefore there is an interest in the behavior of the wave equation along a ray. The first step will then be to transform the wave equation in Cartesian coordinates to a ray-centered coordinate system as shown in figure 3.1. In this system a particular ray is indexed by Ω in initial angle, s measures the distance along the ray from the starting point, and n measures the perpendicular distance from the ray. Following the standard formula for the Laplacian under a change of coordinates, the ray centered wave equation can be written

$$\frac{1}{h}\frac{\partial^2 p}{\partial s^2} + \frac{\partial p}{\partial s}\frac{\partial}{\partial s}\left(\frac{1}{h}\right) + h\frac{\partial^2 p}{\partial n^2} + \frac{\partial h}{\partial n}\frac{\partial p}{\partial n} = \frac{h}{c^2}\frac{\partial^2 p}{\partial t^2}. \tag{3.2}$$

with differential length element

$$dr^2 = dx^2 + dz^2 = h^2 ds^2 + dn^2 \tag{3.3}$$

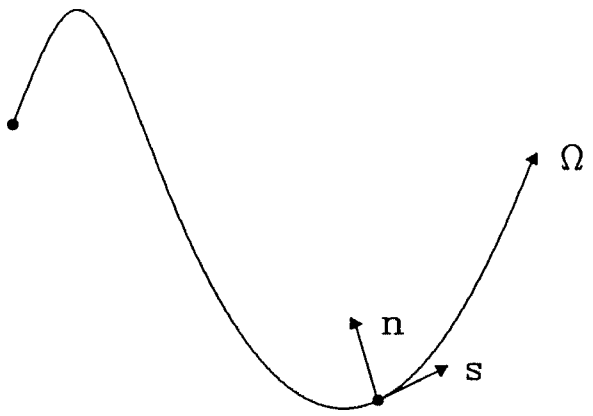

Figure 3.1: Ray Centered Coordinate System.

where

$$h = 1 + \frac{1}{c}\frac{\partial c}{\partial n} n \tag{3.4}$$

is the scale factor for an element of length along the ray.

Since it is known that energy traveling along a ray can be represented by a plane wave, try a time delayed, harmonic solution for the pressure of the following form

$$p(s,n,t) = P(s,n,\omega)\exp\left\{-j\omega\left[t - \int_{s_0}^{s}\frac{ds}{c(s)}\right]\right\}. \tag{3.5}$$

The complex function $P(\cdot,\cdot,\cdot)$ modulates the plane wave which travels along the central ray. It turns out that P will alter the wave by giving it a width and a curvature. To find a solution for P, substitute equation (3.5) into the wave equation (3.2) to get

$$\frac{1}{h}\left\{\frac{\partial^2 P}{\partial s^2} + \frac{2j\omega}{c}\frac{\partial P}{\partial s} - \left[\frac{\omega^2}{c^2} + \frac{j\omega}{c^2}\frac{\partial c}{\partial s}\right]P\right\} +$$

$$h\frac{\partial^2 P}{\partial n^2} + \frac{h\omega^2}{c^2}P - \frac{1}{h^2}\left(\frac{j\omega}{c}P + \frac{\partial P}{\partial s}\right)\frac{\partial h}{\partial s} + \frac{\partial h}{\partial n}\frac{\partial P}{\partial n} = 0. \tag{3.6}$$

This is still an exact wave equation.

To approximate solutions to the wave equation close to the central ray, scale the coordinate perpendicular to the ray according to frequency

$$m = \omega^{1/2} n. \tag{3.7}$$

This expresses the fact that only solutions a certain number of wavelengths from the central ray are to be considered. The wave equation can now be approximated in the vicinity of the central ray by using a Taylor series. This is accomplished by expanding the coefficients of equation (3.6) along the newly scaled coordinate. It is possible to write the wave equation as a Taylor series since all it derivatives exist at all points. The series has terms in powers of $\omega^{-1/2}$. As ω gets larger (or equivalently, as the receiver gets closer to the central ray), it is clear that the lowest order terms contribute the most. After keeping only the first order terms equation (3.6) becomes

$$\frac{\partial^2 P}{\partial m^2} + \frac{2j}{c}\frac{\partial P}{\partial s} - \left(\frac{m^2}{c^3}\frac{\partial^2 c}{\partial n^2} + \frac{j}{c^2}\frac{\partial c}{\partial s}\right)P = 0. \tag{3.8}$$

This is a parabolic wave equation. It is most accurate nearest the central ray and indeed is exact on the ray.

Continuing to seek the solution for the modulating function $P(\cdot,\cdot,\cdot)$, try the following

$$P(s,m) = \sqrt{c}\, A(s) \exp\left(j\frac{1}{2}m^2\Gamma(s)\right). \tag{3.9}$$

where $A(\cdot)$ and $\Gamma(\cdot)$ are complex functions. The exponential form of equation (3.9) forces $P(\cdot)$ to decay away from the central ray. Substituting (3.9) into (3.8) results in

$$j\left(\frac{2}{c}\frac{\partial A}{\partial s} + A\Gamma\right) - Am^2\left(\frac{1}{c}\frac{\partial \Gamma}{\partial s} + \Gamma^2 + \frac{1}{c^3}\frac{\partial^2 c}{\partial n^2}\right) = 0. \tag{3.10}$$

If there are solutions for A and Γ such that

$$\frac{\partial \Gamma}{\partial s} + c\Gamma^2 + \frac{1}{c^2}\frac{\partial^2 c}{\partial n^2} = 0 \tag{3.11}$$

and

$$\frac{\partial A}{\partial s} + \frac{c}{2} A\Gamma = 0 \tag{3.12}$$

then equation (3.10) will be satisfied as well.

To solve equation (3.11), first realize that it is an ordinary non-linear first-order differential equation of the Ricatti type which cannot be solved analytically. Proceed by using a known trick, [9], to simplify the problem. Let

$$\Gamma(s) = \frac{\beta}{\alpha} = \frac{1}{c\alpha}\frac{\partial \alpha}{\partial s} \tag{3.13}$$

then substitute for Γ to get

$$c\frac{\partial^2 \alpha}{\partial s^2} - \frac{\partial c}{\partial s}\frac{\partial \alpha}{\partial s} + \frac{\partial^2 c}{\partial n^2}\alpha = 0, \tag{3.14}$$

a linear equation. Equation (3.14) can also be written as a system of two first–order linear differential equations

$$\begin{aligned} \frac{\partial \alpha}{\partial s} &= c\beta \\ \\ \frac{\partial \beta}{\partial s} &= -\frac{1}{c}\frac{\partial^2 c}{\partial n^2}\alpha \end{aligned} \tag{3.15}$$

which can be easily solved. As a matter of fact equations (3.15) can be solved simultaneously with the ray tracing equations. Also note that α and β do not depend on frequency, so they only have to be calculated one time. This is why the Gaussian beam method is so efficient.

The solution of equation (3.12) is straight forward. Use the expression for Γ given by (3.13) to transform (3.12) into a first-order linear differential equation. Solving this results in

$$A(s) = \Psi \alpha^{-1/2}(s) \tag{3.16}$$

where Ψ is a complex constant.

Finally, the total solution can be written as

$$p(s,n,t) = \Psi \left[\frac{c(s)}{\alpha(s)}\right]^{1/2} \exp\left\{-j\omega\left[t - \tau(s) - \frac{1}{2}\frac{\beta(s)}{\alpha(s)}n^2\right]\right\} \tag{3.17}$$

where

$$\tau(s) = \int_{s_0}^{s} \frac{ds}{c(s)} \tag{3.18}$$

is the time delay calculated along the raypath.

There are two important conditions that the solution of equation (3.14) must fulfill so that (3.17) can be considered physically legitimate. The first is that

$$\alpha \neq 0. \tag{3.19}$$

This condition insures that the solution will remain finite at caustics. The second is that

$$\mathrm{Im}\left(\frac{\beta(s)}{\alpha(s)}\right) > 0. \tag{3.20}$$

This condition guarantees that the modulating function $P(\cdot)$ will decay as one moves away from the central ray. That is to say the beam will make a negligible contribution to the field far from the beam axis.

Any complex solution of (3.14) can be expressed in terms of any two real linearly independent solutions. These solutions can be written in a matrix form as

$$\pi(s) = \begin{pmatrix} \alpha_1(s) & \alpha_2(s) \\ \beta_1(s) & \beta_2(s) \end{pmatrix} \tag{3.21}$$

with initial conditions

$$\pi(s_0) = \begin{pmatrix} 1 & 0 \\ 0 & 1 \end{pmatrix}. \tag{3.22}$$

The determinant of (3.21) is known as the Wronskian and is constant

$$\det \pi(s) = \alpha_1\beta_2 - \alpha_2\beta_1 = 1. \tag{3.23}$$

So the total solution for α and β can be written as the linear combination of the two real independent solutions

$$\alpha = z_1\alpha_1 + z_2\alpha_2, \qquad \beta = z_1\beta_1 + z_2\beta_2 \ . \tag{3.24}$$

with complex coefficients z_1 and z_2. Since the ratio of β to α is what appears in the exponent of equation (3.17), it is possible to eliminate one complex constant by writing

$$\frac{\beta}{\alpha} = \frac{\epsilon\beta_1 + \beta_2}{\epsilon\alpha_1 + \alpha_2} \tag{3.25}$$

where

$$\epsilon = S_0 + jL_0 = \frac{z_1}{z_2}. \tag{3.26}$$

Now there are only two real constants, S_0 and L_0, instead of two complex constants to specify.

The beam equation can be rewritten in a more physically meaningful way as

$$p(s,n,t) = A(s)\exp\left\{-j\omega\left[t - \tau(s) - \frac{1}{2}K(s)n^2\right] - \frac{n^2}{L^2(s)}\right\} \tag{3.27}$$

where the beam magnitude (including cylindrical spreading) is given by

$$|A(s)| = \left|\Psi\left[\frac{c(s)}{r\alpha(s)}\right]^{1/2}\right| = |\Psi|\sqrt{\frac{c}{r}}\left[(S_0\alpha_1 + \alpha_2)^2 + L_0^2\alpha_1^2\right]^{-1/4} \tag{3.28}$$

the beam phase is given by

$$\arg A(s) = \arg\Psi - \frac{1}{2}\arctan\frac{L_0\alpha_1}{S_0\alpha_1 + \alpha_2} \tag{3.29}$$

the beam curvature is given by

$$K(s) = \mathrm{Re}\left(\frac{\beta(s)}{\alpha(s)}\right) = \frac{(S_0\alpha_1 + \alpha_2)(S_0\beta_1 + \beta_2) + L_0^2\alpha_1\beta_1}{(S_0\alpha_1 + \alpha_2)^2 + L_0^2\alpha_1^2} \tag{3.30}$$

and the beam half-width is given by

$$L(s) = \left[\frac{\omega}{2}\mathrm{Im}\left(\frac{\beta(s)}{\alpha(s)}\right)\right]^{-1/2} = \sqrt{\frac{-2}{\omega L_0}}\left[(S_0\alpha_1 + \alpha_2)^2 + L_0^2\alpha_1^2\right]^{1/2}. \tag{3.31}$$

This completes the derivation of a single Gaussian beam. Note that the Gaussian beam is an exact solution to the wave equation when the receiver lies on the central ray. What this implies is that the method spatially averages the acoustic field over the width of the beam. That is to say that any spatial inhomogeneities in the sound speed field of dimension less than the width of a beam are smoothed.

Initial Conditions

In the previous section, the behavior of a single Gaussian beam was described by solving the parabolic wave equation near a central ray. If an ideal source is to be modeled, a set of Gaussian beams must be fitted to the initial wave field. The wave field $p(M)$ at the point M can be expressed in terms of a finite sum of Gaussian beams as

$$p(M) = \sum_{\Omega} \Phi(\Omega)\, p_{\Omega}(s, n) \tag{3.32}$$

where the function $\Phi(\Omega)$ is specified by the initial source field and Ω indexes the beams. The trick to this problem is to find the number of beams needed to adequately represent the field and to find the correct initial beam width and curvature. The values of the constants S_0 and L_0, which have not yet been specified, can then be tuned to adjust the initial width and curvature of the beam. In this section, a new analysis which specifies the minimum number of beams needed to model a point source is made. Also, a procedure which minimizes the approximation error is defined.

Insight into this problem can be developed by studying a more restricted case. Suppose that the sound speed is constant. Now we want to model an ideal point source in two dimensions, whose field can be described by

$$A_{\mathrm{IPS}}(r, \theta) = \frac{1}{r} \exp\left\{-j\left(wt - kr + \frac{\pi}{4}\right)\right\}, \tag{3.33}$$

where r is the distance from source and θ is the angle. This function is independent of θ and implies that the function $\Phi(\Omega)$ is a constant. The parameters S_0 and L_0 will also be assumed to be constant from beam to beam. This greatly simplifies the problem.

In order to determine the number of beams needed to approximate the field (3.33), first consider the behavior of a single beam in a homogeneous environment, that is where the sound speed is constant. In this case, the ray paths follow straight lines and the equations for the beam parameters α and β can be simplified to

$$\frac{\partial \alpha}{\partial s} = c\beta \qquad \frac{\partial \beta}{\partial s} = 0. \tag{3.34}$$

Integrating these yields

$$\begin{aligned} \alpha(s) &= c\beta s + \alpha_0 \\ \beta(s) &= \beta_0. \end{aligned} \tag{3.35}$$

Now the expressions for the beam magnitude, phase, curvature, and width can be simplified also. Explicitly, the beam magnitude is

$$|A(s)| = |\Psi| \sqrt{\frac{c}{r}} \left[(S_0 + s)^2 + L_0^2 \right]^{-1/4}, \tag{3.36}$$

the beam phase is

$$\arg A(s) = \arg \Psi - \frac{1}{2} \arctan \frac{L_0}{S_0 + s}, \tag{3.37}$$

the beam curvature is

$$K(s) = \frac{(S_0 + s)}{(S_0 + s)^2 + L_0^2}, \tag{3.38}$$

and the beam width is

$$L(s) = \sqrt{\frac{-2}{\omega L_0}} \left[(S_0 + s)^2 + L_0^2 \right]^{1/2}. \tag{3.39}$$

The next step is to adjust the width of the beam. Suppose a width of l at the receiver is desired. This can be achieved by adjusting the parameters S_0 and L_0 to

the values

$$S_0 = -\frac{\alpha_2}{\alpha_1} \qquad L_0 = -\frac{\omega l^2}{2\alpha_1^2}. \tag{3.40}$$

Doing so results in a beam width and curvature of

$$L(s) = l \qquad K(s) = 0. \tag{3.41}$$

So the solution to the wave equation along the central ray in a homogeneous environment is approximated by a plane wave modulated by a Gaussian shaped weighting function. Also the beam magnitude and phase are

$$|A(s)| = |\Psi| \sqrt{\frac{c}{r}} \left| \frac{2\alpha_1}{\omega l^2} \right|^{1/2} \tag{3.42}$$

$$\arg A(s) = \arg \Psi + \frac{1}{2} \text{atan2}(\frac{\omega l^2}{2\alpha_1}, 0) = \arg \Psi + \frac{\pi}{2}. \tag{3.43}$$

The magnitude rolls off inversely proportional to the square root of the distance from the source just as it should.

Now the effect of the number of beams can be examined. Plot the magnitude and phase of the approximate field as described by equation (3.32) as a function of angle for three different cases. All three cases have the same beam width but differ in the number of beams. The ideal point source field has a constant magnitude and phase. It is clearly seen in figure 3.2 that only the most dense case adequately matches the ideal point source field. The beams in the dense case are conveniently chosen to be spaced exactly one beam width l apart. This implies that there must be enough beams in any matching field so that any two beams are no farther than l meters or one beam width apart.

Minimum Beam Width

As long as there are enough beams so that they are separated by no more than one beam width, any curvature and width can be used. Since the approximations

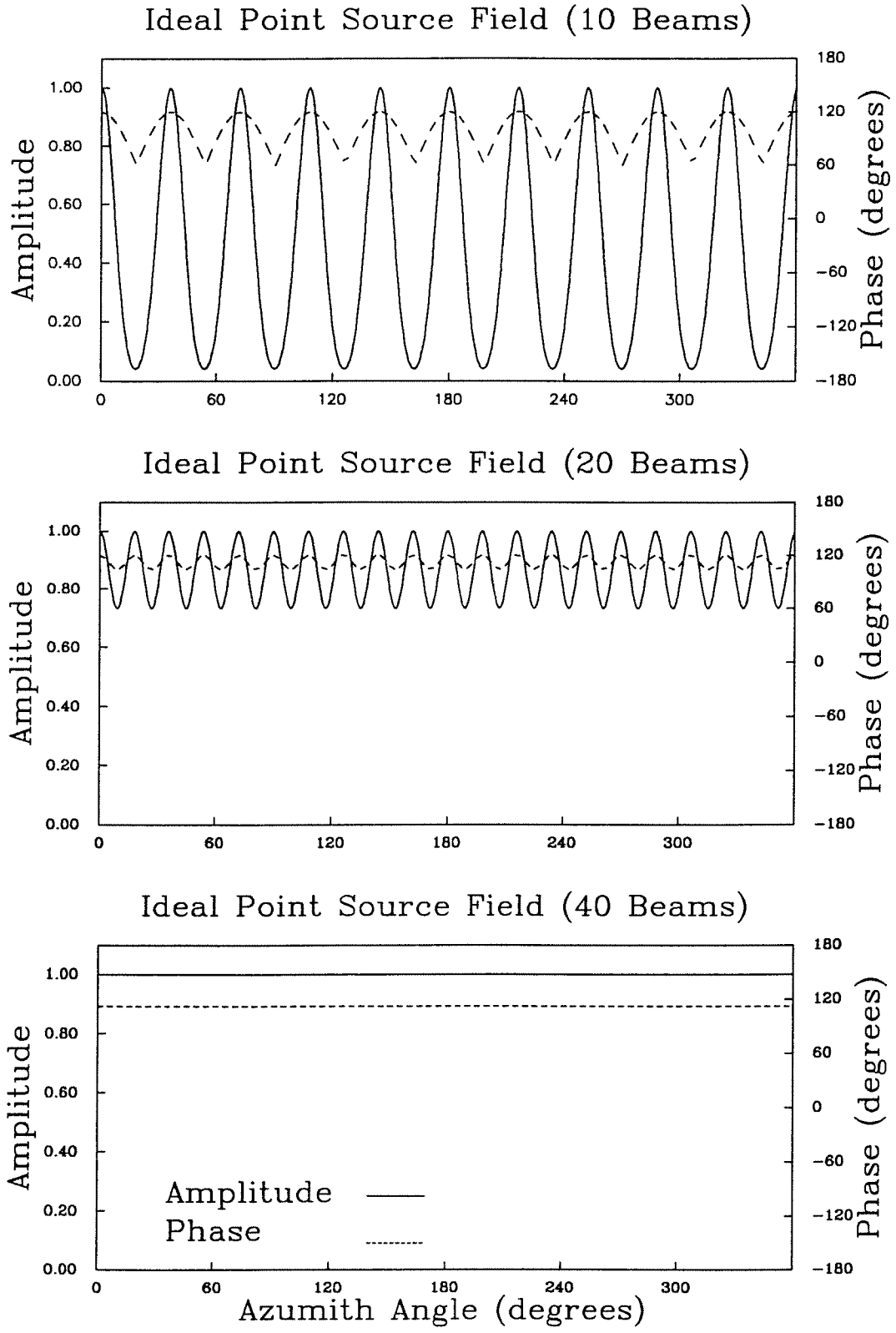

Figure 3.2: Source Matching Field.

made earlier are most accurate nearest the central ray, the parameters S_0 and L_0 are chosen to minimize the width of the beam thus minimizing the contribution of the beam to receivers which are far from the central ray. Doing so minimizes the error in the approximation.

Minimization of the beam width at the receiver is straight forward. Simply form the partial derivative of the beamwidth as shown

$$\frac{\partial L(s)}{\partial L_0} = \frac{1}{2}\sqrt{\frac{-2}{\omega}}\left[\frac{(S_0\alpha_1+\alpha_2)^2+L_0^2\alpha_1^2}{L_0}\right]^{-1/2}\left[\frac{L_0^2\alpha_1^2-(S_0\alpha_1+\alpha_2)^2}{L_0^2}\right]. \tag{3.44}$$

By setting equation (3.44) equal to zero, one can solve for the parameter L_0. After a little effort the result is

$$L_0 = -\left[\frac{S_0\alpha_1+\alpha_2}{\alpha_1}\right]. \tag{3.45}$$

Using this value for L_0 gives the minimum beam width at the receiver.

Now it is time to worry about S_0. For help, return to the homogeneous environment situation and consider the beam curvature

$$K(s) = \frac{1}{2(S_0+s)} \tag{3.46}$$

where the value of L_0 that minimizes the beam width has been used. It is known that the curvature of a wave front generated by an ideal point source is inversely proportional to the distance from the source. Therefore, setting

$$S_0 = 0 \tag{3.47}$$

will best fit the beam's curvature to that of an ideal point source.

There is one more constant to determine, that is the beam constant Ψ. It is necessary that the energy

$$E = \int_{-\infty}^{\infty} |p(s,n,t)|^2\, dn \tag{3.48}$$

along the wavefront (i.e. where $t = \tau(s)$) be well defined. Rewriting equation (3.48) as

$$E = |A|\int_{-\infty}^{\infty} \exp\left\{-\frac{2n^2}{L^2(s)}\right\} dn, \tag{3.49}$$

and using the fact that

$$\int_{-\infty}^{\infty} e^{-n^2/l} dn = \sqrt{\pi l}, \tag{3.50}$$

it is possible to obtain a simple expression for the energy contained in the beam which is

$$E = |A|\, L(s) \sqrt{\frac{\pi}{2}}. \tag{3.51}$$

The energy should be constant with frequency in a homogeneous medium as range increases asymptotically. In this case, since the beam width is

$$L(s) = s \sqrt{\frac{-2}{\omega L_0}}, \tag{3.52}$$

and the magnitude (using $r \propto s$ at long ranges) is

$$|A(s)| = |\Psi| \frac{1}{c} \sqrt{c}, \tag{3.53}$$

the beam constant Ψ can be specified as

$$|\Psi| = \sqrt{\omega} \qquad \arg \Psi = \frac{1}{2} \arctan \frac{L_0}{S_0} + \frac{\pi}{4}. \tag{3.54}$$

Numerical Procedure

So far a description of the behavior of a single beam has been given, and initial conditions to minimize the approximation error have been derived. Also it has been discovered that enough beams must be used so that none are farther apart than one beam width. A new procedure will now be given of how to calculate the acoustic field and the channel impulse response using the Gaussian beam method.

Once the Gaussian beam field due to a source at point $\mathcal{S}$ and a receiver at any point $\mathcal{R}$ in the ocean acoustic channel is known, the impulse response from $\mathcal{S}$ to $\mathcal{R}$ can be written.

$$h(t) = \sum_{i=1}^{N} \mathcal{A}_i \delta(t - \tau_i) \tag{3.55}$$

The advantage of Gaussian beam theory is that for only twice the computational effort of conventional ray theory, accurate values for the $\mathcal{A}_i$'s can be calculated. How to calculate the impulse response (3.55) is the subject of this section.

To gain some insight into the physics of the situation, consider a time front again. As you will recall, a time front is just the connected end points of rays as they move through space. Using Gaussian beam theory, the amplitude and phase of the time front is also known now. In figures 3.3 and 3.4 the calculated magnitude and phase of a time front at $T = 70$ seconds is displayed. This would not be possible with a standard ray trace code. The time front magnitude plot shows how the rays become folded over as they propagate through the channel. The cusps are in reality caustics. The amplitude increases rapidly and peaks at the caustics. Also the phase changes rapidly at the caustic and is constant along each individual sheet or arrival. This is exactly the behavior that is expected in the real ocean.

Now calculate the impulse response at a point. To do this sum a number of Gaussian beams at the receiver point. This yields an amplitude and a phase at that point. It should be pointed out that although α and β are independent of frequency and need be computed only one time, the amplitude and phase will change with signal frequency. Therefore, it is necessary to find the amplitude and phase response over the entire range of frequencies we are interested in. Once this is done, an inverse Fourier transform can be performed to synthesize the time response. In figure 3.5, a point to point impulse response is shown. Notice that the impulse from the source has become a doublet, the linear combination of an impulse and it's Hilbert transform, the effect that is expected when an acoustic signal passes through a caustic. This particular example was calculated using a source at a depth of 1100 meters and a receiver at a range of 100 kilometers and a depth of 1300 meters. The source and receiver were shifted slightly off axis in order to separate the middle arrivals in time and produce a clear diagram. The frequency response was calculated in a range from

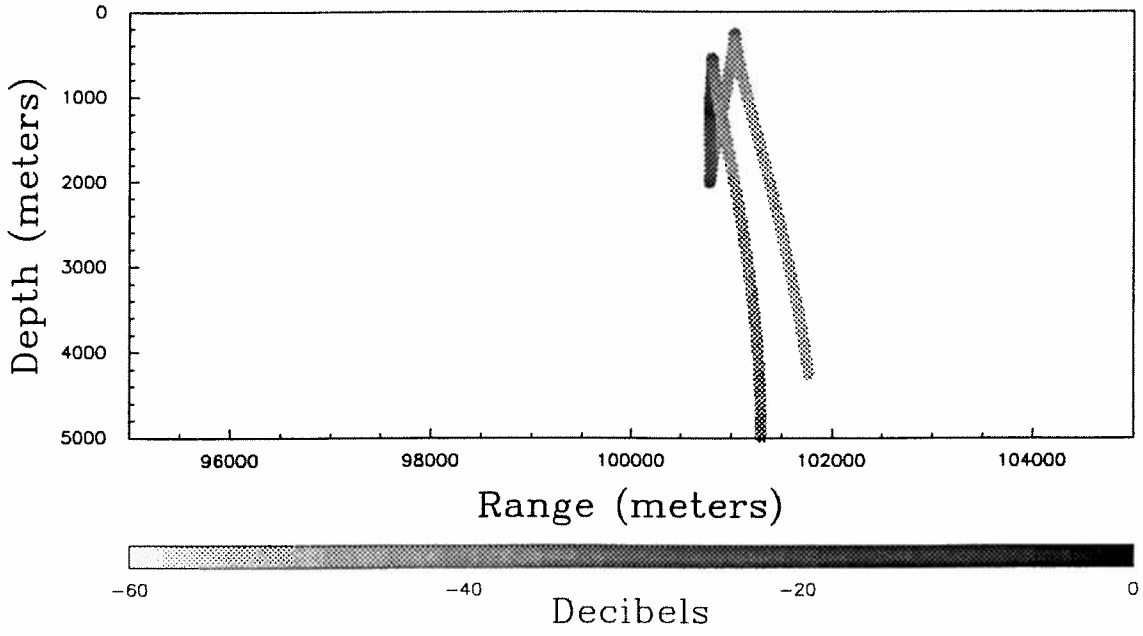

Figure 3.3: Gaussian Beam Time Front Magnitude.

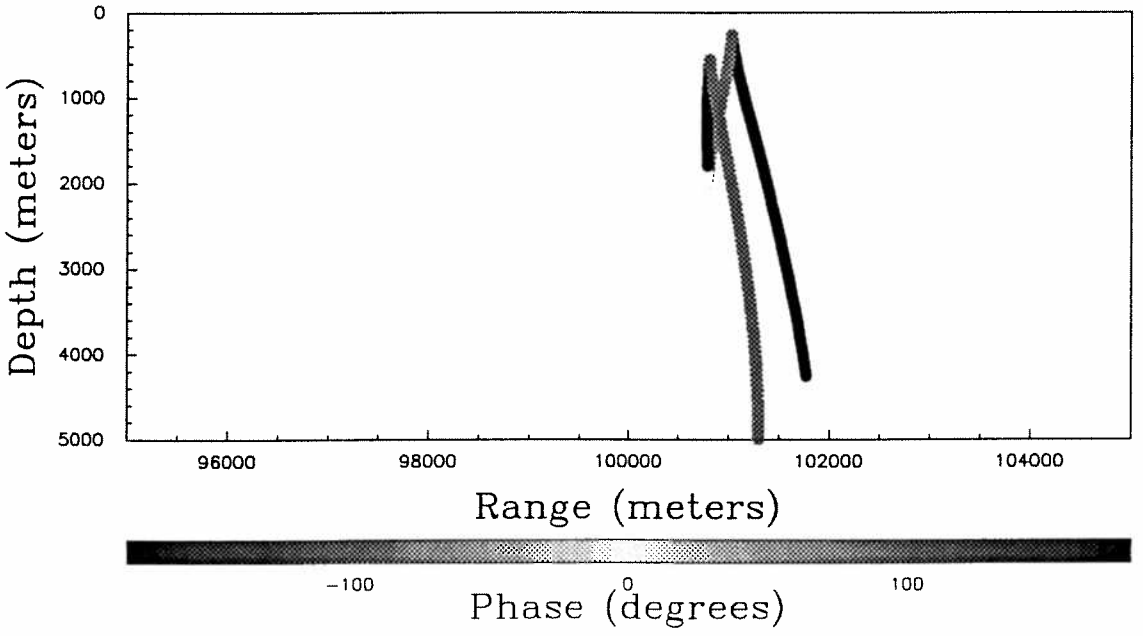

Figure 3.4: Gaussian Beam Time Front Phase.

50 to 1000 Hertz and then the inverse discrete Fourier transform was applied. The plotted result thus has about 2 millisecond time domain resolution. The added low-amplitude oscillation around each peak is simply an artifact due to the application of a rectangular windowing function in the frequency domain.

Although $\mathcal{A}_i$ and τ_i are theoretically weakly dependent on frequency, our best information is that in the real ocean $\mathcal{A}_i$ and τ_i do not change appreciably over the range of frequencies (5–500 Hz) that we are interested in. As shown in figure 3.5, the Gaussian beam method is in good agreement with the complex amplitude weighted, time delayed, multipath model. This suggests that there may be an alternative method of calculating the impulse response. By slicing the time front into its component arrivals, it is possible to avoid the inverse transform. In figure 3.6, the frequency response of the Gaussian beam method is shown. The geometry of this situation is the same as was used in figure 3.5, namely the source was at a depth of 1100 meters and the receiver was at a range of 100 kilometers and a depth of 1300 meters. The amplitude, phase (delay-independent component), and time delay of each path or arrival was plotted as a function of frequency. As hoped each path's parameters are essentially independent of frequency. It is only the interference between paths that produces a variation in field strength with frequency.

Since the frequency response of the Gaussian beam method is essentially flat, the use of the inverse Fourier transform is avoided. Instead, it is necessary to calculate the amplitude, phase, and time delay of each arrival at only one representative frequency. In order for a modal code to calculate a similar impulse response, all modes would have to be evaluated at many frequencies (depending on the time domain resolution needed) and the inverse Fourier transform would have to be performed.

Finally, in figures 3.8 and 3.9, the single frequency (250 Hertz) field due to a point source at a depth of 1200 meters is shown. The ray paths in figure 3.7 are shown to enhance understanding.

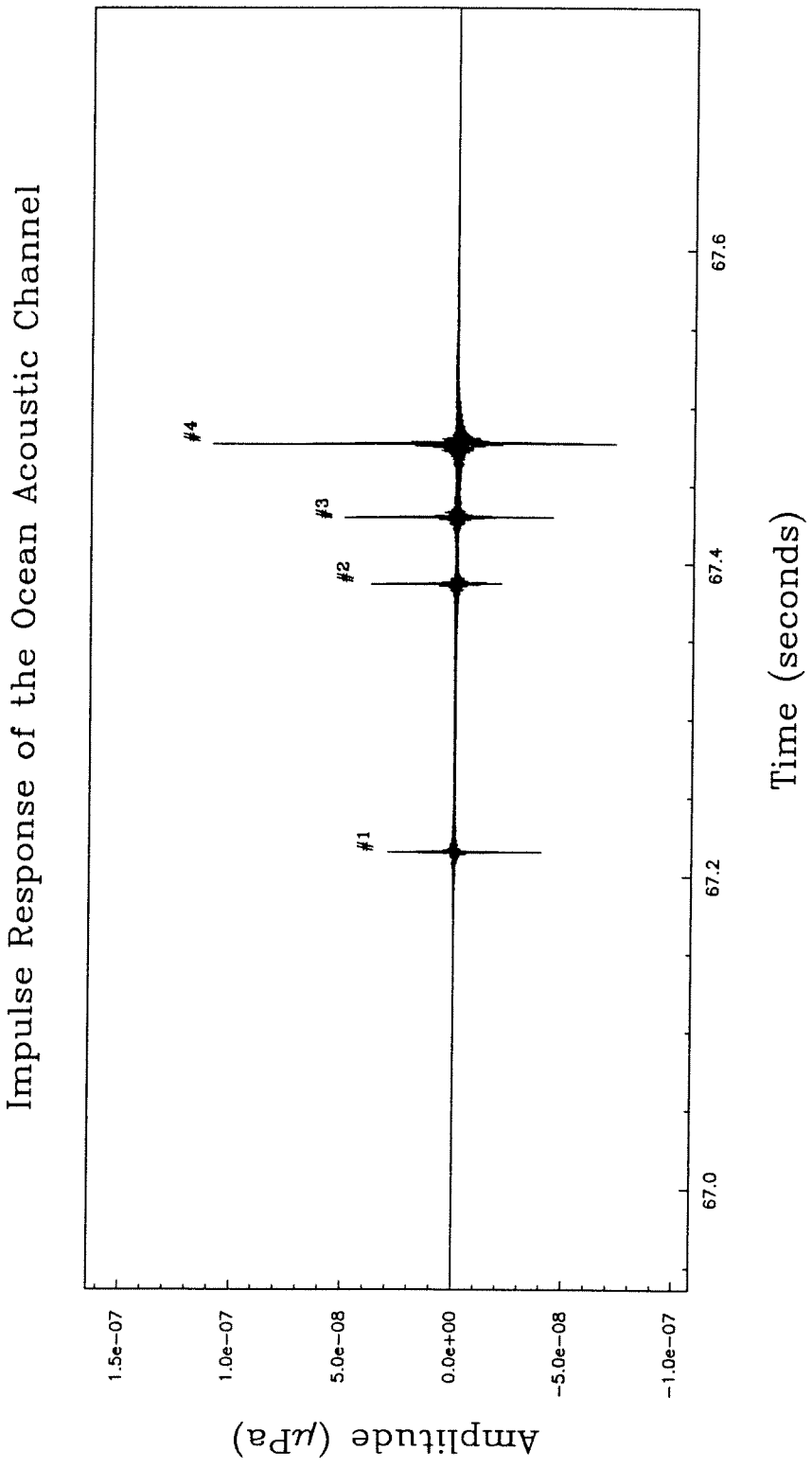

Figure 3.5: Gaussian Beam Impulse Response.

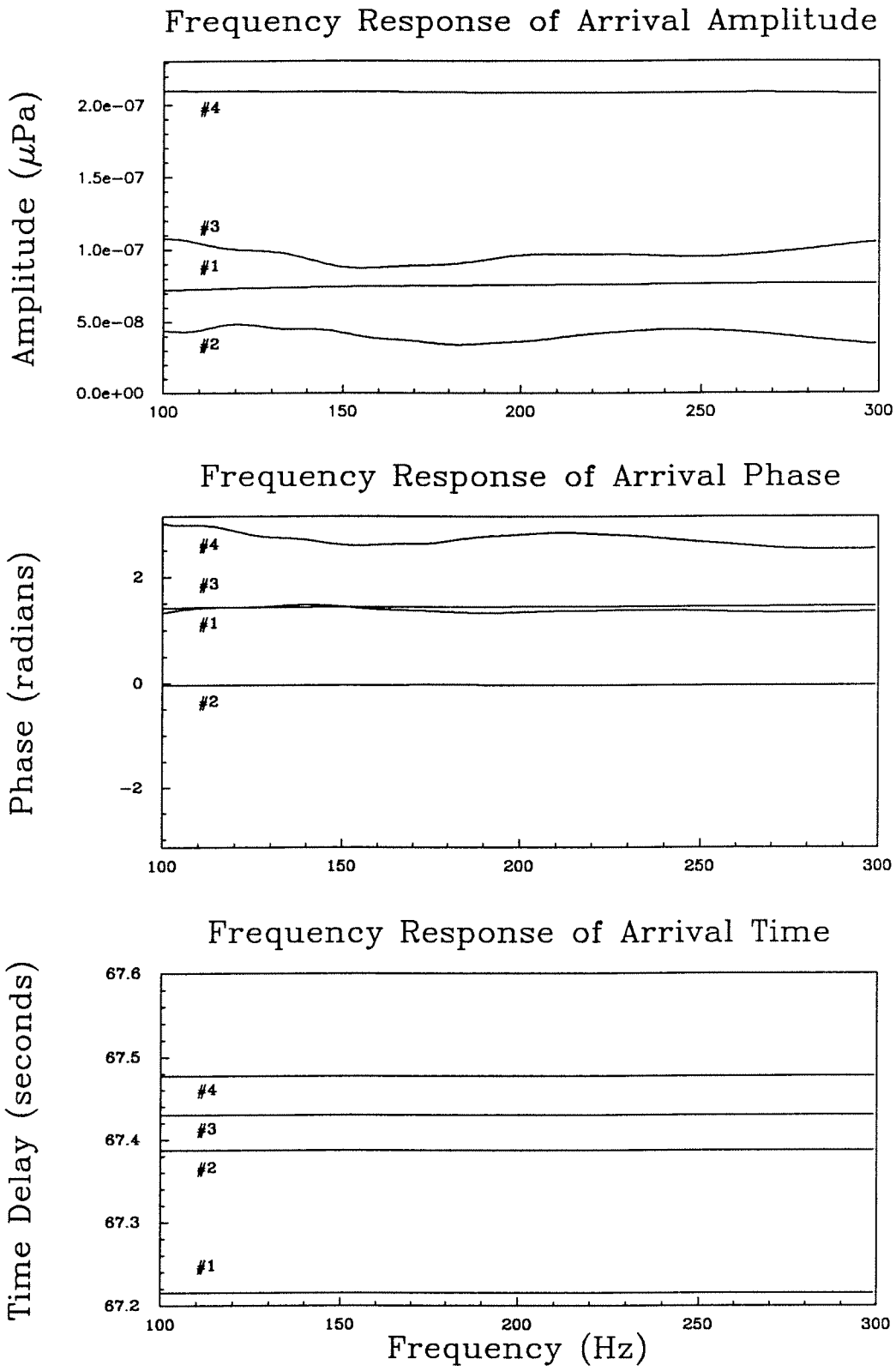

Figure 3.6: Gaussian Beam Frequency Response.

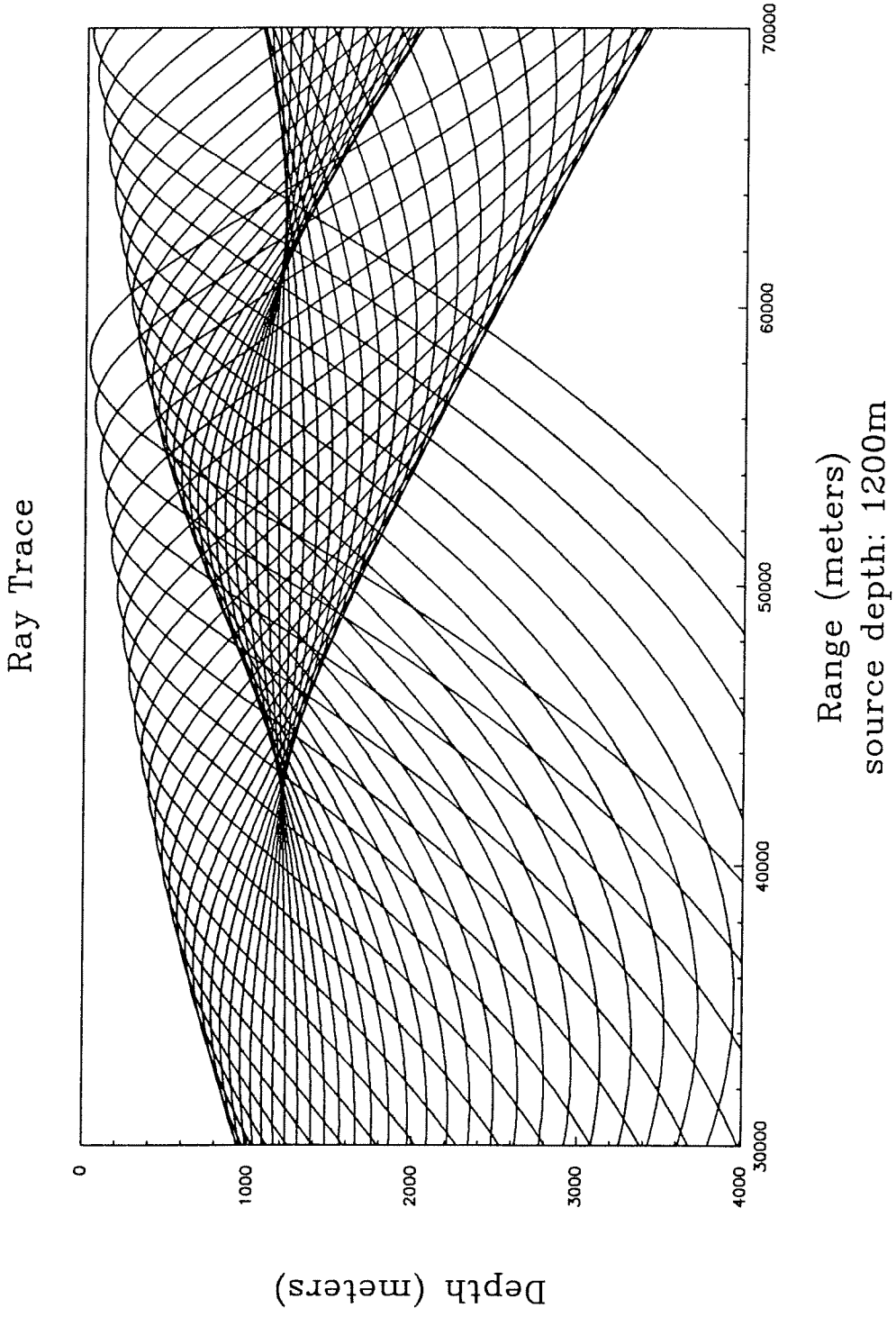

Figure 3.7: Ray Trace.

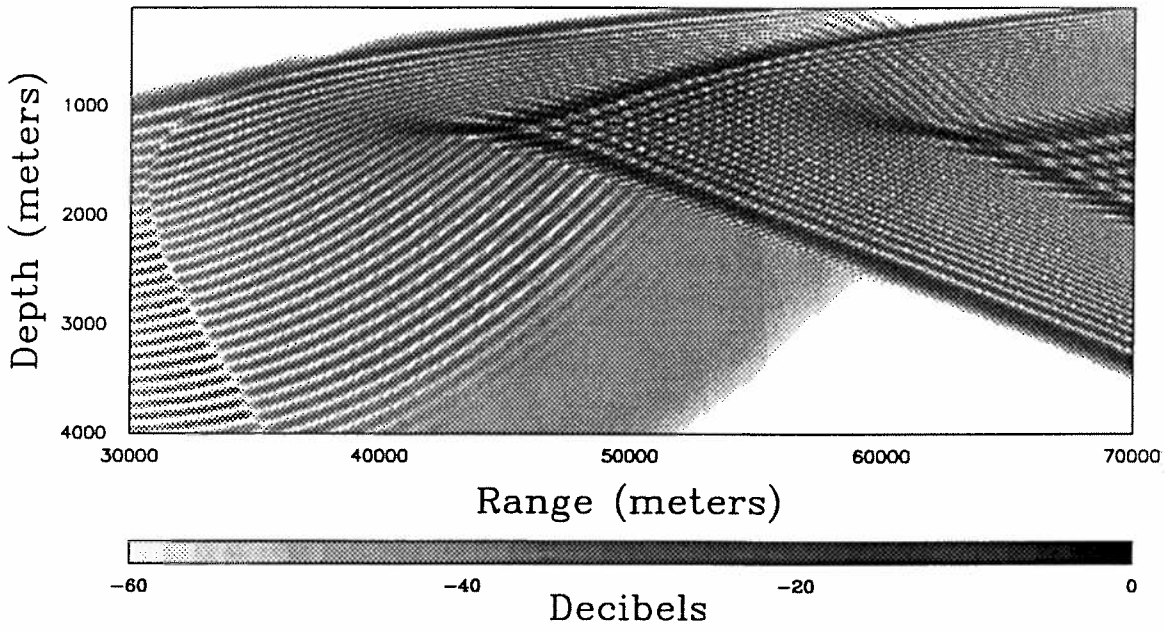

Figure 3.8: Gaussian Beam Acoustic Field Magnitude.

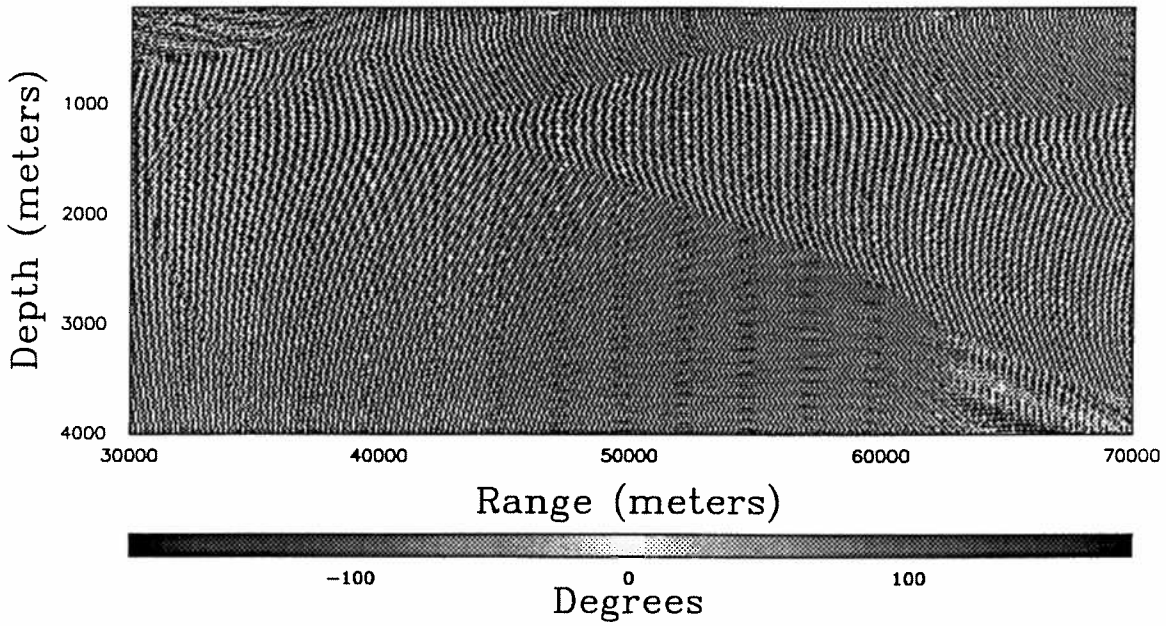

Figure 3.9: Gaussian Beam Acoustic Field Phase.

A direct comparison between the mode method, and the Gaussian beam method can be made. Figures 2.4 and 2.5 show the acoustic field magnitude and phase calculated using the mode model. Figures 3.8 and 3.9 show the acoustic field magnitude and phase calculated using the Gaussian beam method. The Gaussian beam method compares favorably to the mode method. A very similar structure can be seen throughout most of the range–depth space. Areas of disagreement are in the shadow zones where the field has decayed by about 40 decibels.

There are three other points to be made about the calculation of Gaussian beam impulse responses.

The first concerns the estimation of the beam functions when they are calculated on a discrete grid. This is really an interpolation issue. Suppose that the Gaussian beam functions are known at the discrete grid point Q which is near the receiver point P. How does one extrapolate the field at point Q to point P? The simple answer is to adjust the phase to account for the extra delay between the points using a two dimensional Taylor series about point Q, truncated to second order, i.e. a quadratic approximation. Therefore the wave field in the effective vicinity of a specified point of the central ray is

$$u(s_P, n) = u(s_Q, n) \exp\left\{ j\omega \left[\frac{1}{c}(s_P - s_Q) - \frac{1}{c^2}\frac{\partial c}{\partial n} sn - \frac{1}{2c^2}\frac{\partial c}{\partial s}(s_P - s_Q)^2 \right] \right\}. \quad (3.56)$$

.

The second point is that this method eliminates the need for calculation of eigenrays. Normally, to find the time delay of the arrivals at a particular site, one must iteratively shoot rays from the source to the receiver. By varying the initial launch angle of the ray, the end point of the ray can be made to converge to the receiver point. Instead of doing this, the Gaussian beam method can be employed to estimate the arrival time in this manner. First choose the beam on a particular sheet that comes closest to the receiver and then estimate its arrival time with formula (3.56).

The final point to be made concerns the number of beams to be used in the

summation (3.32). Since our beam width has been fixed by minimum approximation error considerations, the number of beams must be large enough to guarantee one beam width wide beam spacing. Any more than are needed would unnecessarily slow the computer modeling effort. A good estimate of the number of beams needed in the typical ocean acoustic environment can be made by again considering the homogeneous situation. To do this, guess a smallest typical value that will be used for the beam width at the farthest distance a receiver will be located. This is where experience helps. (A good guess is about 100 meters). The inter-beam distance d must be no more than twice the beam width

$$2L(s) > d = s\delta\theta = s\frac{\theta_N - \theta_1}{N-1} \tag{3.57}$$

where $\delta\theta$ is the angular separation between beams expressed in radians, N is the total number of beams, and θ_Ω is the initial angle of beam Ω. Solving for the number of beams

$$N > s\frac{\theta_N - \theta_1}{2L(s)} + 1 \tag{3.58}$$

reveals the number of beams needed for an accurate calculation. For example, if one was interested in the field generated by a source which was 1200 meters deep at a range of one hundred kilometers, the number of beams needed would be greater than

$$N > (s = 100,000)\frac{(\theta_N - \theta_1 = 30.0)\pi/180.0}{2(L(s) = 100.0)} + 1 = 246. \tag{3.59}$$

Here, the ray path length has been approximated by the range, and the angle window used includes just those rays which graze the surface and bottom. These are assumptions which work well in practice. If beams become separated by more than a beam width, the field will contain errors locally. So although equation (3.58) gives a good idea of the number of beams needed, any calculation must monitor the relative positions of adjacent beams to ensure accuracy.

CHAPTER IV

SIGNAL PROCESSING FOR LOCALIZATION

Taking a systems approach, we want to apply statistical communications theory and signal detection and estimation theory to the ocean acoustic situation. It is crucial to realize that this is a multiple source and multiple sensor environment and that sources and sensors are coupled by more than one path. The complexity of the environment limits the signal processor to algorithms which can be implemented efficiently.

The question we wish to answer is this: If $c(x, y, z, t)$, the speed of sound is known everywhere, what good would it do? Would knowledge of the acoustic transfer function improve communications, detection, or localization? Furthermore, if knowledge of the speed of sound is imprecise, how does this affect our ability to do signal processing?

This chapter is about passive source localization techniques. To elaborate, the basic problem is this, if one is able to observe the outputs of a number of hydrophones, how can the signal processor detect and localize sound sources by listening only. The problem is a difficult one, that has a number of important applications.

The problem considered in this chapter is that of locating an underwater sound source with a vertical line array. Progress has been made on this problem in this thesis by developing a new signal processing algorithm, channel matched filtering,

(CMF). This type of processing is shown to be a broadband extension to matched field processing, a recently developed algorithm. CMF is conceptually simpler and easier to implement than broadband matched field processing.

In this chapter, the matched field processing algorithm is described first. Then two extensions to the broadband case of matched field processing are presented. Results in the coherent case are believed to be new. Next the CMF algorithm is motivated and described. The algorithm is a new development, which differs slightly from the algorithm described by Clay, [11], in that only receptions at hypothesized arrival times are back propagated, as opposed to a total deconvolution. Three ad hoc variants on this algorithm are then contrasted with the CMF algorithm. Finally the effect of bandwidth and channel mismatch are explored.

To simplify the problem, only a two dimensional slice of the ocean will be considered. The source signal is unknown except for its statistical characteristics. The environment is assumed to be a deep mid-latitude ocean, and Gaussian beam acoustic modeling as developed in the last chapter will be used to calculate channel impulse responses.

Several others have made progress in this area. Bucker first proposed matched field processing for detection in shallow water [7]. More recently, Porter *et al.* [39], compared matched field processing to high resolution methods. Clay [11], developed the theory of source localization in a waveguide using impulse responses. Baggeroer *et al.* [1] applied the Cramer-Rao bound to find the optimum source resolution.

Matched Field Processing

There are several standard techniques for the passive source localization problem, [22]. Until recently however, none incorporated knowledge of the channel propagation characteristics into the problem, [7] This is not due to lack of advanced signal

processing algorithms, there are many, but due to the difficulty in modeling the channel and implementing such models in a reasonable fashion.

When a passive localization technique is to be used in a homogeneous environment, there are considerable simplifications that can made. It can be assumed that there will only be one path to the receiver, and that the arrival will be a spherical wave. This can be further simplified if the receiver array is at great enough distance from the source such that the wave front could be considered planar across the array. The most basic technique in this instance is to adjust the phase of the array to steer it in different look directions for a CW signal. This method, called beamforming, assumes plane wave arrivals. It works well if bearing angle is the only estimate required. For sources located close to the array, range estimates can be found as well by adjusting the time delay on each array element to compensate for wavefront curvature.

If a multipath environment exists, as in a long range ocean acoustic environment, the standard beamformer fails. A more general method is needed, which incorporates channel modeling into the signal processing, if range and depth estimates are to be made.

As a way of motivating the matched field processor, consider the acoustic field as it varies in space as shown in the last chapter, see figures 3.8 and 3.9. It can clearly be seen that vertical slices of this field at different ranges are quite distinct. By comparing the observed field, measured across an array, to a replica field, calculated for different source positions, the signal processor should be able to ascertain the source range and depth.

Let the source signal be CW, an unmodulated carrier, but with unknown phase and amplitude. Suppose the complex demodulate of the rth hydrophone of the array is

$$y_r = x_r(U) \tag{4.1}$$

where $x_r(U)$ is due to the pressure field generated by the source at position U. One can then form the vector of observations

$$\mathbf{Y} = [y_1, y_2, \ldots, y_R]^T, \tag{4.2}$$

from the complex demodulates of the array. We use the complex demodulate representation because that is the typical measured output of a modern sonar array. Note that the vector is just a set of sample values at a particular time. It also could be thought of as a vector of Fourier coefficients corresponding to a particular frequency. That is to say, suppose an observation is made over a finite time interval at all the hydrophones. Then form the Fourier series corresponding to each individual hydrophone's observation. Now extract the coefficient from each series at the particular known frequency at which the source is operating and form the vector $\mathbf{Y}$.

Lets take a closer look at the signal processing for a simple beamformer to determine the direction of the source. In the homogeneous environment situation with plane wave arrivals, one multiplies each component of $\mathbf{Y}$ by

$$b_r = \exp\{-j\omega\tau_r(\theta)\} \tag{4.3}$$

where ω is the source frequency in radians per second, and $\tau_r(\theta)$ is the time delay at phone r in direction θ. Next form the sum of the multiplied components, essentially an inner product, and look at the beamformer output as a function of direction. The source is estimated to be in the direction $\hat{\theta}$ at which a maximum of the beamformer output occurs.

Inspired by the simple beamformer, one can similarly define a beamformer for a single frequency multipath situation. Generalize the beamformer coefficients b_r such that they are the complex conjugates of the value of the predicted transfer function at the source frequency. These coefficients are now functions of the source range and depth as well as the phone index,

$$b_r = b_r(U) = x_r^*(U), \tag{4.4}$$

where U is the two element vector of the range and depth of the source position. The ambiguity function can then be defined as

$$\begin{aligned} A(U,\hat{U}) &\triangleq \frac{\sum_{r=1}^{R} y_r(U) b_r(\hat{U})}{N\sqrt{\sum_{r=1}^{R} |y_r(U)|^2 \sum_{r=1}^{R} \left|b_r(\hat{U})\right|^2}} \\ &= \frac{\sum_{r=1}^{R} x_r(U) \tilde{x}_r^*(\hat{U})}{N\sqrt{\sum_{r=1}^{R} |x_r(U)|^2 \sum_{r=1}^{R} \left|\tilde{x}_r(\hat{U})\right|^2}}, \end{aligned} \tag{4.5}$$

where U is the unknown source position, and $\hat{U}$ is the hypothesized source position. In the second equality in equation (4.5), we have replaced y_r and b_r with x_r and $\tilde{x}_r$ to denote the actual calculation we will perform using the outputs of the Gaussian beam model described in the last chapter. The tilde is used here to distinguish between what would be the observations and the calculated response. The estimator is therefore a correlator that searches over the possible source positions. This is also known as the Bartlett beamformer or matched field processor. It is basically a standard beamformer but with the steering phases replaced by a replica field. A normalization has also been included in the ambiguity equation, (4.5), so that the value of the function will be unity when $\hat{U} = U$.

It is interesting to plot the magnitude squared of equation (4.5), that is the output power of the beamformer with no added noise, in what may be described as a typical deep ocean situation. Figure 4.1 shows the matched field processor output for a vertical array of 100 hydrophones. The depth of the top phone is 100 meters and the spacing between phones is 30 meters. The source is operating at 250 Hertz and is located at a range of 100 kilometers and a depth of 1200 meters. The matched field processor output is shown on a decibel scale with the peak normalized to 0 dB. The search space is from 80 to 120 kilometers in range, with 100 meter steps, and 20 to 2000 meters in depth, with 20 meter steps.

The surface in figure 4.1 has its peak at the true source location. The sidelobe level is significant though and peaks can be found which are less than 10 db below

the true peak. This picture is encouraging however, and demonstrates the power of the matched field processing technique to resolve the location of a source that would not otherwise be discernible.

Multi-Frequency Matched Field Filtering

The estimate in the previous section was based on a single frequency signal. The matched field processor can be generalized to as many independent frequency components as desired. There are two ways to combine multi-frequency information, incoherently and coherently.

As the signal bandwidth increases, the question becomes: How does one combine the added information present in the observations? As the signal bandwidth increases, we can form more independent observations as the Fourier coefficients,

$$\mathbf{Y}(\omega_k) = [y_{1,k}, y_{2,k}, \ldots, y_{R,k}]^T, \tag{4.6}$$

where

$$\omega_k = \frac{2\pi\ k}{T}, \tag{4.7}$$

defines the discrete spectral index, k; and T is the observation time. Adding to the confusion is the fact that T is also used to denote the transpose of the observation vector, $\mathbf{Y}$, but it should be clear from the context which is which. An implicit assumption is that the Fourier coefficients are statistically independent.

It is possible to form multiple ambiguity functions A_k using equation (4.5), where k indexes the Fourier component that was used. To combine the multiple functions simply add them. The ambiguity equation thus becomes

$$A(U,\hat{U}) = \sum_{k=0}^{N-1} \left| A_k(U,\hat{U}) \right| = \sum_{k=0}^{N-1} \left| \frac{\sum_{r=1}^{R} x_{r,k}(U)\tilde{x}^*_{r,k}(\hat{U})}{N\sqrt{\sum_{r=1}^{R} |x_{r,k}(U)|^2 \sum_{r=1}^{R} \left|\tilde{x}_{r,k}(\hat{U})\right|^2}} \right|, \tag{4.8}$$

where the single frequency components as given in equation (4.5) have been combined incoherently.

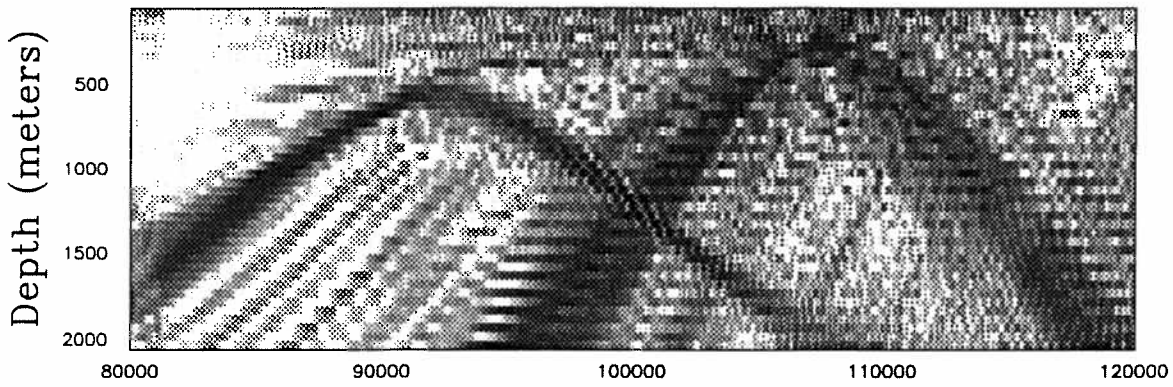

Figure 4.1: Matched Field Processor.

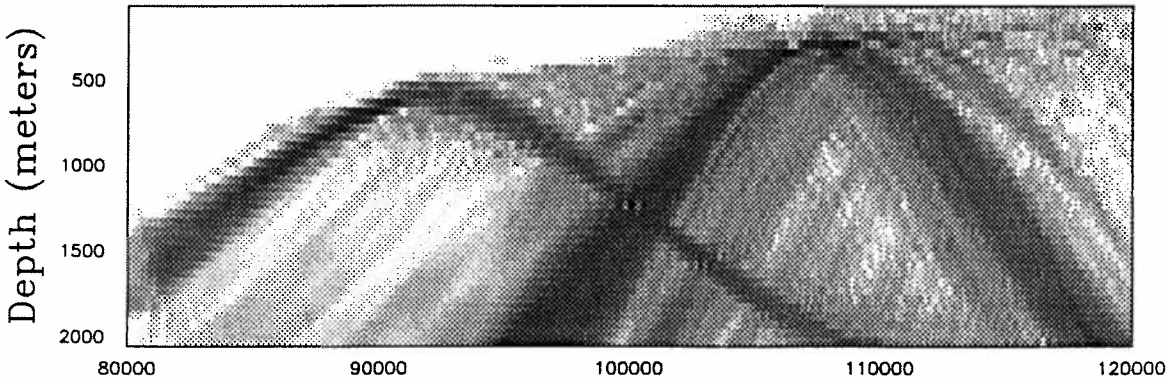

Figure 4.2: Matched Field Processor: Incoherent Case.

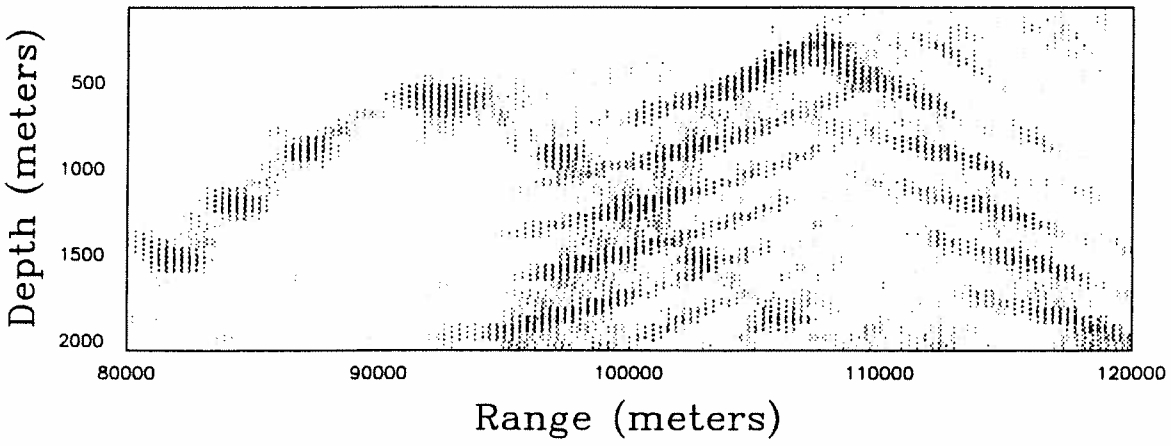

Figure 4.3: Matched Field Processor: Coherent Case.

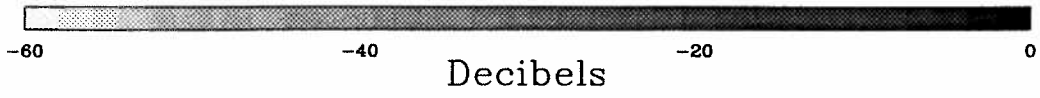

An example is shown in figure 4.2. The geometry is the same as for figure 4.1. The source spectrum is taken to be 11 equal energy lines spread uniformly across a band from 200 to 300 Hertz. The source has been correctly localized. There is a major improvement from the single frequency case. The surface is considerably smoother and the sidelobe levels are much further below the peak level.

There is another method of combining broadband information that will be considered here. By moving the absolute value sign outside the summation, the single frequency components of the ambiguity function can be combined coherently. This only makes sense if the phase relationship between the spectral lines is known, that is if the signal is known exactly except for amplitude and starting time. Coherent and incoherent combination are solutions to quite different signal problems.

To be more specific, the coherent multi-frequency ambiguity function is

$$A(U,\hat{U}) = \left| \sum_{k=0}^{N-1} A_k(U,\hat{U}) \right|, \tag{4.9}$$

where the multiple ambiguity functions are combined before calculating the magnitude. An example has been plotted in figure 4.3. The geometry is the same as previously given for figure 4.1. The source spectrum is taken to be 11 equal energy lines, whose phases are constant, spread uniformly across a band from 200 to 300 Hertz. Again the source has been correctly localized and there is an improvement in the sidelobe levels. The surface is not as smooth as before however.

Minimum Variance Distortionless Response Beamformer

There is another algorithm that is worth mentioning. It is the minimum variance distortionless response beamformer (MVDR). This technique goes by several different names in the literature. It is also known as the maximum likelihood method (MLM), and as Capon's method, [22].

MVDR has useful imaging properties. It tends to suppress the sidelobes in the

ambiguity function thus giving it a more focused appearance. MVDR has therefore been labeled a high resolution method. The algorithm attempts to form the maximum likelihood estimate of the source range and depth parameters subject to the constraint that it passes the source waveform through to its output undistorted.

One must be careful. A direct analogy may be drawn to the comparison of matched filters versus inverse filters in the scalar time delay estimation problem with a known signal in Gaussian noise. Using the standard notation, the received signal spectrum Y is

$$Y(\omega) = X(\omega) + N(\omega), \tag{4.10}$$

where X is the known signal, and $|N(\omega)|^2$ is the power spectral density of noise. If the observation interval is $(0, T)$, the optimum processor for time delay estimation in the maximum likelihood sense is a matched filter [8],

$$H(\omega) = \frac{X^*(\omega)}{E \mid N(\omega) \mid^2} = \frac{1}{N_0} \mid X(\omega) \mid^{\xi} e^{-j \arg X(\omega)}, \tag{4.11}$$

where $\xi = 1$, and the noise power spectral density has been assumed to be a constant N_0, for simplicity. The output waveform of this filter is the shifted autocorrelation function of $x(t)$, whose maximum value is the maximum likelihood estimate of the time delay. If the value of ξ is set to -1, the processing is referred to as inverse filtering. The output of the filter is a delta function centered at the time delay. The sharpness of the processing has increased infinitely; but at what cost? If the signal spectrum has deep nulls present, the inverse filter will apply high gain to any noise in the system, thus destroying the estimate.

The lesson to be learned here is that at high signal to noise ratios, high resolution processing produces sharp results. At low signal to noise ratios, however, one is much better off using the matched filter, which as a maximum likelihood estimator (without a constraint) achieves minimum estimator variance. The two methods are trying to solve two different problems. The matched filter gives the best time delay estimate, while the inverse filter attempts to estimate the total input waveform.

Another drawback of MVDR processing is that it requires the inversion of a matrix whose dimension is the number of hydrophones used in the array. This greatly increases the amount of calculation required over matched field processing. However a total dismissal of the idea is not appropriate. There are occasions where the MVDR may be very useful, such as when there are multiple targets present or if the ambient noise on the array is highly directional or spatially correlated. Since the usual ocean acoustic situation for passive localization has low signal to noise ratio the MVDR beamformer will not be discussed further.

Channel Matched Filtering

As seen in the last section, matched field processing is an effective technique for the localization of an underwater source. Also, the method becomes more effective as more frequency components are used. It is possible however, to have a much different viewpoint than that of the last section. This viewpoint is based on characterizing the channel with time domain impulse responses instead of frequency domain transfer functions. This is appropriate for broadband sources and becomes possible because impulse responses can be quickly and efficiently calculated with the Gaussian beam method.

As shown in the last chapter, the ocean acoustic channel between a source and a single hydrophone can be modeled as a linear time–invariant filter whose impulse response function is

$$c^U(\tau) = \sum_{p=1}^{P} \mathcal{A}_p \delta(\tau - \tau_p) \tag{4.12}$$

where U represents the unknown position of the hydrophone relative to the source, p is the path index, P is the total number of paths, τ_p is the path time delay, and $\mathcal{A}_p$ is the complex valued path attenuation coefficient. We will use this deterministic model and ignore any variability of the ocean since it is our objective to develop

new signal processing strategies based on a known acoustic transfer function. We choose to use a complex baseband representation here so that our previous work with complex Fourier coefficients and the matched field processor will be included. The complex impulse response function, (4.12), is the impulse response for a demodulated channel.

The new processing strategy investigated in this thesis is the *reverse* propagation of the received signal waveform through a linear filter which approximates the ocean channel. Suppose we wish to find the source waveform from the waveform observed at the hydrophone. For the time being, we will assume that the observation,

$$y(t) = c^U(t) * x(t), \tag{4.13}$$

at the hydrophone is noiseless. Here the observation is shown as the convolution of the emitted source signal, $x(t)$, and the channel impulse response. The reverse (or backwards) propagating filter is defined as

$$b^{\hat{U}}(\tau) = \sum_{p'=1}^{P'} \mathcal{B}_{p'} \delta(\tau + \tau_{p'}), \tag{4.14}$$

where $\hat{U}$ is the hypothesized position of the source relative to the hydrophone, and the $\mathcal{B}_{p'}$'s and $\tau_{p'}$'s are related to the forward coefficients and time delays respectively, in a manner to be described shortly. Note that the number of paths in the reverse direction, P', depends on the hypothesized position $\hat{U}$. After the filter, the output is

$$w(t) \triangleq y(t) * b^{\hat{U}}(t) = \sum_{p=1}^{P} \sum_{p'=1}^{P'} \mathcal{A}_p \mathcal{B}_{p'} x(t - \tau_p + \tau_{p'}). \tag{4.15}$$

If the reverse propagating filter has correctly hypothesized the source position, $w(t)$ becomes

$$w(t) = \sum_{p=1}^{P} \mathcal{A}_p \mathcal{B}_p x(t) + \sum_{p=1}^{P} \sum_{p' \neq p}^{P} \mathcal{A}_p \mathcal{B}_{p'} x(t - \tau_p + \tau_{p'}). \tag{4.16}$$

The first term has the desired property of reconstructing the original unknown source waveform. The second term is a self–interference term.

Let us now examine how we might choose the coefficients, $\mathcal{B}_{p'}$, of the reverse propagating filter. Three choices come to mind.

$$\mathcal{B}_{p'} = |\mathcal{A}_p|^{\xi} e^{-j \arg(\mathcal{A}_p)} \tag{4.17}$$

where $\xi = 1, 0$, or -1. These correspond to a *channel matched*, a *channel phase matched*, and a *channel inverse* filter respectively. As ξ varies between 1 and -1, we might expect that we could trade signal–to–noise (or interference) ratio for *sharpness* of response. Another variation that can be used is if we let $\xi = 1$ and let $\arg(\mathcal{A}_p) = 0$; this is known as the *channel time delay filter.*

If one knew the signal spectrum and the channel transfer function to the hydrophone, the transfer function of the matched filter for the received waveform would be

$$X^*(\omega)C^*(\omega), \tag{4.18}$$

where $C(\omega)$ is the transfer function of the channel. Thus the *channel matched* filter is nothing but the channel half of the matched filter. In other words, since we don't have any knowledge of the source's spectrum, $X(\omega)$, we do the reasonable thing and assume its value is unity for all values of ω.

Next, let us assume that we have an array of hydrophones. Each hydrophone reception is back–propagated to a hypothesized source location and then the filter outputs are summed to get

$$a(t; U, \hat{U}) \triangleq \sum_{r=1}^{R} \sum_{p=1}^{P} \sum_{p'=1}^{P'} \mathcal{A}_{r,p}(U) \mathcal{B}_{r,p'}(\hat{U}) x(t - \tau_{r,p}(U) + \tau_{r,p'}(\hat{U})) \tag{4.19}$$

where r is the receiver hydrophone index and R is the number of receiver hydrophones; p and p' are the path indices and P and P' are the number of paths between the array and U and $\hat{U}$ respectively. The function $a(t; U, \hat{U})$ is a time domain focusing function. It can be expected to peak when $\hat{U} = U$.

Let us assume that we are using channel matched filtering. There are two cases which can occur. First suppose that the back–propagating filters exactly compensate

for the channel. Then we have

$$a_{\mathrm{CMF}}(t;U,\hat{U}=U) = \sum_{r=1}^{R}\sum_{p=1}^{P}\mathcal{A}_{r,p}(U)\mathcal{A}^{*}_{r,p}(U)x(t) + \sum_{p=1}^{P}\sum_{p'\neq p}^{P}\sum_{r=1}^{R}\mathcal{A}_{r,p}(U)\mathcal{A}^{*}_{r,p'}(U)x(t-\tau_{r,p}(U)+\tau_{r,p'}(U)) \quad (4.20)$$

The first term reconstructs the original signal and the second is a self–interference term. The hope is that as the number of receiver hydrophones, R, and the number of paths, P, increase, the gain applied to the reconstruction increases faster than that of the interfering term. On the other hand, when the back–propagating filters incorrectly hypothesize the source position,

$$a(t;U,\hat{U}) = \sum_{r=1}^{R}\sum_{p=1}^{P}\sum_{p'=1}^{P'}\mathcal{A}_{r,p}(U)\mathcal{A}^{*}_{r,p'}(\hat{U})x(t-\tau_{r,p}(U)+\tau_{r,p'}(\hat{U})) \quad (4.21)$$

In this case we have only the self–interference term. Adding many signal waveforms in this misaligned fashion, we hope that the power in $a(t;U,\hat{U}\neq U)$ is less than in $a(t;U,\hat{U}=U)$ where the aligned waveforms are added.

It is useful to perform a normalization

$$\tilde{a}(t;U,\hat{U}) \triangleq \frac{a(t;U,\hat{U})}{\sqrt{\sum_{r=1}^{R}|y_r(t)|^2\sum_{r=1}^{R}\sum_{p'=1}^{P'}\left|\mathcal{B}_{r,p'}(\hat{U})\right|^2}}. \quad (4.22)$$

This assures that $|\tilde{a}| \leq 1$ by an application of the Schwarz inequality. Further processing of the time domain focusing function resembles standard detection theory. The source waveform, $x(t)$, is a complex valued waveform which is either unknown or a random process of some type. An ambiguity function can be formed in the time domain as an energy detector or its expected value

$$\left|A(U,\hat{U})\right|^2 \triangleq \int_0^T \left|\tilde{a}(t;U,\hat{U})\right|^2 dt. \quad (4.23)$$

This ambiguity function reduces to the form in equation (4.5) when the source signal is assumed to be CW. It should be noted, however, that the reverse is not true. That is to say that multiple frequency matched field processing and channel matched

filtering are not equivalent. The channel matched filtering algorithm uses the fact that only time delays corresponding to real path delays have non-zero amplitude coefficients, whereas a time domain representation of multiple frequency matched field processing uses all time delays and does not distinguish between zero and non-zero coefficients. This means that channel matched filtering has a greater computational efficiency than matched field processing.

The ability of an array of back–propagating filters to localize a source depends on the complexity of the arrival structure. We expect that the more complicated the structure the easier it becomes to localize a source. This happens because more structure is equivalent to more information about the channel. Thus we expect the multipath channel characteristic to be to our advantage.

An example of channel matched filtering is given in figure 4.4. In this type of processing, the back propagating filter coefficients are the complex conjugates of the forward path coefficients.

$$\mathcal{B}_{p'} = \mathcal{A}_p^* \tag{4.24}$$

The geometry in the example is the same as that of the previously displayed matched field processors. There are 100 hydrophones in the array, spaced 30 meters apart. The top phone is at a depth of 100 meters. The source is located at a range of 100 kilometers and at a depth of 1200 meters. The source spectrum is assumed to be that of a low-pass filtered white Gaussian random process, with autocorrelation function

$$R_x(\tau) = P_x e^{-\tau/\tau_x}, \tag{4.25}$$

where τ_x was chosen to give a $1/e$ *bandwidth* of 100 Hertz.

An ambiguity surface can now be calculated using equations, (4.23) and (4.25). This is done by assuming that the source waveform is a wide sense stationary ergodic random process and realizing that the variance of the mean value of (4.23) becomes very small if the time–bandwidth product is large. Therefore the mean value of (4.23) can be calculated using the autocorrelation function (4.25).

The result shown in figure 4.4 is quite good. By using a wideband signal the localization properties of the ambiguity surface are greatly improved over the previously shown matched field results. This is not meant to say that a multiple frequency matched field processor has inferior performance with the same bandwidth, but to merely point out the advantage a wideband signal provides in this localization problem, and to show how channel matched filtering naturally lends itself to wideband processing.

An example of the corresponding channel phase filtering is given in figure 4.5. For this type of filtering the backpropagating filter coefficients are given by

$$\mathcal{B}_{p'} = \frac{\mathcal{A}_p^*}{|\mathcal{A}_p|}, \tag{4.26}$$

which results in the time domain focusing function

$$a_{\mathrm{CPF}}(t; U, \hat{U}) \triangleq \sum_{r=1}^{R} \sum_{p=1}^{P} \sum_{p'=1}^{P'} \mathcal{A}_{r,p}(U) \frac{\mathcal{A}_{r,p'}^*(\hat{U})}{|\mathcal{A}_{r,p'}(\hat{U})|} x(t - \tau_{r,p}(U) + \tau_{r,p'}(\hat{U})). \tag{4.27}$$

The expected value of the power in this function, the ambiguity function, is plotted in figure 4.5. The geometry and source parameters are as previously given. The channel phase filtering is able to localize the source even better than the channel matched filter case. This might be expected since, as mentioned earlier, the channel phase filter is a wideband all–pass filter.

Finally, an example of channel time delay filtering is given in figure 4.6. In this instance the channel amplitude and phase characteristics are ignored and the matching process is only applied to the channel time delay. The coefficients in this case are

$$\mathcal{B}_{p'} = 1, \tag{4.28}$$

and the backpropagating filter merely realigns the multiple path arrivals. The resulting time domain focusing function is

$$a_{\mathrm{CTDF}}(t; U, \hat{U}) \triangleq \sum_{r=1}^{R} \sum_{p=1}^{P} \sum_{p'=1}^{P'} \mathcal{A}_{r,p}(U) x(t - \tau_{r,p}(U) + \tau_{r,p'}(\hat{U})). \tag{4.29}$$

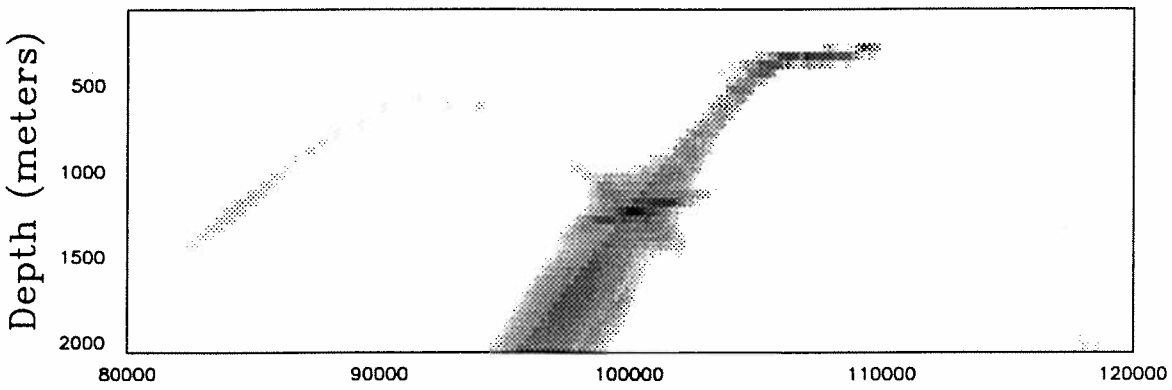

Figure 4.4: Channel Matched Filter.

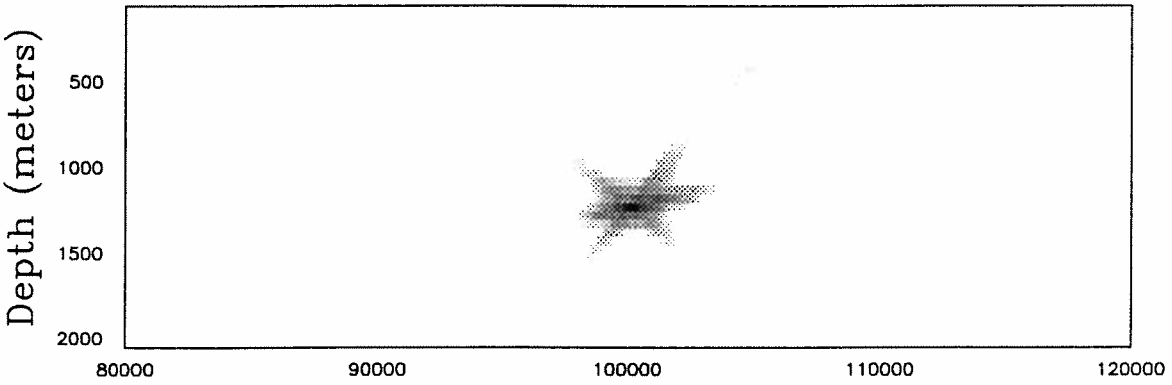

Figure 4.5: Channel Phase Filter.

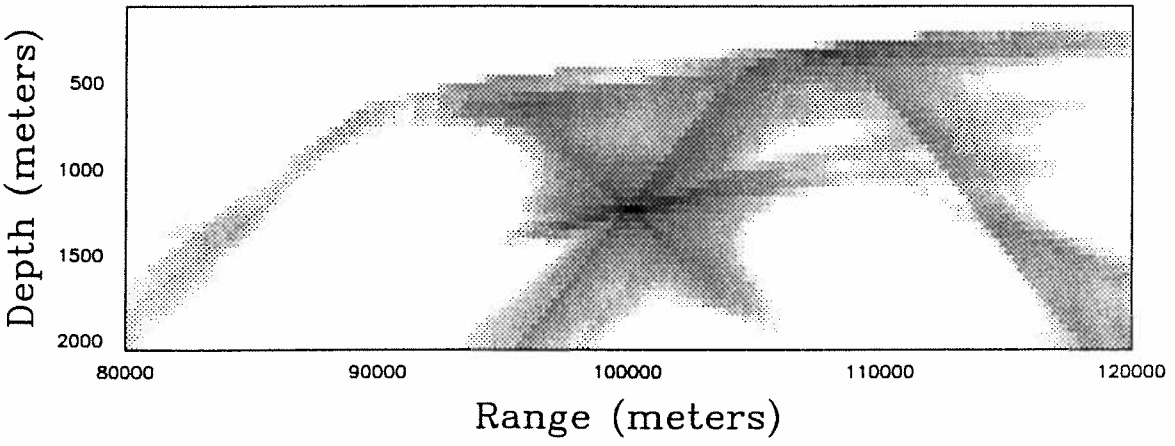

Figure 4.6: Channel Time Delay Filter.

The ambiguity surface is plotted in figure 4.6 with the same geometry and source parameters as the other processing. The displayed surface still localizes the source fairly well but the peak is much broadened. This might be expected since we are using only part of the channel propagation characteristics available to us, i.e. the time delay, and not the amplitude or phase.

Motivation for trying these variants on the channel matched filtering procedure is that there may be occasions when our knowledge of the propagation characteristics is not exact, and we wish to explore the robustness of these methods to channel uncertainty. Physically the amplitudes of the multipath coefficients are the most unstable. It is hoped that using only phase and time delay in channel phase filtering or just time delay in channel time delay filtering would yield some immunity to amplitude variations. These issues will be explored in subsequent sections.

Environmental Sensitivity

A major problem in source localization has been the question of how to relax the assumption of absolute knowledge of the sound speed field. Up until now, the basic premise has been that the sound speed field, and hence the point–to–point impulse response, is known exactly. A more realistic situation is that the sound speed field is known imprecisely.

It is a natural step for a systems-oriented researcher to impose a probabilistic structure on this field. Fortunately, there is a natural physical parameterization of the field. Even though we will not impose a stochastic model on the sound speed field, it is useful to employ a parameterization based on internal waves.

The ocean is a giant heat pump. Warm water moves toward the poles and cold water moves toward the equator. Variations driven by solar radiation and tides, excite traveling density waves known as internal waves. These waves cause time and

space varying deviations from the equilibrium sound speed field. In this section, the effect of internal waves upon the previously considered source localization algorithms is explored.

Internal Waves

Ocean variability is a very complex phenomena but its main component is thought to be internal waves. Internal waves are density waves that move slowly through the interior of the ocean. The spectral energy peaks for waves with periods of about 10 minutes to several hours.

A discussion of internal waves following Flatté, [18], is in Appendix B. It is shown in this appendix that the vertical and horizontal fields are separable. The important point is that one can calculate sound speed perturbations that are the sum of several vertical eigenfunctions associated with the structure of these perturbation fields. The contemporary model of the physics of the situation constrains the sound speed deviations to a sum of computable functions. This greatly reduces the degrees of freedom of the system. It is believed that most of the internal wave energy can be found in the first 3 modes, [23]. Typical deep ocean internal wave modes are shown in figure 4.7.

The horizontal variation in the sound speed field is usually treated as a random field whose characteristics have been measured. As mentioned above, the most energetic waves have a period of about 10 minutes. A diagram of spectral energy, [18], versus horizontal wavenumber is show in figure B.2.

Experimentally it has been shown that it is the amplitude of acoustic arrivals that varies the most. Amplitude stability is on the order of ten minutes. Time of arrival is actually quite stable, having variations less than a few milliseconds over periods of days [18]. Even crude simulations of internal wave effects match this behavior, [3].

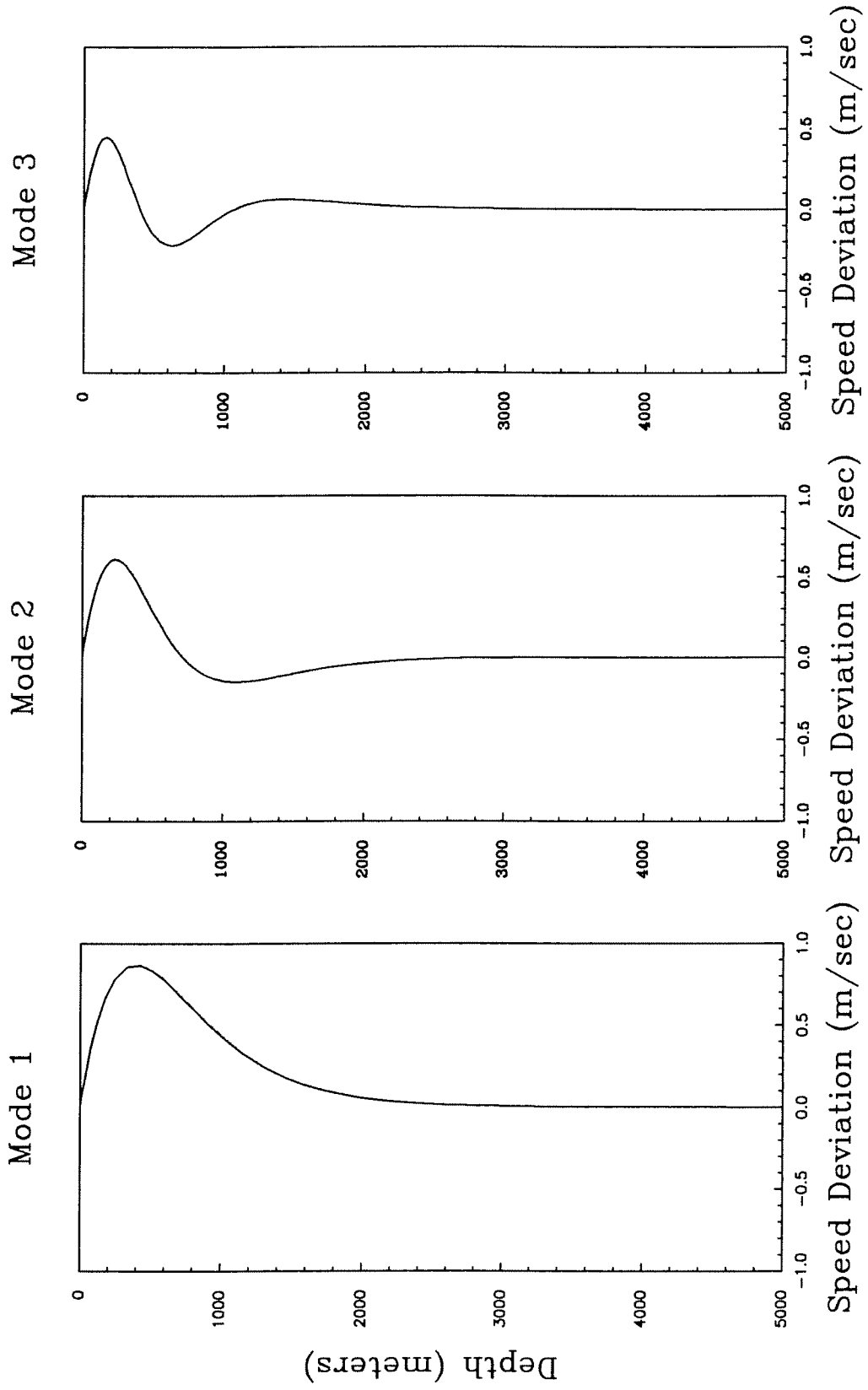

Figure 4.7: Internal Wave Sound Speed Deviations.

Shown in figure 4.8 are the effects of an internal wave perturbation on the point-to-point impulse response of a source and receiver separated by 100 kilometers. The amplitude is affected by a much greater amount than the time delay or phase.

It is necessary to explain just how the perturbation was added. The computer code used for the impulse response calculation did not handle range-varying sound speed profiles. This is not due to any theoretical constraints; it simply was not coded. Simple internal wave action can be simulated by adding an amount of the first mode of sound speed deviation shown in figure 4.7. The amount added was equal to a maximum positive deviation of 1 meter/second, a physically reasonable perturbation. This is a snapshot of an internal wave traveling perpendicular to the source–receiver plane. The sound speed profile is given by the combination of equations (2.1) and (B.22)

$$c'(z) = c(z)(1 + \theta_{iw} 2.5 n^2(z)\zeta), \tag{4.30}$$

where $c(z)$ is the Munk profile described previously, ζ is the deviation as described in Appendix B, and θ_{iw} is a parameter which sets the amount of internal wave sound speed deviation.

Sound Speed Mismatch

A measure of the robustness of the performance of source localization algorithms are their effectiveness under mismatched conditions. Suppose that the true sound speed field is slightly different from the one used in the algorithm. The estimates will be degraded if the true model set is not represented among the candidate models. Displaying the ambiguity surface under these conditions will give some idea of the degradation. Others have considered this problem, [39], but with unrealistic mismatch conditions.

It is widely hypothesized that the most likely perturbation from the baseline

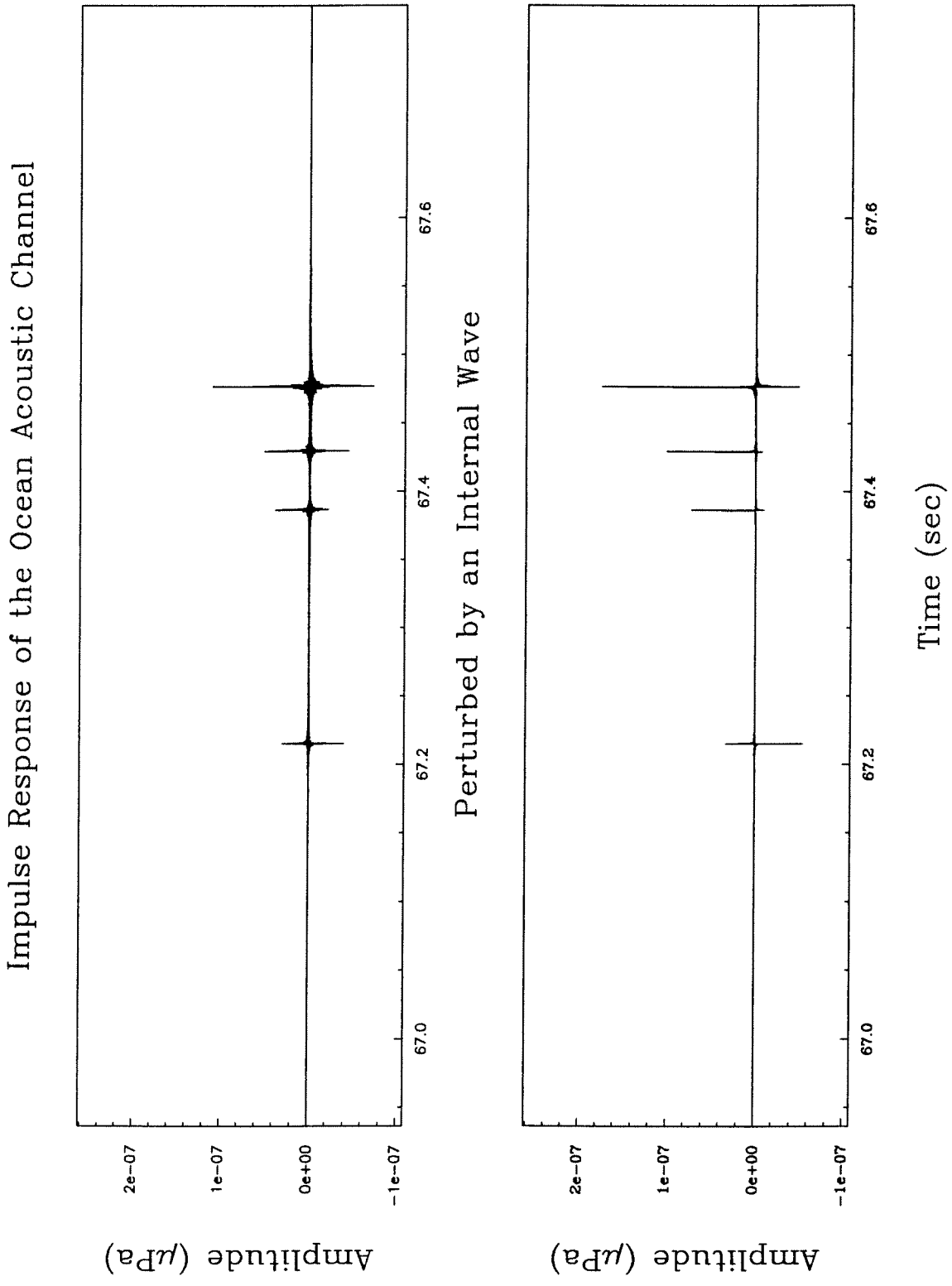

Figure 4.8: Internal Wave Impulse Response.

sound speed field is that due to internal waves. To make life simple, (i.e. in order to calculate an answer in a reasonable amount of time), a representative perturbation can be added to the sound speed profile in the same manner as the last section. A single, first order mode as shown in figure 4.7, is added to the baseline Munk profile so that the maximum deviation is 1 meter/sec.

The next six figures, 4.9 – 4.14, show the behavior of the six localization algorithms previously considered. The geometry and signal characteristics are the same as used before. The array consists of 100 hydrophones oriented vertically. The true source location is 100 kilometers from the array at a depth of 1200 meters. For the matched field processor the signal is a sine wave of unknown amplitude and phase, but known frequency (250 Hertz). In the broadband case the signal is modeled as a wide sense stationary Gaussian random process whose power spectrum is constant across a 100 hertz band centered at 250 Hertz and zero outside the band.

The matched field algorithms show the most degradation as might be expected. The peaks in the ambiguity surface are broadened and sidelobe magnitudes become large enough to give false indications of source location. In the single frequency case 4.9, the mismatch caused some blurring and actually makes the ambiguity surface seem smoother than that shown in figure 4.1. The peak has moved to a new location at a range of about 110 kilometers and depth of about 300 meters. The multi-frequency matched field algorithms perform better. They display false peaks in the ambiguity surface, but at least there is a peak at the true source location as well.

The broadband impulse response based algorithms seem to be more robust to the mismatch. The peaks are broadened and seem to be split into a narrow doublet, but in no case are false peaks found. (In figure 4.14 the search space extends only to 110 kilometers but the same scale as the previous figures was used.)

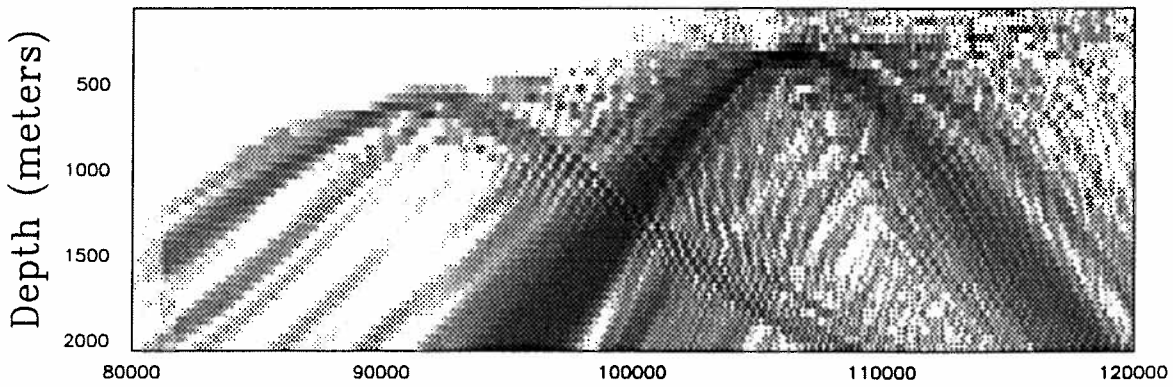

Figure 4.9: Mismatched Matched Field Processor.

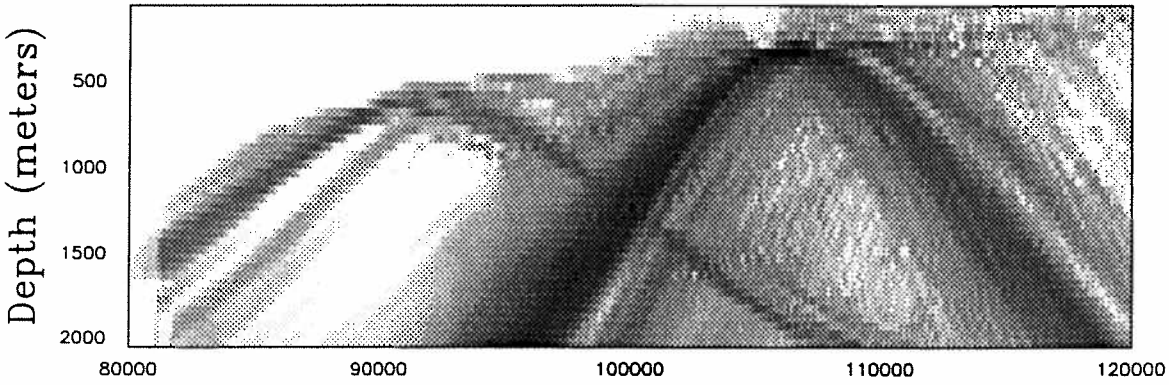

Figure 4.10: Mismatched Matched Field Processor: Incoherent Case.

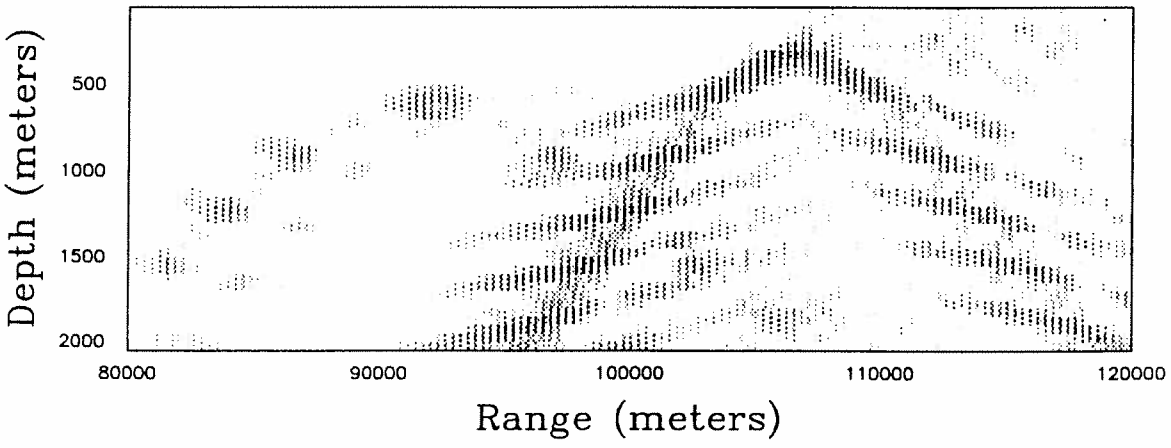

Figure 4.11: Mismatched Matched Field Processor: Coherent Case.

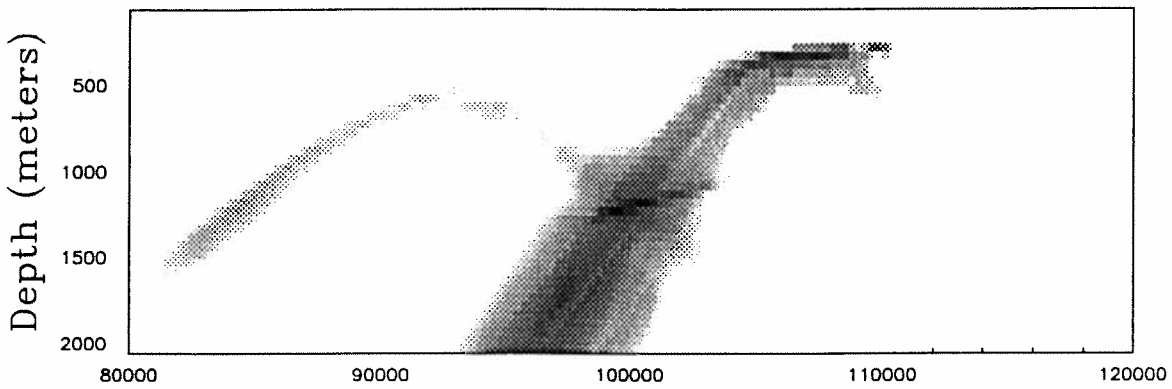

Figure 4.12: Mismatched Channel Matched Filter.

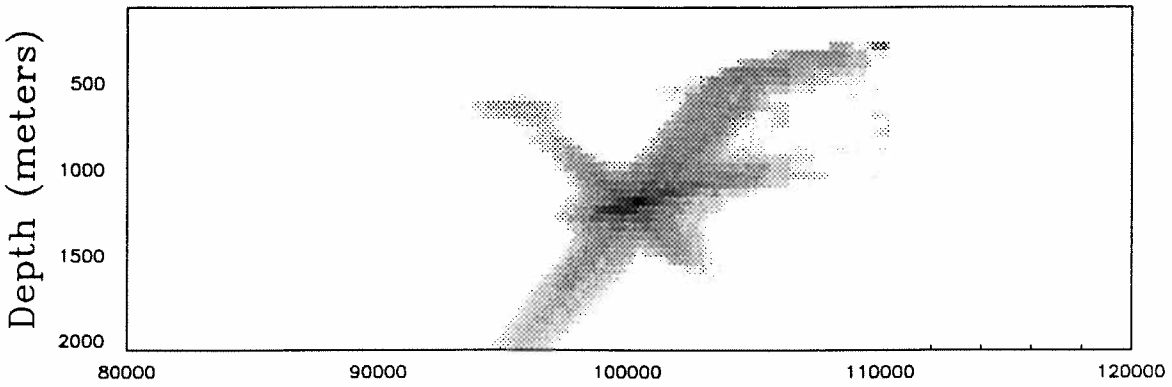

Figure 4.13: Mismatched Channel Phase Filter.

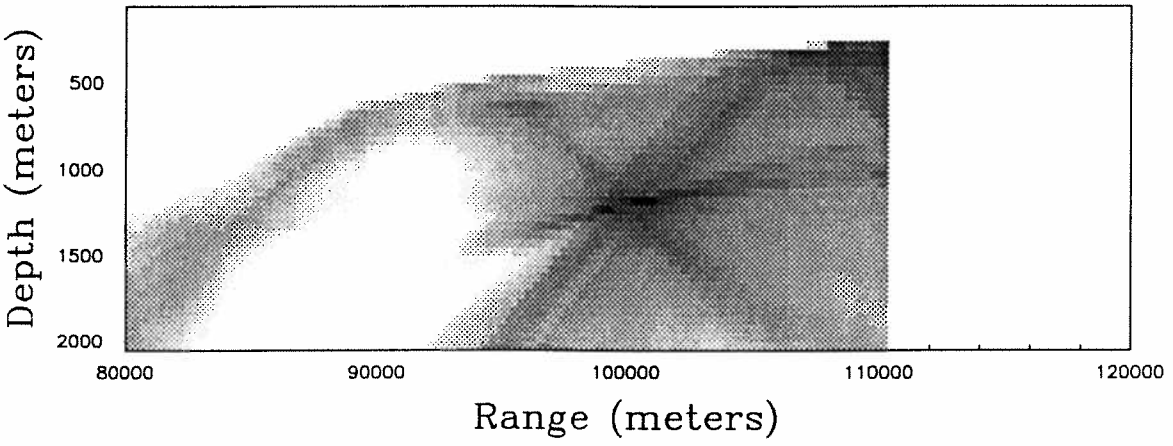

Figure 4.14: Mismatched Channel Time Delay Filter.

Bandwidth

In this section we explore the effect of bandwidth on the channel matched filtering algorithm. Specifically, we want to see how well the depth localization works with different bandwidth signals and we want to confirm that channel matched filtering reduces to matched field processing in the narrowband case.

First, let's see how the bandwidth of the signal spectrum affects the ambiguity surface. As done previously in equation (4.25), the source spectrum is that of a low-pass filtered white Gaussian random process, with autocorrelation function

$$R_x(\tau) = P_x e^{-\tau/\tau_x}, \tag{4.31}$$

where the value of τ_x is the $1/e$ *bandwidth* of the source. By varying the value of τ_x, we can see the effect of signal bandwidth on the channel matched filtering algorithm.

Ambiguity surfaces were calculated as a function of depth at the known true range of 100 kilometers, using equations, (4.23) and (4.31).

The effect of varying bandwidth is shown in figure 4.15. The same geometry was used here as in previous examples. The search depth varies between 0 and 2000 meters. The true source depth is 1200 meters. Three graphs are shown for the three cases of the channel matched, channel phase matched, and channel time delay matched filters. As the bandwidth is varied, graphs are superimposed on each other. The bandwidths in hertz were 1, 2, and 5×10^n, where $-4 \leq n \leq 3$.

The obvious effect of signal bandwidth is on the level of ambiguity at depths away from the true depth. The wider the bandwidth, the better the localization properties of all three algorithms. As was true in previous examples, the channel matched filter correctly localizes the source for all bandwidths; the channel phase filter is the narrowest above 50 hertz but losses its sharpness below 10 or 20 hertz source bandwidth, t also correctly localizes the source; the channel time delay filter

is wider than the others and is only able to correctly localize the source when the source bandwidth is greater than 20 Hertz.

Finally, it should be pointed out that the behavior of the channel matched filtering algorithms as the bandwidth approaches zero, is the same as the matched field processing algorithm. In fact, one can see the graphical evidence of a narrowband limit as the signal bandwidth becomes small in figure 4.15. This is the performance of monochromatic matched field processing.

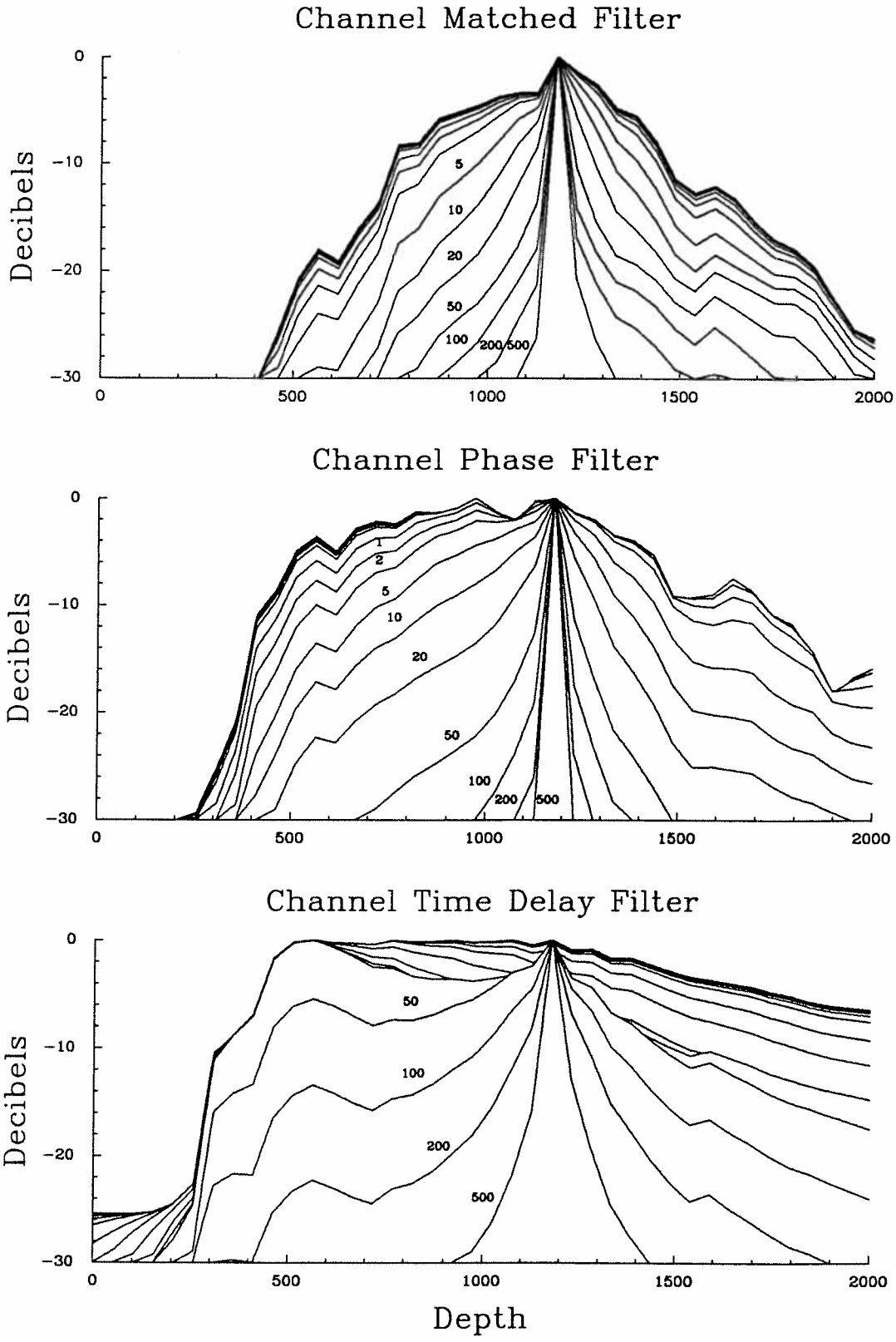

Figure 4.15: The Effect of Bandwidth on Depth Resolution.

CHAPTER V

CONCLUSIONS

At this point, a brief review of the work done is presented and is implications are discussed.

This research is a response to the question: If the sound speed profile were known everywhere exactly, what good would it do the signal processor? It is largely exploratory in nature. Attempts were made to to implement some simple signal processing techniques and performance measures to find out if they would work and how well they performed. The answer found here is that, yes, simple techniques work when combined with a sophisticated channel model.

The research was divided into two parts. The first half concerned the development and implementation of a sophisticated yet computationally efficient ocean acoustic propagation model. The Gaussian beam theory of Porter and Bucker [38] was refined to provided an accurate description of important acoustic effects such as the behavior at caustics, and phase changes. Specific contributions in the area of acoustic modeling include the ability to calculate impulse responses as opposed to merely calculating the single frequency field strength. Previously, impulse responses were found by calculating the frequency domain transfer function of the channel and then synthesizing the time domain response via Fourier techniques. In this research, a simple method of finding the impulse response was developed by slicing the spatial

timefront into its component sheets. Another important development in this work was the calculation of the 90 degree phase change as a wavefront moves past a caustic. Its modeling allows one new insight into timefront analysis. An exploration of the initial condition problem inherent in Gaussian beam modeling was undertaken. Although this question was not answered definitively, a procedure was defined that meets a minimum error criterion.

The second half of the research was an investigation of signal processing techniques combined with serious channel modeling. It seemed pretty obvious that it would be necessary to build a matched filter that would compensate for the channel characteristics. This strategy has worked well. First, an implementation of the matched field processing algorithm in a realistic deep ocean acoustic environment was constructed. This was performed for two reasons; to show that the algorithm would work with Gaussian beam modeling; and to provide a benchmark for other algorithms. Next the multi-frequency matched field processing algorithm was implemented for two cases, incoherent and coherent recombination of the ambiguity surface. This shows the work (in the computational sense) involved in extending MFP to the case of periodic broadband signals. Two methods of multi-frequency MFP were developed to show the improvement in the result when one has some knowledge of the signal spectrum as measured by the peak width of the ambiguity surface.

The new contribution to the field of ocean acoustic signal processing presented in this dissertation, is the development and implementation of channel matched filtering. CMF is a reverse propagation algorithm that efficiently implements broadband source localization using impulse responses. Its advantages over matched field processing is that it is inherently a broadband algorithm and is especially apt for long range deep water multipath propagation. The algorithm does not change depending upon the type of signal expected and therefore, even if nothing is known about the

signal, no assumptions (such as periodicity) need to be made to use CMF. Another contribution was the development and implementation of channel phase filtering, and channel time delay filtering, variations on the channel matched filtering theme. These are ad hoc schemes for source localization. They are significant because they are still able to localize a source even when the knowledge of the channel is not complete.

Finally the performance of the different signal processing strategies was considered. First, the ability to localize sources when the model of the channel does not match the true channel was investigated. It was found that the CMF algorithms and its variants were able to tolerate the type of mismatch caused by ocean internal waves to a higher degree than the matched field processing algorithm. Secondly, the effect of the signal bandwidth on the depth localization performance was explored. Bandwidth was found to have a strong effect on performance with bandwidth greater than 10 Hertz reducing the ambiguity and sharpening the precision.

Since this research was an exploratory investigation of the feasibility of techniques rather than an exhaustive analysis of a particular procedure, a number of areas worthy of further study have been identified. First, it is necessary to test the validity of the Gaussian beam model against a normal mode benchmark such as the SNAP model, [25]. Hopefully, by tuning the Gaussian beam model, ocean acoustic modelers will get an effective tool for use in deep ocean environments. Secondly, a rigorous performance analysis of the signal processing needs to be done. By putting this problem in a parameter estimation framework, the question of optimality of the methods, in relation to the Cramer-Rao performance bound could be calculated. Effects that could be tested via this bound include uncertainties array position and movement (Doppler effects), signal power and bandwidth, and directional noise fields. And lastly but perhaps of greatest practical importance, a large number of examples need to be run for specific static and dynamic ocean models, with range varying

sound speed, at ranges of 1 megameter or more, to continue the exploration of the applicability of CMF detection and localization.

APPENDICES

APPENDIX A

COMPUTER MODELING

A listing of the computer code that was written to implement the Gaussian beam acoustic model is given in this appendix.

The code itself is comprised of seven subroutines written in the C language. It has been used extensively on an Apollo workstation, but also is portable enough to work on a PC compatible microcomputer or any UNIX machine.

This code enables the user to generate acoustic field and impulse responses. Also it can be used to do ray tracing, to produce time fronts, or to find eigenrays. The code assumes a Munk sound speed profile. A more general range dependent profile can be used however by substituting the appropriate subroutine. Runge–Kutta numerical integration is used to perform the approximate calculation of the ray paths.

The first step is to initialize the rays with the routine `rayinit`. Input variables are the source depth and the number of rays. If just one ray is to be traced, then the initial angle of the ray must be specified as well. Next the rays are propagated to the receiver location by the routine `prop`. If a non–zero number is input as the propagation time though, the rays will all be integrated for the same amount of time. This allows the user to generate a timefront. Finally, there are two routines to calculate the output in the desired form. The routine `field` returns the magnitude and phase response of a cw source. The routine `imp` returns the impulse response.

The header file:

```
/*
 *          ocean.h
 */

double      **rayinit();
void        prop();
double      *field();
double      *imp();
void        ruku();
void        sys();
void        ssp();
```

The source code file:

```
/*
 *          ocean.c
 *
 *          ocean acoustics subroutines
 */

#include    <stdio.h>
#include    <math.h>
#include    "ocean.h"

/*          global variables */

int         nrays;
double      angdown;
double      angup;
double      cbottom;
double      cinit;
double      csurface;
double      phimax;
double      dt      = 0.1;
double      pi      = 3.1415926;
double      zbottom = 5000.0;
double      ztop    = 0.0;
```

```
/*
 *          Initialize rays at source_depth with number_of_rays
 *          evenly spaced between surface and bottom grazing
 *          angles. If number_of_rays is one then initialize
 *          only one ray leaving source at angle theta. Returns
 *          pointer to ray state variable.
 */

double      **rayinit ( source_depth, theta, number_of_rays)
double      source_depth, theta;
int         number_of_rays;
{
    int     i;
    double  dcz, dczz, phi;
    double  **x;

    nrays = number_of_rays;
    ssp ( source_depth,  &cinit,    &dcz, &dczz);
    ssp ( ztop,    &csurface, &dcz, &dczz);
    ssp ( zbottom, &cbottom,  &dcz, &dczz);
    angup   = -acos(cinit/csurface);
    angdown =  acos(cinit/cbottom);
    phimax = angdown;
    if (fabs(angup) < fabs(angdown))
      phimax = angup;
    if (nrays == 1)
      phimax = theta;

    x = (double **) malloc((unsigned) nrays*sizeof(double*));
    for ( i=0; i<nrays; i++) {
      phi = phimax - 2.0*i*phimax/(nrays - 1);
      x[i] = (double *) malloc((unsigned) 10*sizeof(double));
      x[i][0]  = 0.0;              /* source range */
      x[i][1]  = cos(phi)/cinit;   /* ray run      */
      x[i][2]  = source_depth;     /* source depth */
      x[i][3]  = sin(phi)/cinit;   /* ray rise     */
      x[i][4]  = 1.0;              /* alpha_0      */
      x[i][5]  = 0.0;              /* beta_0       */
      x[i][6]  = 0.0;              /* alpha_1      */
      x[i][7]  = 1.0;              /* beta_1       */
      x[i][8]  = 0.0;              /* time         */
      x[i][9]  = 0.0;              /* cross        */
    }
    return (x);
}
```

```
/*
 *          Propagate rays to receiver at range, rrange and
 *          depth, rdepth if ptime is zero; else propagate
 *          rays for amount of time, ptime. The two dimensional
 *          pointer x is the ray state variable returned by the
 *          routine rayinit.
 */

void        prop ( x, rrange, rdepth, ptime)
double      **x;
double      rrange; /* receiver range */
double      rdepth; /* receiver depth */
double      ptime;  /* propagation time */
{
    int     i, j;

    double  dist, old_dist;
    double  old_x[10];

    if (ptime == 0.0) {
      for ( i = 0; i < nrays; i++) {
        old_dist = x[i][1]*(rrange - x[i][0]) +
                   x[i][3]*(rdepth - x[i][2]);
        do {
          for (j= 0; j<10; j++)  old_x[j] = x[i][j];
          dt = old_dist*fabs(dt/old_dist);
          ruku ( x[i], dt);
          if ( x[i][6] <= 0.0) {
            if ( x[i][4]*old_x[4] <= 0.0) {
              if ( -x[i][4] < 0.0) x[i][9]++;
              if ( -x[i][4] > 0.0) x[i][9]--;
            }
          }
          dist = x[i][1]*(rrange - x[i][0]) +
                 x[i][3]*(rdepth - x[i][2]);
        }  while (dist*old_dist > 0.0);

        if ( fabs(dist) > fabs(old_dist) ) {
          for (j= 0; j<10; j++)  x[i][j] = old_x[j];
        }
      }
    }
```

```
    else {
      for ( i = 0; i < nrays; i++) {
        while (x[i][8] < ptime) {
          old_x[4] = x[i][4];
          ruku ( x[i], dt);
          if ( x[i][6] <= 0.0) {
            if ( x[i][4]*old_x[4] <= 0.0) {
              if ( -x[i][4] < 0.0) x[i][9]++;
              if ( -x[i][4] > 0.0) x[i][9]--;
            }
          }
        }
      }
    }

    return;
}
```

```
/*
 *          Calculate field at point, rrange, rdepth, at frequency
 *          freq. Returns pointer to two element double precision
 *          array with first element magnitude and second element
 *          phase of signal. The two dimensional pointer x is the
 *          ray state variable returned by the routine rayinit.
 */

double      *field ( x, freq, rrange, rdepth)
double      **x;
double      freq, rrange, rdepth;
{
    int     i, imax;

    double  amp, ampmin;
    double  arg, phase;
    double  c, dcz, dczz;
    double  den;
    double  k, l;
    double  lz, min;
    double  omega, psi;
    double  real, im;
    double  s, n;
    double  time;
    double  *z;

    ampmin = 0.0;
    for ( i = 0; i < nrays; i++) {
      amp = -fabs(x[i][6]);
      if ( amp < ampmin) {
        ampmin = amp;
        imax   = i;
      }
    }

    omega = 2*pi*freq;
    i = imax;
    min = 100.0;
    if (x[i][6] == 0)
      lz = -omega*min*min/(2.0*x[i][4]*x[i][4]);
    else if (x[i][4] == 0.0)
      lz = -2.0*x[i][6]*x[i][6]/(omega*min*min);
    else
      lz = -fabs(x[i][6]/x[i][4]);
```

```
    psi = sqrt(-lz/freq);

    real = 0.0;
    im   = 0.0;
    for ( i = 0; i < nrays; i++) {
      ssp ( x[i][2], &c, &dcz, &dczz);
      den   = lz*lz*x[i][4]*x[i][4] + x[i][6]*x[i][6];
      k     = c*(lz*lz*x[i][5]*x[i][4] + x[i][7]*x[i][6])/den;
      l     = -2.0*den/(omega*lz);
      s     = c*(x[i][1]*(rrange - x[i][0]) +
              x[i][3]*(rdepth - x[i][2]));
      n     = c*(x[i][3]*(rrange - x[i][0]) -
              x[i][1]*(rdepth - x[i][2]));

      amp   = exp(-n*n/l)*sqrt(c/(sqrt(den)*fabs(x[i][0])))/psi;
      arg   = atan2 ( -lz*x[i][4], x[i][6]) - pi*x[i][9];
      time  = x[i][8] + s/c + s*n*dcz*x[i][1]/c -
              s*s*dcz*x[i][3]/(2.0*c) + k*n*n/(2.0*c);
      phase = omega*time + arg;

      real = real + amp*cos(phase);
      im   = im   + amp*sin(phase);
    }

    z      = (double *) malloc ( 2*sizeof(double));
    *z     = sqrt(real*real + im*im);
    *(z+1) = atan2(im,  real);

    return (z);
}
```

```
/*
 *          Calculate impulse response at a point, rrange, rdepth,
 *          at frequency freq. Returns pointer to (3*N+1) element
 *          double precision array where N is the number of
 *          arrivals. The first element is N, followed by the
 *          magnitude, phase, and time delay of each arrival.
 *          The two dimensional pointer x is the ray state
 *          variable returned by the routine rayinit.
 */

#define     NS   50

double      *imp ( x, freq, rrange, rdepth)
double      **x;
double      freq, rrange, rdepth;
{
    int     i, imax;
    int     sheet_number;

    double  amp, ampmin;
    double  arg, phase;
    double  c, dcz, dczz;
    double  den;
    double  dist, slope, dmin;
    double  k, l;
    double  lz, min;
    double  last_dist, last_slope;
    double  omega, psi;
    double  real, im;
    double  s, n;
    double  time, toa;
    double  *z;

    double  shamp[NS], shphase[NS], shtoa[NS];

    ampmin = 0.0;
    for ( i = 0; i < nrays; i++) {
      amp = -fabs(x[i][6]);
      if ( amp < ampmin) {
        ampmin = amp;
        imax   = i;
      }
    }
```

```
omega = 2*pi*freq;
i = imax;
min = 100.0;
if (x[i][6] == 0)
  lz = -omega*min*min/(2.0*x[i][4]*x[i][4]);
else if (x[i][4] == 0.0)
  lz = -2.0*x[i][6]*x[i][6]/(omega*min*min);
else
  lz = -fabs(x[i][6]/x[i][4]);

psi = sqrt(-lz/freq);
for ( i = 0; i < nrays; i++) {
  ssp ( x[i][2], &c, &dcz, &dczz);
  den   = lz*lz*x[i][4]*x[i][4] + x[i][6]*x[i][6];
  k     = c*(lz*lz*x[i][5]*x[i][4] + x[i][7]*x[i][6])/den;
  l     = -2.0*den/(omega*lz);
  s     = c*(x[i][1]*(rrange - x[i][0]) +
          x[i][3]*(rdepth - x[i][2]));
  n     = c*(x[i][3]*(rrange - x[i][0]) -
          x[i][1]*(rdepth - x[i][2]));

  amp   = exp(-n*n/l)*sqrt(c/(sqrt(den)*fabs(x[i][0])))/psi;
  arg   = atan2 ( -lz*x[i][4], x[i][6]) - pi*x[i][9];
  time  = x[i][8] + s/c + s*n*dcz*x[i][1]/c -
          s*s*dcz*x[i][3]/(2.0*c) + k*n*n/(2.0*c);
  phase = omega*time + arg;

  dist  = (rrange - x[i][0])*(rrange - x[i][0]) +
          (rdepth - x[i][2])*(rdepth - x[i][2]);

  if ( i == 0) {
    last_dist    = dist;
    last_slope   = -1.0;
    sheet_number = 0;
    real         = amp*cos(phase);
    im           = amp*sin(phase);
    toa          = time;
    dmin         = dist;
  }
  else {
     slope = dist - last_dist;
     if ((last_slope > 0.0) && (slope < 0.0)) {
       shamp[sheet_number]   = sqrt ( real*real + im*im);
       shphase[sheet_number] = atan2 ( im, real);
       shtoa[sheet_number]   = toa;
```

```
            sheet_number++;
            real   = 0.0;
            im     = 0.0;
            dmin   = HUGE;
          }
          real = real + amp*cos(phase);
          im   = im   + amp*sin(phase);
          if (dist < dmin) {
            dmin = dist;
            toa  = time;
          }
          last_dist  = dist;
          last_slope = slope;
        }
      }
      shamp[sheet_number]   = sqrt (real*real + im*im);
      shphase[sheet_number] = atan2 ( im, real);
      shtoa[sheet_number]   = toa;
      sheet_number++;

      z = (double *) malloc ( (unsigned)
                              (3*sheet_number + 1)*sizeof(double));
      *z = sheet_number;
      for ( i=0; i<sheet_number; i++) {
        *(z+3*i+1) = shamp[i];
        *(z+3*i+2) = atan2( sin(shphase[i] - omega*shtoa[i]),
                            cos(shphase[i] - omega*shtoa[i]));
        *(z+3*i+3) = shtoa[i];
      }

      return (z);
}
```

```
/*          runge kutta integrator */

#define     NI   9

void        ruku (y, dt)
double      y[];
double      dt;
{
    int     i;
    double  d[NI], e[NI], xzero[NI];

    for ( i=0; i<NI; i++)
      xzero[i] = y[i];

    sys (y, d);

    for ( i=0; i<NI; i++) {
      e[i] = d[i]*dt;
      y[i] = xzero[i] + e[i]/2.0;
    }

    sys (y, d);

    for ( i=0; i<NI; i++) {
      e[i] = e[i] + 2.0*d[i]*dt;
      y[i] = xzero[i] + d[i]*dt/2.0;
    }

    sys (y, d);

    for ( i=0; i<NI; i++) {
      e[i] = e[i] + 2.0*d[i]*dt;
      y[i] = xzero[i] + d[i]*dt;
    }

    sys (y, d);

    for ( i=0; i<NI; i++)
      y[i] = xzero[i] + (e[i] + d[i]*dt)/6.0;

    return;
}
```

```
/*          ray dynamics */

void        sys (y, d)
double      y[], d[];
{
    double  c, cc, dcnn, dcx, dcz, dczz;

    ssp (y[2], &c, &dcz, &dczz);

    cc  = c*c;
    dcx = 0.0;

    d[0]  = cc*y[1];
    d[1]  = -dcx/c;
    d[2]  = cc*y[3];
    d[3]  = -dcz/c;

    dcnn  = dczz*d[0]*d[0]/(d[0]*d[0] + d[2]*d[2]);

    d[4]  = cc*y[5];
    d[5]  = -dcnn*y[4]/c;
    d[6]  = cc*y[7];
    d[7]  = -dcnn*y[6]/c;

    d[8]  = 1.0;

    return;
}
```

```
/*          munk sound speed */

#define     BETA                        1040.0
#define     C0                          1482.0
#define     EP                          0.006
#define     Z0                          1200.0

void        ssp (z, pc, pdcz, pdczz)
double      z, *pc, *pdcz, *pdczz;
{
    double  diff, value;

    diff   = 2.0*(z - Z0)/BETA;
    value  = exp(-diff);
    *pc    = C0*(1.0 + EP*(value + diff - 1.0));
    *pdcz  = 2.0*C0*EP*(1.0 - value)/BETA;
    *pdczz = 4.0*C0*EP*value/(BETA*BETA);

    return;
}
```

APPENDIX B

LINEAR INTERNAL WAVES

A short description of linear internal waves is given in this appendix. Internal waves are slowly moving density waves that travel through the ocean. They are ultimately driven by solar energy. The differences in adsorbed radiation at different global locations results in differences in temperature. The temperature differences are effective, through the thermodynamic equation of state, as space varying density and pressure fields. The classical equations of motion describe nature's attempt to drive these fields to an equilibrium state. The motion is complicated by the presence of the gravitational field and by the rotation of the earth.

Following the derivation by Flatté [18], begin with the assumption of an inviscid, incompressible fluid which is allowed to have a variable density. Let ρ be the density of the fluid, $\mathbf{u}$ be the velocity of a fluid element with components (u, v, w), p be the pressure, and $\hat{\mathbf{k}}$ be a unit vector in the vertical direction. Define the convective derivative as

$$D_t = \frac{\partial}{\partial t} + \mathbf{u} \cdot \nabla. \tag{B.1}$$

The equations of motion can now be expressed as follows:

$$\rho D_t \mathbf{u} = -\nabla p + \rho g \hat{\mathbf{k}}, \tag{B.2}$$

$$D_t \rho + \rho \nabla \cdot \mathbf{u} = 0, \tag{B.3}$$

$$\nabla \cdot \mathbf{u} = 0, \tag{B.4}$$

where (B.2) is Newton's second law, (B.3) is the equation of continuity, and (B.4) is a result of the incompressibility of the fluid.

It turns out that variations in the fields, ρ, $\mathbf{u}$, and p are small and they are perturbations around the static equilibrium point, $\mathbf{u} = 0$. So the equations of motion reduce to the hydrostatic pressure equation

$$\nabla p_0 = \rho_0 g \hat{\mathbf{k}}, \tag{B.5}$$

where ρ_0 is the equilibrium density distribution.

Now define the time varying parts of the density (ρ') and pressure (p') as

$$p = p_0 + p', \qquad \rho = \rho_0 + \rho'. \tag{B.6}$$

If we assume that all motions are infinitesimal about the equilibrium point we can linearize the above equations. Neglecting all second-order terms, we can write:

$$\rho_0 \frac{\partial \mathbf{u}_H}{\partial t} = -\nabla_H p', \tag{B.7}$$

$$\rho \frac{\partial w}{\partial t} = -\frac{\partial p'}{\partial z} + \rho' g, \tag{B.8}$$

$$\nabla_H \cdot \mathbf{u}_H + \frac{\partial w}{\partial z} = 0, \tag{B.9}$$

$$\frac{\partial \rho}{\partial t} + w \frac{\partial \rho_0}{\partial z} = 0, \tag{B.10}$$

where the index H indicates the horizontal components and z is the depth coordinate.

By trying a plane wave solution of the form

$$w = W(z) e^{j(kx - \omega t)}, \tag{B.11}$$

for the vertical component of the velocity, where x is the range coordinate, and eliminating variables other than w from the linearized equations of motion, the linear internal wave equation,

$$\frac{\partial^2 W}{\partial z^2} + \left(\frac{n^2(z) - \omega^2}{\omega^2 - \omega_i^2} \right) k^2 W = 0, \tag{B.12}$$

can be obtained. Here $n(z)$ is the Brunt–Väisälä frequency,

$$n = \left(\frac{g}{\rho}\frac{d\rho}{dz}\right)^{1/2} = n_0 e^{-z/B}, \tag{B.13}$$

which is a measure of the stability of the water column, and ω_i is the inertial or Coriolis frequency,

$$\omega_i = 2\Omega \sin(\text{ latitude }), \tag{B.14}$$

$$\Omega = \frac{2\pi}{24\,\text{hours}}, \tag{B.15}$$

which compensates for the rotation of the earth.

The solution of the linear internal wave equation, (B.12), is subject to the boundary conditions,

$$W(0) = 0 \tag{B.16}$$

$$W(z_{\text{bottom}}) = 0. \tag{B.17}$$

This suggests a solution technique similar to that used in Chapter 2 for the modal propagation of sound waves. An orthonormality condition can also be derived from equation (B.12)

$$D_1 \int_{z_{\text{bottom}}}^{0} \left[n^2(z) - \omega_i^2\right] W(k,m,z) W(k,m',z)\, dz = \delta_{mm'}, \tag{B.18}$$

where we shall use $D_1 \approx \rho_1$ a constant. A plot of the first three internal wave displacement modes is shown in figure B.1, assuming a Munk sound speed profile.

The horizontal components of velocity have plane wave solutions also, but since there are no boundary conditions to be satisfied, the spectrum of allowable solutions is continuous. The displacement of an isodensity surface can thus be represented as the weighted sum of the propagating modes, explicitly,

$$\zeta = \sum_{k_x,k_y,m} G(k_x,k_y,m) W(k,m,z) e^{j(k_x x + k_y y - \omega t)}, \tag{B.19}$$

where

$$k^2 = k_x^2 + k_y^2. \tag{B.20}$$

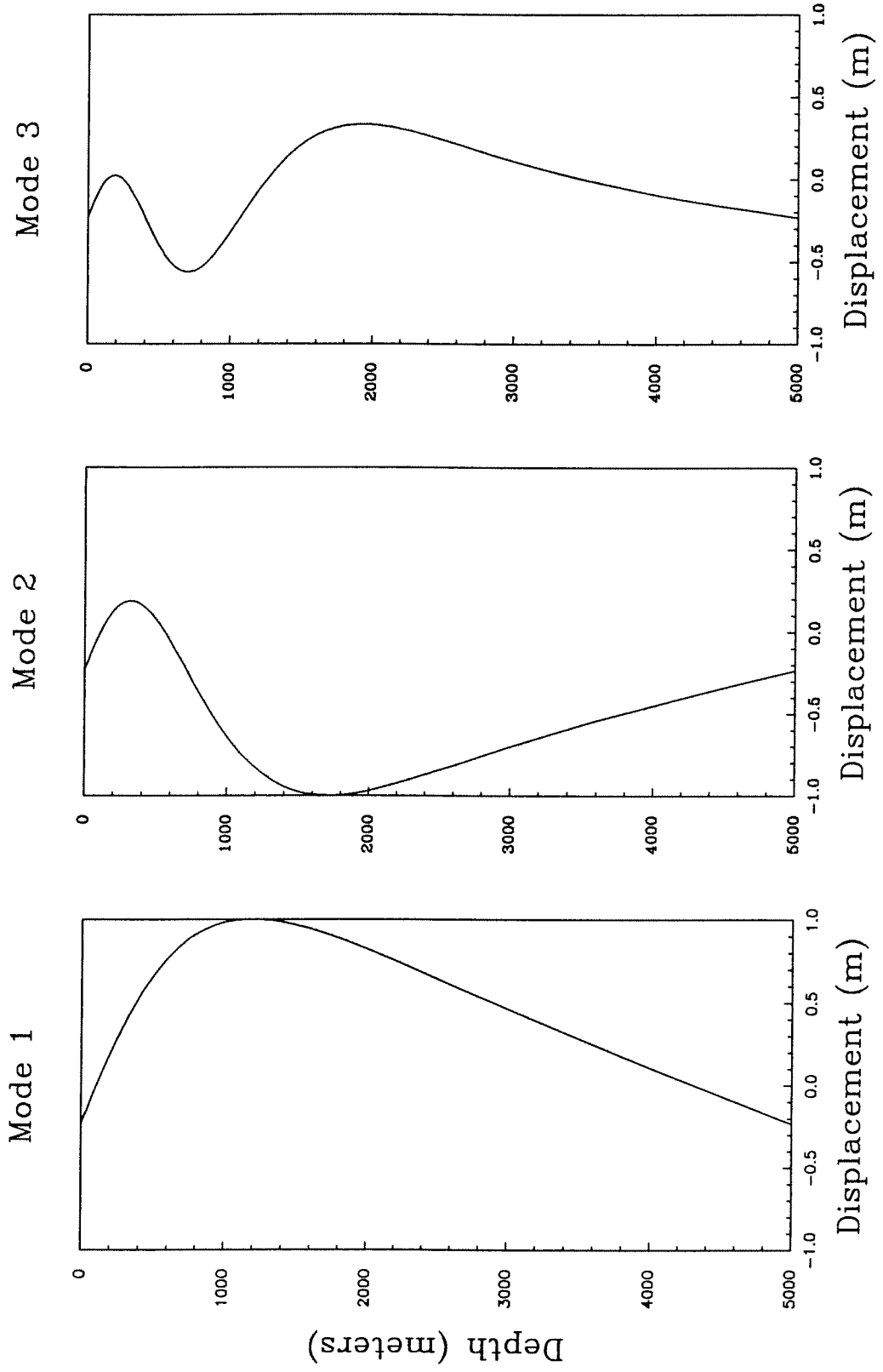

Figure B.1: Internal Wave Density Modes.

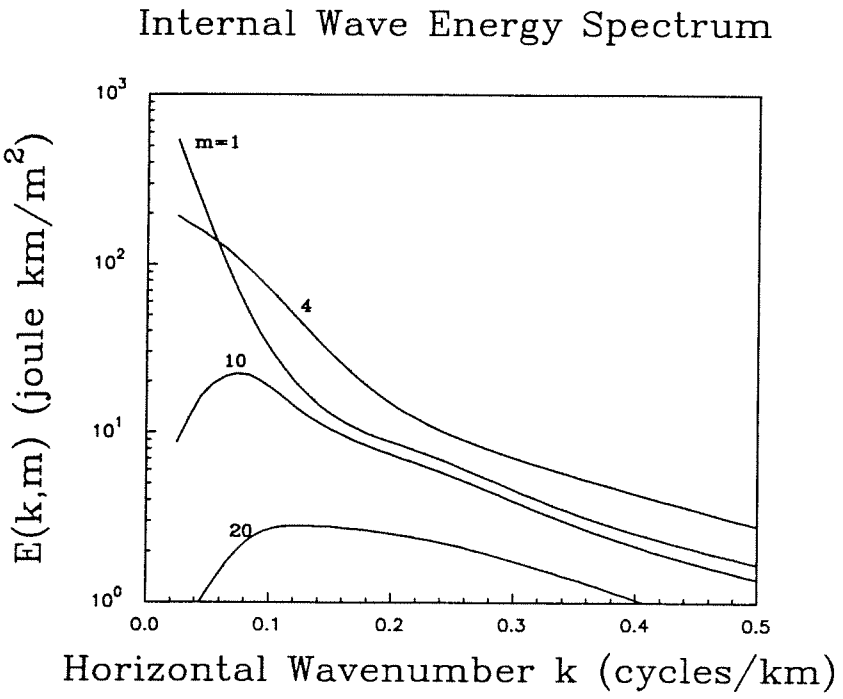

Figure B.2: Internal Wave Energy Spectrum.

Here $G(k_x, k_y, m)$ represents the energy present in the mth mode that is traveling in the direction $k_x\hat{\mathbf{i}} + k_y\hat{\mathbf{j}}$. The spectrum, G, has been measured extensively and it is known that most of the energy is carried in the first few modes modes. The magnitude squared of G,

$$E(k_x, k_y, m) = |G(k_x, k_y, m)|^2 \tag{B.21}$$

is the energy. Figure B.2, [18] shows a typical energy spectrum as a function of horizontal wavenumber.

All that remains is to relate the displacement to the change in sound speed. Flatté asserts that

$$\frac{\delta C}{C} = 2.5n^2(z)\zeta. \tag{B.22}$$

Sound speed changes corresponding to the displacement modes shown in figure B.1 are plotted in figure 4.7.

BIBLIOGRAPHY

BIBLIOGRAPHY

[1] A. B. Baggeroer, W. A. Kuperman, and Henrik Schmidt, "Matched Field Processing: Source localization in correlated noise as an optimum parameter estimation problem", *Journal of the Acoustic Society of America*, 1988, **83**, 571–587.

[2] T. G. Birdsall, *The Theory of Signal Detectability: ROC Curves and Their Character*, Ph.D. Thesis, The University of Michigan, 1966.

[3] T. G. Birdsall, *Personal communication.*

[4] Gary E. J. Bold, "Simulation of nonlinear acoustic systems using bilinear transform and higher-order simulators", *Journal of the Acoustic Society of America*, 1985, **78**, 1902–1904.

[5] Gary E. J. Bold, "EECS 750 Notes: Physics of underwater sound", *The University of Michigan*, Fall 1985.

[6] Gary E. J. Bold, T. G. Birdsall, and Kurt Metzger Jr. "Long Range Arrival structure using Timefront Analysis" *Journal of the Acoustic Society of America*, 1986, *80 Supplement 1*, S63.

[7] Homer P. Bucker, "Use of calculated sound fields and matched-field detection to locate sound sources in shallow water", *Journal of the Acoustic Society of America*, 1976, **59**, 368–373.

[8] G. C. Carter, "Time Delay Estimation for Passive Sonar Signal Processing", *IEEE Transactions on Acoustics, Speech, and Signal Processing*, 1981, **29**, 463–470.

[9] V. Červený, M. M. Popov, and I. Pšenčík, "Computation of wave fields in inhomogeneous media — Gaussian beam approach", *Geophysical Journal of the Royal Astronomical Society*, 1982, **70**, 109–128.

[10] V. Červený and I. Pšenčík, "Gaussian beams in elastic 2-D laterally varying layered structures", *Geophysical Journal of the Royal Astronomical Society*, 1984, **78**, 65–91.

[11] C. S. Clay, "Optimum time domain signal transmission and source location in a waveguide", *Journal of the Acoustic Society of America*, 1987, **81**, 660–664.

[12] C. S. Clay and Saimu Li, "Time domain signal transmission and source location in a waveguide: Matched filter and deconvolution experiments", *Journal of the Acoustic Society of America*, 1988, **83**, 1377–1383.

[13] B. Cornuelle, et. al., "Tomographic Maps of the Ocean Mesoscale. Part 1: Pure Acoustics", *Journal of Physical Oceanography*, 1985, **15**, 133–152.

[14] Bruce Cornuelle and Bruce M. Howe, "High Spatial Resolution in Vertical Slice Ocean Acoustic Tomography", *Journal of Geophysical Research*, 1987, **92**, 11,680–11,692.

[15] Dan E. Dudgeon and Russell Mersereau, *Multidimensional Digital Signal Processing*, Prentice-Hall, 1984.

[16] Matthew Dzieciuch and T. G. Birdsall, "Spatial Matched Processing for Multipath Propagation", *Journal of the Acoustical Society of America*, 1987, *82 Supplement 1*, S73.

[17] Matthew Dzieciuch, "Passive Sonar Detection and Position Estimation", *NATO SACLANT ASW Research Center, Summer Research Report*, La Spezia, Italy, 1985.

[18] Stanley M. Flatté, ed., *Sound transmission through a fluctuating ocean*, Cambridge University Press, 1979.

[19] Benjamin Friedlander, "On the Cramer–Rao Bound for Time Delay and Doppler Estimation", *IEEE Transactions on Information Theory*, 1984, **30**, 575–580.

[20] Benjamin Friedlander, "Accuracy of Source Localization Using Multipath Delays", *IEEE Transactions on Aerospace and Electronic Systems*, 1988, **24**, 346–359.

[21] Adrian E. Gill, *Atmosphere–Ocean Dynamics*, Academic Press, 1982.

[22] S. Haykin, Ed., *Array Signal Processing*, Prentice-Hall, 1985.

[23] Bruce Miller Howe, *Ocean Acoustic Tomography: Mesoscale Velocity*, Ph.D. Thesis, The University of California, San Diego, Scripps Institution of Tomography, 1966.

[24] E. T. Jaynes, "Prior Information and Ambiguity in Inverse Problems", *Proceedings of the Symposium in Applied Mathematics of the American Mathematical Society and the Society for Industrial and Applied Mathematics*, 1983, **14**, 151–166.

[25] Finn B. Jensen and Melchiorre C. Ferla, "SNAP: The SACLANTCEN Normal-Mode Acoustic Propagation Model", *SACLANT ASW Research Centre Memorandum*, SM-121, 1979.

[26] D. H. Johnson, "The Application of Spectral Estimation Methods to Bearing Estimation Problems", *Proceedings of the IEEE*, 1982, **70**, 1018–1028.

[27] Joseph B. Keller and William Streifer, "Complex Rays with an Application to Gaussian Beams", *Journal of the Optical Society of America*, 1971, **61**, 40–43.

[28] Gordon S. Kino, *Acoustic Waves: Devices, Imaging, and Analog Signal Processing*, Prentice-Hall, 1987.

[29] L. Ljung and T. Söderström, *Theory and Practice of Recursive Identification*, MIT Press, 1983.

[30] L. Ljung, *System Identification: Theory for the User*, Prentice-Hall, 1987.

[31] Dietrich Marcuse, *Light Transmission Optics*, Van Nostrand Reinhold, 1982.

[32] Kurt Metzger, *Personal communication.*

[33] G. Müller, "Efficient calculation of Gaussian beam seismograms for two dimensional inhomogeneous media", *Geophysical Journal of the Royal Astronomical Society*, 1984, **79**, 153–166.

[34] Jacques Munier and Gilles Y. Delisle, "Spatial Analysis in Passive Listening Using Adaptive Techniques", *Proceedings of the IEEE*, 1987, **75**, 1458–1471.

[35] Walter H. Munk, "Sound channel in an exponentially stratified ocean, with application to SOFAR", *Journal of the Acoustic Society of America*, 1974, **55**, 220–226.

[36] Walter H. Munk and Gordon O. Williams, "Acoustic Oceanography", *Nature*, 1977, **267**, 774–778.

[37] Walter Munk and Carl Wunsch, "Ocean acoustic tomography: a scheme for large scale monitoring", *Deep–Sea Research*, 1979, **26A**, 123–161.

[38] Michael Porter and Homer P. Bucker, "Gaussian beam tracing for computing ocean acoustic fields", *Journal of the Acoustic Society of America*, 1987, **82**, 1349–1359.

[39] Michael Porter, Ronald Dicus, and R. G. Fizell, "Simulations of Matched-Field Processing in a Deep-Water Pacific Environment", *IEEE Journal of Oceanic Engineering*, 1987, **12**, 173–181.

[40] R. P. Porter and A. J. Devaney, "Generalized Holography and Computational Solutions to Inverse Problems", *Journal of the Optical Society of America*, 1982, **72**, 1707–1713.

[41] William H. Press, Brian P. Flannery, Saul A. Teukolsky, and William T. Vettering, *Numerical Recipes in C*, Cambridge University Press, 1988.

[42] J. C. Stienberg and T. G. Birdsall, "Underwater sound propagation in the straights of Florida", *Journal of the Acoustic Society of America*, 1966, **39**, 301–315.

[43] A. Tarantola and B. Valette, "Inverse Problems = Quest for Information", *Journal of Geophysics*, 1982, **50**, 159–170.

[44] Ivan Tolstoy and C.S. Clay, *Ocean Acoustics: Theory and Experiment in Underwater Sound*, McGraw–Hill Book Company, 1966.

[45] Robert J. Urick, *Principles of Underwater Sound for Engineers*, McGraw–Hill Book Company, 1967.

[46] H. L. Van Trees, *Detection, Estimation, and Modulation Theory*, John Wiley & Sons, 1968.

[47] Mati Wax and Thomas Kailath, "Optimum Localization of Multiple Sources by Passive Arrays", *IEEE Transactions on Acoustics, Speech, and Signal Processing*, 1983, **31**, 1210–1217.

[48] Mati Wax and Thomas Kailath, "Decentralized Processing in Sensor Arrays", *IEEE Transactions on Acoustics, Speech, and Signal Processing*, 1985, **33**, 1123–1129.

[49] Mati Wax and Ilan Ziskind, "On Unique Localization of Multiple Sources by Passive Sensor Arrays", *IEEE Transactions on Acoustics, Speech, and Signal Processing*, 1989, **37**, 996–1000.

[50] P. Whittle, "The Analysis of Multiple Stationary Time Series", *J. Royal Statistical Society*, 1953, **15**, 125–139.

[51] Stephen Wolfram, *Mathematica*, Addison–Wesley Publishing Company, 1988.

[52] Carl Wunsch, "Using Data with Models, Ill-posed and Time-dependent Ill-posed Problems", *NATO Advanced Study Institute, Summer School on Geophysical Tomography*, Les Houches, France, August 1989.

[53] Amnon Yariv, "Phase Conjugate Optics and Real-Time Holography", *IEEE Journal of Quantum Electronics*, 1978, **14**, 650–660.